UNIVERSITÄTSKLINIKUM HAMBURG-EPPENDORF

Klinik und Poliklinik für Neurologie

Prof. Dr. med. Tim Magnus
Prof. Dr. med. Götz Thomalla

Role of extracellular vesicles mRNA in neuroinflammation in a mouse model of stroke

Dissertation

zur Erlangung des Grades eines Doktors der Medizin
an der Medizinischen Fakultät der Universität Hamburg.

vorgelegt von:

Paul Christian Max Kügler
aus Kiel

Hamburg 2024

Angenommen von der
Medizinischen Fakultät der Universität Hamburg am: 27.01.2025

Veröffentlicht mit Genehmigung der
Medizinischen Fakultät der Universität Hamburg.

Prüfungsausschuss, der/die Vorsitzende: PD Dr. Bastian Cheng

Prüfungsausschuss, zweite/r Gutachter/in: PD Dr. Berta Puig Martorell

Content

1. Aim of the study

Ischemic stroke occurs when a cerebral artery is occluded, resulting in hypoxia and cell damage in the adjacent brain parenchyma. Many pathological events are triggered in the ischemic region, leading to cell death and irreversible damage (Dirnagl et al., 1999, Iadecola et al., 2020, Khoshnam et al., 2017). This results in stroke being the second leading cause of death and one of the first of disability in the world (Feigin et al., 2022, GBD 2019 Stoke Collaborators, 2021). At present, the limited therapeutic strategies of thrombolysis or mechanical thrombectomy only focus on reperfusion and many patients suffer from disability even years after the event (Campbell et al., 2019). Thus, the development of new strategies that could target neuronal survival after ischemic stroke is of urgent need.

During ischemic stroke, one very important event is neuroinflammation, where microglia and astrocytes become activated and peripheral cells like macrophages, neutrophils and lymphocytes invade the ischemic area. Depending on the temporal pattern, neuroinflammation can be detrimental but also needed for the recovery after stroke (Iadecola et al., 2020). Targeting neuroinflammation at the right time could be a powerful therapeutic strategy. A recently discovered way for cells to communicate with each other is through extracellular vesicles (EVs). These are particles released by every cell type. Their cargo, including proteins, lipids and different RNA types, can be internalized and used by recipient cells (Russell et al., 2019, Valadi et al., 2007, van Niel et al., 2018). While the transfer of proteins and RNA subpopulations, mainly microRNA (miRNA), have been described, the possibilities of messenger RNA (mRNA) are at present not well understood.

The aims of the present work were, first, to optimize a protocol for isolating small EVs (sEVs) to achieve the gold standard of the guidelines for analyzing sEVs, MISEV2018 (Théry et al., 2018), which was recently updated to MISEV2023 (Welsh et al., 2024); second, to characterize the resulting sEV population in order to verify the new protocol; and third, to get an overview of upregulated and downregulated mRNAs in sEVs on pathways associated with neuroinflammation. To do so, the NanoString nCounter® Technology, a hybridization method to count single mRNAs, was used. The goal was to find mRNAs in EVs related to immunological pathways that could potentially alter the phenotype of recipient cells and, therefore, to understand the communication system behind the complex process of neuroinflammation after stroke.

2. Introduction

2.1. Stroke

Stroke was defined by the World Health Organization (WHO) in 1970 as “rapidly developing clinical signs of focal (or global) disturbance of cerebral function, with symptoms lasting 24 h or longer, or leading to death, with no apparent cause other than of vascular origin” (Coupland et al., 2017). It can be classified into two major groups: ischemic stroke and hemorrhagic stroke. Ischemic stroke is a focal ischemia due to artery occlusion in the central nervous system (CNS) and is generally the leading cause of stroke. In contrast, hemorrhagic stroke can occur through intracerebral or subarachnoid collection of blood, which is not caused by trauma (Sacco et al., 2013). Because of this fundamental distinction between ischemia and hemorrhage and their pathophysiology, it is crucial to search for their essential characteristics separately. Therefore, this dissertation is dedicated to ischemic stroke.

The classic clinical presentation of a stroke containing focal neurological deficits, like motoric or sensible dysfunction or deficits in hearing or speaking, are caused by thrombosis or embolism of cerebral arteries, resulting in their occlusion and, therefore, reduced cerebral blood flow and hypoxia in the cerebral segment supplied by the artery. Arterial embolism is often caused by atrial fibrillation (Hankey, 2017). Risk factors for ischemic stroke are hypertension, diabetes, hypercholesterinemia, smoking, vascular heart disease and carotid stenosis (Kuriakose and Xiao, 2020, Moskowitz et al., 2010). Because collateral arteries supply parts of the ischemic brain parenchyma, hypoxia and brain cell damage are not uniform. The ischemic segment can be subdivided into (i) ischemic core, where the blood flow is maximally reduced, resulting in rapid cell death and necrosis and (ii) the peripheral parts, called the ischemic penumbra, where the persisting cerebral blood flow of the collateral arteries is sufficient to keep cells alive for a limited amount of time. During this limited therapeutic time window, the critical therapy is to salvage as much of the penumbra as possible before irreversible damage, like in the stroke core, occurs (Baron, 2018). Possible therapeutic options are intravenous thrombolysis (IVT) and mechanical thrombectomy. IVT is only applicable within the first 4.5 h and mechanical thrombectomy is a possible therapeutic option in the first 6 h after the initial onset of stroke symptoms. New studies indicate a prolongation of this time period to 24 h (Mendelson and Prabhakaran, 2021). The

therapeutic options have many exclusion criteria and can, therefore, not be given to all ischemic stroke patients (Iadecola et al., 2020, Rinaldo et al., 2019). Patients often have severe disability even months and years after stroke (Yoshimura et al., 2022), and so, intensive research in order to understand the pathophysiological mechanisms in the penumbra and potential new treatment options must be conducted.

2.1.1. Epidemiology

Stroke is the second leading cause of death in the world (Internet reference 1: WHO, 2020), with over 7.6 million new ischemic strokes and over 3.4 million new intracerebral hemorrhages each year. Globally, ischemic stroke makes up 87% of all strokes (Saini et al., 2021). According to the GEDA study of 2015, the 12-month prevalence of the adult population in Germany (>18 years old) is 1.6% (Busch and Kuhnert, 2017).

2.1.2. Pathophysiology

Hypoxia caused by occlusion of a cerebral artery not only causes energy failure, which starts within minutes (Moskowitz et al., 2010) leading to necrosis in the ischemic core, but also starts various other pathophysiological effects leading to continuous cell death in the penumbra, even hours and days after the stroke event (Zhao et al., 2022). Excitotoxicity, peri-infarct depolarization, oxidative stress and inflammation are the major pathogenic factors triggered by hypoxia in the penumbra (Fig. 1) (Dirnagl et al., 1999, Iadecola et al., 2020, Khoshnam et al., 2017).

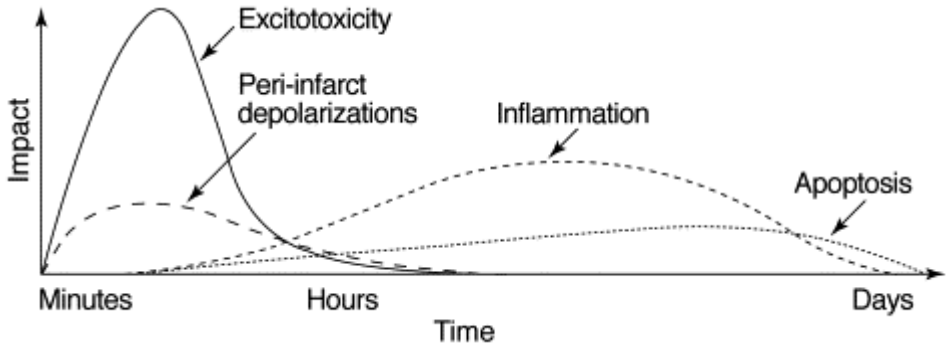

Figure 1: Pathological events after stroke. The x-axis shows the pathological events over time while the y-axis reflects the impact on the final outcome after focal ischemia. These mechanisms do not operate isolated and are mutually dependent. Figure extracted from (Dirnagl et al., *1999).*

The primary energy source that allows the cells of the brain to perform their various functions is adenosine triphosphate (ATP), generated by oxidative phosphorylation at the mitochondria. ATP is used, among other metabolic processes to maintain the sodium/potassium (Na^+/K^+)-ATPase pump, that maintains the resting potential (high extracellular concentration of Na^+ compared to intracellular and the high intracellular concentration of K^+ compared to extracellular) and regulates the volume of the cells (Pape et al., 2018). Failure of ATP supply, induced by the lack of oxygen in the area after occlusion of an artery, leads to the failure of the Na^+/K^+-ATPase pump and, as a consequence, there is a detrimental release of K^+ to the extracellular space and the entry of Na^+ inside the cell. This leads to peri-infarct cell depolarization and cell swelling due to osmosis (Frenguelli, 2019, Lipton, 1999). Additionally, the calcium (Ca^{2+})-ATPase and the Na^+/Ca^{2+}-exchanger (crucial for the Ca^{2+} regulation) no longer function, resulting in a high Ca^{2+} concentration within the cell. Ca^{2+}-dependent proteases and lipases are then activated by the acutely high concentration of Ca^{2+}, causing the cells to lose essential structures leading to cell death (Lipton, 1999). The collapse of ionic gradients additionally leads to increased extracellular glutamate concentration. As glutamate is the primary excitatory neurotransmitter within the CNS, the drastic excitatory events in the penumbra also result in increased intracellular Ca^{2+}-concentration, initiating the so-called excitotoxicity leading to cell death (Shen et al., 2022).

Besides peri-infarct depolarizations and excitotoxicity, oxidative stress through a high concentration of reactive oxygen species (ROS) is another participant in the pathophysiology of ischemic stroke. ROS are highly active molecules that can cause dysfunction of DNA, proteins and lipids (Briyal et al., 2023) when their production exceeds the brain's ability to detoxify them (Adibhatla and Hatcher, 2010). The primary sources of ROS are nicotinamide adenine dinucleotide phosphate (NADPH) oxidases. These are enzymes, which can transfer an electron from NADPH to oxygen and can be induced by N-methyl-D-aspartate (NMDA) receptor signaling (Brennan et al., 2009). NMDA receptors are activated through extracellular glutamate. Therefore, the increased ROS production is also linked to the increased extracellular glutamate concentration. Additionally, there is evidence that ROS can promote proinflammatory events inducing neuroinflammation (Chen et al., 2020).

Despite the various adverse effects contributing to neuronal damage in the penumbra, there is also evidence for the activation of pathways positively influencing cell survival and neuronal protection. For instance, astrocytes were found to limit cell death in the penumbra

via anti-excitotoxicity-effects and the release of neurotrophins (Liu and Chopp, 2016). They also participate in neurogenesis, synaptogenesis and axonal remodeling (Zhao et al., 2022).

2.2. Cells related to the neurovascular unit

Understanding the roles of the different cells of the CNS and their intercellular communication and signaling to the extracellular matrix is fundamental for explaining all aspects of ischemic stroke. The neurovascular unit (NVU) is a relatively recent concept that emphasizes complex interactions between endothelial cells, smooth muscle cells, the extracellular matrix and cells of the brain parenchyma, like astrocytes, neurons and microglia with the general function to control brain homeostasis. Also under ischemic conditions, these interactions have to be taken into account highlighting the importance of understanding stroke not only as an interplay between neurons and occluded blood vessels, but as a complicated scheme, consisting of multiple different cell types (Lo et al., 2003, Ozaki et al., 2019). Although oligodendrocytes and microglia are not included in the definition of the NVU, they play a crucial role in maintaining it (Wang et al., 2021).

The **cerebrovascular endothelial cells**, together with astrocytes end-feet serve as the cellular wall called the blood brain barrier (BBB) between the blood vessel lumen and brain tissue. The high selectivity of the BBB is created by high expression of transport proteins, lack of fenestration, tight junctions (TJs) and low expression of leucocyte adhesion molecules.. The BBB ensures essential functions within the CNS, like low paracellular permeability, proteostasis, maintaining ionic balance, immune surveillance and regulation of the CBF (Candelario-Jalil et al., 2022, Schaeffer and Iadecola, 2021).

Damage to brain tissue during or after an ischemic stroke not only compromises the BBB but also affects the whole NVU. Ischemia induces BBB permeability through the activation of microglia and astrocytes. The following induced secretion of cytokines and the activation of matrix metalloproteinases (MMPs) initiate the BBB breakdown, leading to cerebral edema and increased invasion of peripheral cells, which is further enhanced by proinflammatory signals from pericytes (Wang et al., 2021, Yang et al., 2019). Invasion of peripheral cells is also triggered by platelet activation, initiated seconds after vessel occlusion, leading to the presentation of P-selectins and other adhesion molecules at the surface of endothelial cells. P-selectins are crucial for slowing down circulating leukocytes and direct them to the vessel wall. The hemostasis system, triggered by platelet activation,

plaque disruption and the complement system (activated by coagulation processes), launch further recruiting, adhesion and transmigration of leukocytes (Anrather and Iadecola, 2016, Iadecola and Anrather, 2011, Nakamura and Shichita, 2019). Proinflammatory cytokines lead to the presentation of adhesion molecules on the endothelial cell's surface. Thus, endothelial cells also participate in the beginning of inflammation and leucocyte recruitment by expressing adhesion molecules on their apical surface (Yilmaz and Granger, 2010). Furthermore, the increased ROS production leads to platelet aggregation and increased endothelial permeability (Khoshnam et al., 2017, Wei et al., 1996).

Astrocytes play many critical housekeeping roles in the normal function of the brain, including structuring the BBB, neural metabolism, support the synaptic transmission, surveillance over the extracellular space, stabilization of cell-cell communications and defense mechanisms (Liddelow et al., 2017, Liu and Chopp, 2016). Many of these functions require the formation of barriers, e.g., the envelope of synapses limiting the diffusion of neurotransmitters and local communication molecules. Astrocytes are also necessary for delivering water and solutes from the blood vessels to the brain tissue (Yao et al., 2014). Thus, astrocytic end feet can control nutrient and water exchange/outward flow and influence blood flow by releasing vasoactive molecules, such as prostaglandins and nitric oxide (NO) (Candelario-Jalil et al., 2022, Gordon et al., 2007).

Interestingly, astrocytes have a neuroprotective role in the early stages of stroke within the first hours, while in subacute or chronic stages, astrocytes can have positive as well as negative effects. The different effects of astrocytes can partly be explained by the proliferation of activated astrocytes, leading to glial scar formation (Liu and Chopp, 2016, Zhang et al., 2021c). By creating a barrier around the stroke area, tissue can be remodeled and the local immune system can be controlled. However, in the subacute or chronic stages, this barrier can limit neuron repair (Wang et al., 2012). There are two different populations of activated astrocytes. A1 astrocytes are shown to be harmful to other brain cells , while A2 astrocytes upregulate many neurotrophic factors, turning them to the helpful and protective side. These terms are in analogy to the M1/M2 macrophages. Liddelow *et al*. could show the role of microglia as the main inducers of A1 astrocytes through secretion of IL-6, TNF-α and C1q (Liddelow et al., 2017). Astrocytes additionally play a role in the disruption of the BBB by releasing MMPs, NO, glutamate and endothelins, promoting the apoptosis of endothelial cells and downregulation of tight junctions (Michinaga and

Koyama, 2019). Furthermore, they increase white blood cell crossing of the BBB, leading to neuroinflammation (Zhang et al., 2021c).

Oligodendrocytes produce myelin, which is fundamental for neuronal signal transduction, and offer trophic support to neurons. It has been shown that cell swelling occurs in oligodendrocytes as early as 30 min after stroke and most of the oligodendrocytes die within 3 h after arterial occlusion (Pantoni et al., 1996). Excitotoxicity induces apoptosis and necrosis in oligodendrocytes. The following demyelination of axons has severe consequences for axonal function, metabolism and survival. On the other hand, neuroinflammatory cytokines, such as IL-6 and IL-11, released after stroke, directly impact oligodendrocytes and oligodendrocyte progenitor cells, controlling their proliferation and differentiation (Mifsud et al., 2014, Xu et al., 2020). Stimulation of these effects might facilitate neuronal recovery.

Microglia are the native immune cells of the brain and part of the NVU. Multiple receptors on their surface can detect neurotransmitters and neuropeptides released by neurons and other glial cells, allowing microglia to monitor the CNS function. In their resting state, microglia have multiple processes covering large brain areas connecting to neurons, astrocytes and blood vessels. Microglia change their morphology upon activation and increase their phagocytic and pro- and anti-inflammatory capacity (Colonna and Butovsky, 2017). Microglia are, on the one side, able to enhance neuronal recovery by clearing cell debris, releasing neurotrophic factors like IGF-1 and controlling local inflammation. They are also able to prevent or reduce excitotoxicity and intracellular edema. The activation of neuronal NMDA receptors by high extracellular concentrations of glutamate causes the release of neuronal ATP, which can activate microglia (Dissing-Olesen et al., 2014). They migrate to the damaged tissue and wrap around the swollen axons. This microglia wrapping can reduce axonal permeability and prevent excitation and, thus, reduce cell death (Kato et al., 2016). On the other side, microglia can also release proinflammatory cytokines, like TNF, IL-1 and IL-6, take part in BBB disruption and promote the stimulation of other immune cells.

These two polarizations of microglia are described, like astrocytes before, as M1 microglia, being proinflammatory and mainly harmful to the recovery after stroke, and M2 microglia, which can enhance neuronal recovery. Many publications highlight the differences between M1 and M2 microglia (Hu et al., 2015, Ma et al., 2017, Qin et al., 2019, Szalay et al., 2016,

Wang et al., 2021, Wen et al., 2020, Xu et al., 2020). Within the first hour after stroke, most microglia infiltrating the ischemic brain tissue are M2 microglia. In this state, the microglia are able to enhance their phagocytic activity to clear cell debris and inhibit neuron death (Hu et al., 2012). However, the beneficial effect of M2 microglia is transient for the first week after stroke. Although the activation of M1 microglia occurs later than the activation of the M2 phenotype, it dominates the stroke area after the first week and can persist for over a month (Hu et al., 2012). In addition to the influence of timing on the positive or negative effects of microglia, the existence of different subpopulations of microglia is also dependent on the localization. For instance, microglia in the ischemic core and penumbra are phenotypically different (Hu et al., 2015). In summary, the functional role of microglia is extremely complex and not fully understood. Communication with other cells after stroke seems to regulate numerous processes determining the destiny of ischemic brain tissue (Xu et al., 2020). Because positive and negative effects have been attributed to M1 and M2 microglia, this dichotomic categorization of microglia is outdated and more recent research has revealed that, in fact, microglia is always activated and acquire several states depending on the brain area, sex or disease type (Paolicelli et al., 2022). As this is a fairly new concept, further investigation is required to understand the positive and negative effects of the different microglia states in stroke (Xu et al., 2020).

Long-term cerebral function after stroke depends on neuronal survival which, in turn, depends on the other brain cells. Hence, the therapeutic approach has shifted from focusing on neurons to a more holistic strategy based on the study of the NVU and all their components. The multiple interactions between them and their effects on neurovascular repair, disruption of the BBB and post-stroke inflammation need to be understood for the development of new therapies (Moskowitz et al., 2010, Wang et al., 2021).

2.3. Inflammation after ischemia

Focal ischemia can trigger a strong inflammatory response initiated within hours after insult, causing delayed tissue damage after ischemia. This sterile inflammation involves the activation of brain resident cells like microglia, perivascular macrophages (PVMs) and astrocytes, as well as infiltrating peripheral immune cells like neutrophils, myeloid cells, dendritic cells and lymphocytes, through the disrupted BBB (Iadecola et al., 2020). A

complex interplay between these different cells develops over the first few days after stroke and can have beneficial or detrimental effects on the ischemic lesion.

As mentioned before, the dying cells in the ischemic lesion release many molecules, which initiate a complex inflammation cascade. These molecules include lipopeptides, heat shock proteins, the nuclear protein high-mobility group box 1 (HMGB1) and ATP. These danger associated molecular patterns (DAMPs) can activate immune cells through pattern recognition receptors (PRRs) like Toll-like receptors (TLRs) which then secrete proinflammatory cytokines, such as interleukin 1 (IL-1), tumor necrosis factor (TNF), ROS and MMPs (Candelario-Jalil et al., 2022).

The temporal dynamic of activated cells is important to keep in mind when describing the immune response after an ischemic stroke. Not only are different immune cells activated at different time points after stroke, but their effects can also change within a few days. Within hours after stroke, microglia are the first cells to be activated by DAMPs (Moskowitz et al., 2010). Macrophages, from perivascular and peripheral origin, together with neutrophils infiltrate the brain parenchyma and are the majority of immune cells 3 days after stroke. At this time point, dendritic cells and lymphocytes also invade the ischemic area. However, their presence constitutes a smaller fraction compared to other immune cells (Fig. 2) (Gelderblom et al., 2009).

The role of **macrophages** is similar to that of microglia (Gelderblom et al., 2009). They can produce proinflammatory cytokines and act as phagocytic cells, but also participate in the resolution of neuroinflammation after stroke by releasing growth factors (Amantea et al., 2015). The origin of macrophages can be either from a perivascular or a meningeal site or they can be blood-borne (Moskowitz et al., 2010). PVMs are located in the perivascular space and play an important role in maintaining the BBB. They are also associated with the NVU (Iadecola, 2017). Furthermore, like microglia, they can be subdivided into pro- and anti-inflammatory macrophages (M1/M2 macrophages). In normal conditions, PVMs participate in the maintenance of BBB permeability and are, therefore, essential for brain homeostasis. In the case of neuroinflammation, PVMs proliferate and migrate to the ischemic area and mediate the permeability of the BBB (Zheng et al., 2022b). They can also induce chemotaxis of neutrophils (Pedragosa et al., 2018).

The injured neurons, activated astrocytes and microglia release chemokines, for instance CCL2, which promotes the migration of circulating monocytes towards the inflammation

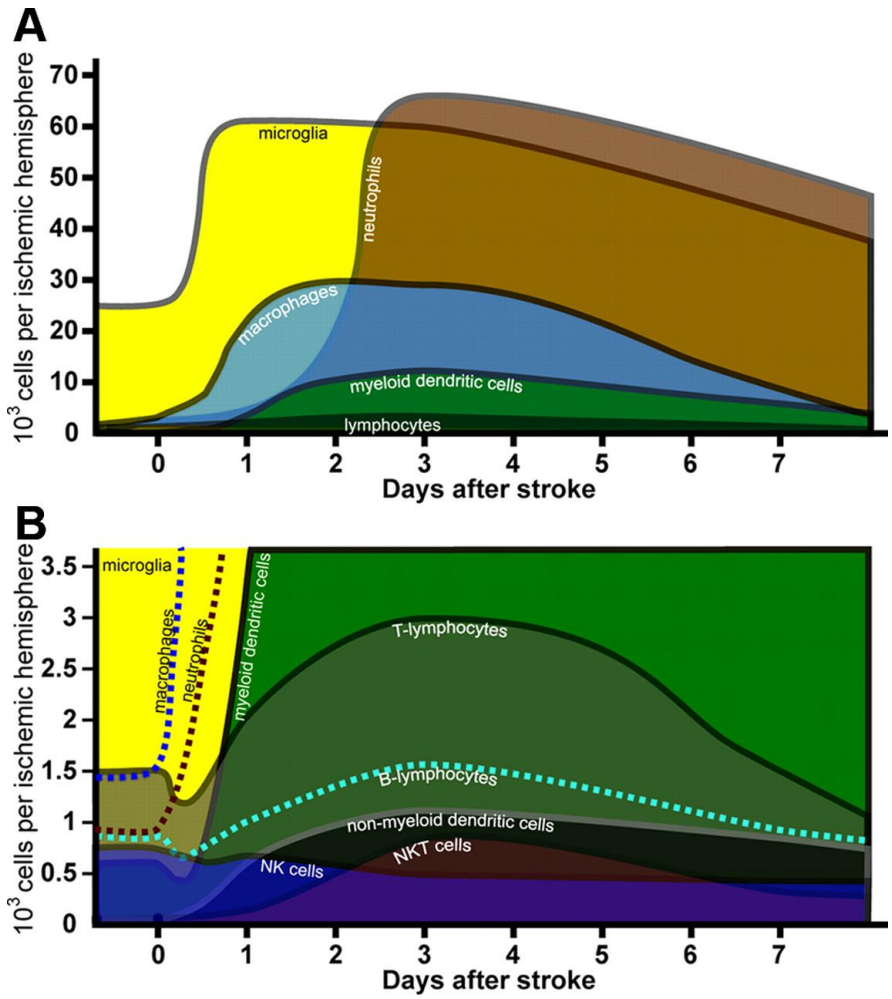

Figure 2: Temporal progression of inflammation following stroke. The data is extrapolated from results collected at 12 h, 1, 3 and 7 d after reperfusion. The x-axis shows the number of days after stroke, the y-axis shows the absolute number. Extracted from (Gelderblom et al., *2009).*

area. Unlike microglia, which persist in the proinflammatory M1 state even weeks after stroke, macrophages maturing from the circulating monocytes change their phenotype to the anti-inflammatory M2 state in the chronic phase after stroke. Therefore, some hints support the idea of M2 macrophages having a beneficial role in post-stroke recovery (Wicks et al., 2022).

As previously mentioned, **neutrophils** comprise most of the immune cells in the ischemic area at around 3 days post-stroke and are the first peripheral cells to infiltrate the CNS (Cai et al., 2020). Their increase in numbers correlates to the extent of tissue damage and poor neurological outcomes (Gelderblom et al., 2009). Like microglia and macrophages, neutrophils can also be divided into a proinflammatory state (N1) and an anti-inflammatory state (N2) (Cai et al., 2020). N1-neutrophils can enhance secondary brain damage by releasing ROS, proteases like MMPs, cytokines and chemokines.

Lymphocytes are part of the adaptive immune system and its depletion results in significantly smaller infarct areas (Liesz et al., 2009, Zhang et al., 2021a). Studies have revealed various effects of its different subsets, such as T helper cells, regulatory T cells, cytotoxic T cells and B cells. T cells appear to infiltrate the ischemic area during the first few days after stroke. Both, antigen-dependent and antigen-independent, effects of T cells take place. The negative effects of T cells are direct cytotoxicity, increasing neuronal apoptosis, promoting microglia and macrophages to increase the secretion of proinflammatory cytokines and increase peripheral immune cell infiltration. Positive effects, mostly from regulatory T cells, are inhibition of TNF-secretion from microglia, increased neuronal stem cell proliferation, reduced production of MMP and the promotion of reparative microglia and oligodendrocyte differentiation (Zhang et al., 2021a).

In conclusion, there is compelling evidence for the essential role of the immune system in stroke. Various specific immune cell populations have been found to participate in neuroinflammation after stroke, with either advantageous or disadvantageous impacts on the outcome (Iadecola et al., 2020). In the early stages after stroke, the activation of microglia, astrocytes and macrophages further damages the brain, in addition to the detrimental effects of ischemia. In contrast, in later stages, reparative pathways are induced by many different immune cells. This dual role makes the immune system a problematic target for therapeutic intervention. The study of neuroinflammation is an active field of research and requires further analysis to be fully understood.

2.4. Extracellular Vesicles

2.4.1. Definition

EVs are lipid-bilayer membrane particles released by every cell type into the extracellular space (Russell et al., 2019). EVs carry biological active molecules, like proteins, lipids and different types of RNA (miRNA, mRNA) and DNA from the cell of origin which can be transferred to other cells. EVs can be classified into two different groups depending on their biosynthetic pathway. Other classifications are based on the EV's size or type of markers (Gould and Raposo, 2013). Exosomes originate at the endosomal pathway and have a size range from 30 – 150 nm. Their release is highly regulated and occurs when the multivesicular bodies (MVBs) containing intraluminal bodies (ILVs) fuse with the plasma

membrane releasing the ILVs, then called exosomes, into the extracellular space (Budnik et al., 2016). Microvesicles are ectosomes formed by outward budding of the plasma membrane and have a diameter ranging from 100 nm to 1 µm. Another type of ectosomes are apoptotic bodies, which are also shed from the plasma membrane but only by cells undergoing apoptosis (Fig. 3). They have a diameter between 0.8 and 5 µm (Colombo et al., 2014, Galvanin et al., 2019, van Niel et al., 2011, Welsh et al., 2024).

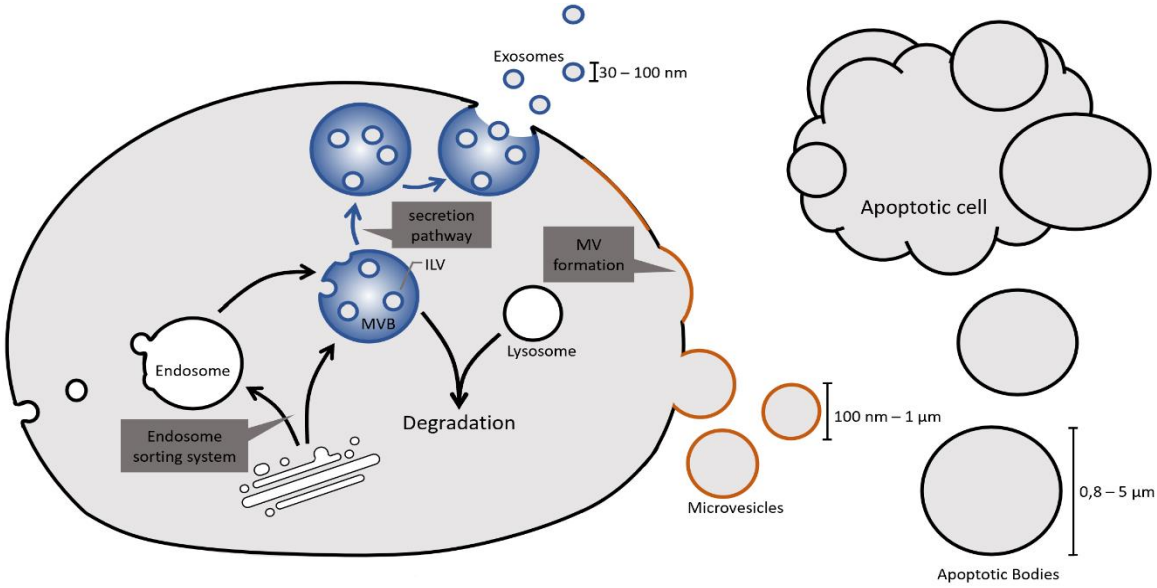

Figure 3: Origin of EVs. On the left cell, the origin of exosomes (blue) and microvesicles (orange) are shown. Exosomes originate from intraluminal vesicles (ILVs) formed at multivesicular bodies (MVBs). Microvesicles are formed by outward budding of the plasma membrane. On the right, an apoptotic cell, releasing an apoptotic body, is shown. The illustration is not true to scale. Figure extracted from (Kügler, 2021).

Exosomes and microvesicles are sometimes classified as such based on physical characteristics, including size, density or biochemical composition (different biomarkers). However, recent recommendations by the International Society of Extracellular Vesicles (ISEV) recommend to use the nomenclature of exosomes, microvesicles and apoptotic bodies only in the case that the origin of EVs, such as MVB or plasma membrane, is explicitly assessed in the study (MISEV 2018 and 2023 guidelines). Otherwise, the use of sEVs (with a diameter of <200nm), or medium/large (mEVs/lEVs) with a diameter of >200 nm is recommended (Gould and Raposo, 2013, Théry et al., 2018, Welsh et al., 2024, Witwer and Théry, 2019).

2.4.2. History

EVs have been known for several years to be part of the extracellular compartment of different tissues, although they were named “membrane microparticles” (George et al.,

1982) or sole “vesicles” (Anderson, 1969) instead of EVs. Before the 1980s, these vesicles were assumed to be established by outward budding of the plasma membrane, which is only applicable to microvesicles. In 1983, a more complex idea of how EVs could be secreted was formed. Pan *et al*. (Pan and Johnstone, 1983) and Harding *et al*. (Harding et al., 1983) investigated the fate of transferrin receptors in late reticulocytes maturing into erythrocytes. Pan *et al*. described a selective loss of the transferrin receptor over vesicle-like structures. Their studies also indicate a segregation pathway for how internalized transferrin receptors during iron delivery could be released (Pan and Johnstone, 1983). Harding *et al*. came to the same results by observing colloidal-gold-transferrin with the addition of detecting the transferrin-receptor in so-called multivesicular endosomes (Harding et al., 1983). In 1987, the connection between MVBs and exosomes was defined (Couch et al., 2021, Johnstone et al., 1987).

2.4.3. EVs biogenesis and physiology

Exosomes are formed at the endocytic pathway, at the MVBs, which are part of a highly dynamic endosomal sorting system within the cell, including early endosomes, late endosomes and lysosomes. Endosomes are formed by the internalization of the plasma membrane. During their maturation, the endosomal membrane invaginates and buds into the endosomal lumen forming ILVs containing ubiquitinated proteins to be degraded. When MVB fuse with lysosomes, ILVs will be delivered for degradation. However, MVBs can also be selectively sorted to fuse with the plasma membrane, releasing then ILVs to the extracellular space as exosomes (Colombo et al., 2014). Two principal mechanisms are involved in the biogenesis of exosomes. The first one is dependent on the endosomal sorting complex required for transport (ESCRT) for the formation of the ILVs, whereas a second one is ESCRT-independent and involves the activation of ceramides, phosphatidic acid or Rab31-flotillin-dependent lipid raft formation (Arya et al., 2024, van Niel et al., 2011). For the sorting and fusion of MVB with the plasma membrane and release of ILVs, the participation of various GTPases, including RAB11, RAB25 and RAB27 is of fundamental importance (Abels and Breakefield, 2016). The sorting of MVBs to the secretory pathway (to the plasma membrane) instead of degradative pathway (to lysosomes) depends on multiple pathways, including those associated with intracellular trafficking, autophagy and several alterations can promote more one pathway or the other. Furthermore, different cell

types, tissue conditions and other experimental settings can alter the cell's capability to secrete exosomes (Kalluri and LeBleu, 2020).

Microvesicles, on the other hand, are directly formed at the plasma membrane. Their generation involves mechanisms similar to exosome biogenesis, such as ESCRT factors and GTPases, although many other proteins are involved (Jin et al., 2022, van Niel et al., 2018). Besides, the biogenesis of microvesicles also requires a physical outward bending of the plasma membrane. This is achieved by the translocation of phospholipids from the inner part of the plasma membrane to the outer one driven by aminophospholipid translocases, scramblases and calpain (van Niel et al., 2018). Influx of calcium though extracellular signals can be an initiator of the secretion of microvesicles by inducing the enzymes required for the lipid rearrangement (Abels and Breakefield, 2016). Furthermore, modulating parts of the cytoskeleton is necessary. This is regulated by the ADP ribosylation factor 6 (ARF6). ARF6 initiates the contraction of actomyosin at the formation site of microvesicles and bends the plasma membrane further, leading to the shedding of microvesicles from the plasma membrane (Clancy et al., 2021, Tricarico et al., 2017).

Once released into the extracellular space, EVs can be found in every biofluid and tissue of the human body. To be part of the intercellular communication system, EVs must interact with specific recipient cells. This precise targeting of EVs to induce a particular function in another cell is currently a subject of active research (van Niel et al., 2018). For instance, EVs can also cross the BBB in both directions, from the vascular system to brain tissue and from brain tissue to the vascular system (Elsharkasy et al., 2020, Saint-Pol et al., 2020). Thus, EVs were found to transport functional cargo from hematopoietic cells across the BBB to neurons (Ridder et al., 2014). The presence of specific ligand/receptor interactions promote EVs' affinity to specific recipient cells, as showed by Prada *et al.*, who found differential movements and uptake of EVs at the surface of astrocytes compared to microglia (Prada et al., 2016).

Once near the recipient cell, EVs interact to the cell surface through various mechanisms eliciting a response. Tetraspanins, integrins, lipids, lectins, heparan sulfate proteoglycans, and constituents of the extracellular matrix facilitate the interaction with the recipient cell. On the one hand, EVs can remain at the cell surface by binding to specific receptors and promote a response in the recipient cell by secondary intercellular signaling or antigen presentation. On the other hand, EVs can be internalized via endocytosis, phagocytosis or

directly fusing with the plasma membrane. With the latter, the EV cargo is released directly into the cytoplasm of the recipient cell. Endocytosis directs the EVs to the endosomal system where they can have two fates: either they fuse with lysosomes, leading to their degradation, which can result in trophic support for the cell (van Niel et al., 2018), or they can release their content to the cytoplasm through a mechanism of endosomal escape which can then elicit a specific function in the recipient cell (Joshi et al., 2020).

2.4.4. EVs cargo

As briefly described above, EVs can carry a variety of proteins, lipids and nucleic acids. The EV cargo sorting process depends on the cell type, biogenesis and physiologic conditions of the EV donor cell (Abels and Breakefield, 2016). The cargo, either membrane associated or soluble, needs to be delivered to the ILV's formation site to produce exosomes or to the membrane budding site in the case of microvesicles. Notably, the mechanisms responsible for sorting or loading proteins into EVs remain to be illuminated. However, EV proteome analysis can indicate which proteins might be involved in the sorting process. Several studies have revealed that a dominant proportion of the EV proteome is part of the EV biogenesis system. One example is the tetraspanin family, which includes CD9, CD37, CD63, CD81 and CD82 (Rädler et al., 2023). These proteins can modulate lipid membrane curvature, making them important members in the EV biogenesis (Jankovičová et al., 2020). Van Niel *et al*. have found CD63 to be involved in ESCRT-independent protein sorting (van Niel et al., 2011). Different posttranslational modifications, like ubiquitination or farnesylation, cause proteins to be segregated to the ILV formation site (Maas et al., 2017, Rädler et al., 2023, van Niel et al., 2018). Several thousand different proteins have been identified in EVs since their discovery and multiple websites like ExoCarta and Vesiclepedia work as compendiums of EV cargo (Chitti et al., 2023, Keerthikumar et al., 2016). It is proven that proteins delivered to a recipient cell via EVs can provide biologically active information for the cell (Toh et al., 2018).

While the role of proteins in EVs has been extensively analyzed, the importance of EV-DNA has yet to be fully understood. Genomic, mitochondrial and viral DNA has been found in EVs from many different cell types (Lázaro-Ibáñez et al., 2019). Notably, DNA is mainly found in cancer cell-derived EVs (Elzanowska et al., 2021, Malkin and Bratman, 2020). Several studies have indicated the presence of large DNA fragments encompassing all

chromosomes with a representation of the entire genome with no specific chromosome region showing a higher abundance in EVs. Furthermore, as indicated by the analysis of cancer cell derived exosomes, EV-DNA shows the same mutations as the donor cell (Kahlert et al., 2014, Thakur et al., 2014). This lack of selectivity might be explained by the role of EVs in cellular homeostasis and clearing the cell from cytoplasmic DNA. (Takahashi et al., 2017). The presence of histones and other DNA binding proteins in EVs could indicate that the DNA is actively transferred into EVs. However, multiple studies have found that most of the DNA associated with EVs is not incorporated, but mostly attached to the surface of the EV, as they remain sensitive to extracellular DNases (Lázaro-Ibáñez et al., 2019, Liu et al., 2022). Other studies with purified exosomes could not detect extracellular DNA. Thus, the presence of DNA associated with EVs could also indicate contaminated EVs during the isolation protocol (Jeppesen et al., 2019). Overall, further investigations related to DNA in EVs are necessary to fully understand their presence and biological impact.

In 2007, Valadi *et al*. discovered mRNA in exosomes, which could influence protein production in the recipient cell (Valadi et al., 2007). Exosomes were derived from cell lines and the RNA presence was confirmed by agarose gel electrophoresis, spectrophotometry and Bioanalyzer. About 1300 different mRNA transcripts were detected, of which 270 were present in exosomes and not detectable in the EV-producing cell, indicating an active transfer of specific mRNA into EVs. These observations made in 2007 opened a new range of studies highlighting the potential meaning behind EV transfer of nucleic acid cargo.

Further studies have identified other RNA species, which were generalized with the term of extracellular RNA (exRNA). As intracellular RNA, exRNA consists of coding (mRNA) and non-coding RNA (Tkach and Théry, 2016). Non-coding RNA encompasses miRNA, rRNA, long and short non-coding RNA, transfer RNA (tRNA), piwi-interacting RNA (piRNA), vault RNA and Y RNA (Abels and Breakefield, 2016, Kügler, 2021, Murillo et al., 2019). The functions of exRNA range from the protein-coding function of mRNA (Brosius and Raabe, 2016) to the regulation of gene expression (miRNA), mRNA degradation (miRNA) (Hombach and Kretz, 2016, Huntzinger and Izaurralde, 2011), RNA interfering or silencing (siRNA) (Mattick and Makunin, 2006), mRNA translation (tRNA) (Gebetsberger and Polacek, 2013) and splicing (snRNA) (Hombach and Kretz, 2016). There is not direct relation between the type of EV and the RNA cargo and thus, the exRNA profile released by one cell type is difficult to define and depends very much on the condition of the cell (Everaert et al., 2019, Turchinovich et al., 2019). Multiple published isolation methods can

also influence the exRNA pattern (O'Brien et al., 2020, Srinivasan et al., 2019), including separating EVs from other exRNA carriers. In short, apart from EVs, lipoproteins, which are known for transporting cholesterol and fatty acids through the vascular system, are also vesicular carriers for exRNA (Allen et al., 2018, Vickers et al., 2011). Non-vesicular carriers include several ribonucleoproteins (RNPs), like Argonaute2 (Ago2), which are able to carry miRNA in plasma and protect it, like EVs or lipoproteins, from extracellular RNases (Arroyo et al., 2011). Besides the influence of isolation methods, the sheer quantity of RNA in EVs must be considered. On average, there is only 1 miRNA in 1 to 100 EVs and 1 intact long RNA, like mRNA, in 1000 EVs, even though full-length mRNA is smaller than 1 kilobase (kb) (O'Brien et al., 2020, Wei et al., 2017). In the case of brain isolated EVs, we could calculate that mRNA was present in around 1 out of 1,000,000 EVs (Bub et al., 2022).

As mentioned above, encased within the double lipid membrane of EVs, RNA is shielded from extracellular RNases. The process of loading RNA cargo into EVs is not fully understood. There is evidence for the necessity of multiple sorting proteins and RNAs, which select distinct RNA to be incorporated into EVs. Specific sequences in the 3' untranslated region (UTR) of mRNAs enriched in EVs could act as a zip code, where a RNP or miRNA can bind, targeting the mRNA to the EV formation site (Rädler et al., 2023). Additionally, specific RNA sequence motifs can also be necessary to attract RNA binding proteins (RBP). 25% of the EV protein content consists of RBPs (O'Brien et al., 2020). The Y-box binding protein 1 (YBX1) is an RBP, that recognizes the structural motifs ACCAGCCU, CAGUGAGC and UAAUCCCA, enriched in exosomal mRNAs. Interestingly, the degree of enrichment in the RNAs containing these motifs correlated with the location of the motif within the mRNA sequence. To clarify, Kossinova *et al.* found mRNA enriched in exosomes when a specific motif (CAGUGAGC) was found in the 5'UTR, whereas no enrichment could be found when the motif was in the 3'UTR (Fabbiano et al., 2020, Kossinova et al., 2017). RNAs inside EVs have been identified as full-length (Bub et al., 2022) or fragmented (Batagov and Kurochkin, 2013, O'Brien et al., 2020).

Once internalized by the recipient cell, the mRNA can either undergo translation to generate functional proteins or assist other RNAs in their function (Skog et al., 2008, Sork et al., 2018). For instance, when exosomes derived from mouse cell lines were incubated with human cells, selected mouse proteins were found, which could not be produced by the recipient human cells (Colombo et al., 2014, Valadi et al., 2007). Some studies shown that the proportion of mRNA being translated into proteins in the recipient cell is negligible

(Hung and Leonard, 2016), meaning that mostly, the endocytosed EVs undergo degradation at the lysosomes. However, there is also evidence of the generation of active proteins from mRNA from EVs, implying that cargo escape from the endosomal system is essential for delivering functional mRNA to the recipient cell and promoting significant protein synthesis (O'Brien et al., 2020). An overview of EV-RNA can be seen in Fig. 4.

2.5. The EV's role in stroke

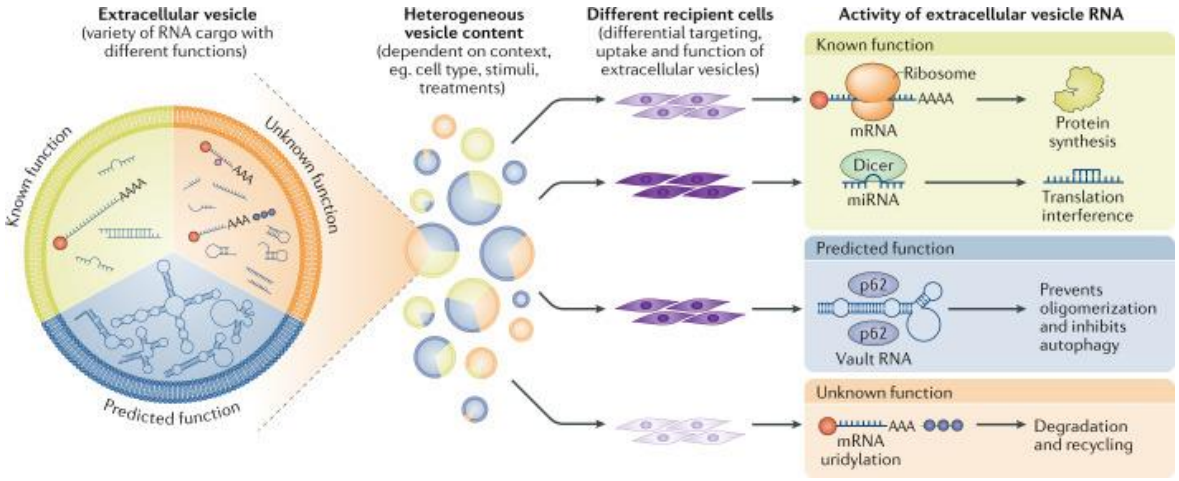

Figure 4: Fundamentals of EV-RNA functions. The cell type, stimuli or treatments of EV donor cells highly impact the release of EVs and their cargo, including RNA. Despite the ongoing investigations into EV-RNA, there are still many unknown functions when the RNA is delivered into the recipient cell. Figure extracted from (O'Brien et al., 2020).

EVs have been analyzed in various physiological and pathological, in *in vivo* or *in vitro* settings. This is also the case for the pathological setting of an ischemic stroke. All cells of the CNS, including neurons, glial and vascular cells and peripheral cells, when infiltrating the CNS under pathological conditions, can produce EVs to communicate with other cells (Lizarraga-Valderrama and Sheridan, 2021). In the last several years, many positive and negative effects of EVs in the context of stroke have been discovered. Many studies documenting the functions of EVs are performed in cell culture, which makes it challenging to compare the findings with *in vivo* experiments. Moreover, there are additional experimental difficulties that complicate the interpretation of results. For example, as mentioned above, EV isolation often leads to heterogenous EV populations, especially when isolated from tissues.

The alterations at the cellular level and mechanisms of neuroinflammation occurring after stroke might change the existing EV population, although it has to be pointed out that the role of EVs and their cargo in stroke pathophysiology is beginning to be understood (Budnik

et al., 2016). Many studies have assessed the role of EVs after hypoxic damage *in vitro* showing that EVs can have a positive effect. For example, it has been shown that EVs participate in the protection from ROS. Thus, EVs isolated from oligodendrocytes subjected to oxygen glucose deprivation (OGD), as a stroke *in vitro* model, contain enzymes like SOD1, catalase and peroxiredoxin, which lead neurons, as recipient cells, to have a higher oxidative stress tolerance (Frohlich et al., 2014). Additionally, in *in vitro* models of oxidative stress and nutrient deprivation, another finding of the same group was the activation of pro-survival pathways in neurons when treated with oligodendrocyte-derived exosomes (Frohlich et al., 2014).

Under OGD conditions, it has been shown that EVs from microglia have several positive impacts on other cells. These EVs can promote angiogenesis and repress neuronal cell injury by sending large amounts of TGF-β1 to neurons as recipient cells. Furthermore, TGF-β1 in microglia-derived EVs can stimulate the polarization of residing microglia into the anti-inflammatory M2 phenotype (Zhang et al., 2021b). Existing M2 microglia secrete EVs with a high abundance of miR-124, which results in decreased glial scar formation, astrocyte proliferation and migration after stroke (Li et al., 2021b). Further positive effects of EVs in stroke were shown by Li *et al*., who found that EVs from brain endothelial cells can reduce infarct volume and BBB-disruption. OGD-conditioned endothelial cells were treated with endothelial cell-derived EVs, which resulted in reduced permeability of endothelial cell monolayers. Further *in vivo* experiments with permanent middle cerebral artery occlusion (pMCAO)-rats showed that injection of endothelial cell-derived EVs can reduce the infarct volume (Li et al., 2023). Additionally, endothelial cells-derived EVs can inhibit neuronal apoptosis, improve neuronal behavior and increase cerebral blood flow after stroke (Sun et al., 2022). Besides these positive effects of EVs in stroke, EV cargo enhancing the postischemic inflammation has also been described (Couch et al., 2017, Yang et al., 2018). It is known that EVs can participate in inflammation as carriers of neuroinflammatory signals (Budnik et al., 2016).

Besides to investigate the involvement of EVs in the pathophysiological mechanisms of stroke, to search for potential new biomarkers is another goal when studying EVs. With the ability of EVs to cross the BBB (Saint-Pol et al., 2020), they could be used as diagnostic markers, which can be collected peripherally from either CSF or blood. Isolation of EVs specifically from brain can be done by checking proteins present in neurons such as cell adhesion molecule L1 (L1CAM), in astrocytes, such as glial fibrillary acidic protein (GFAP)

or in microglia such as transmembrane protein 119 (TMEM119). It has been shown that, for example, the amount of endothelial cells-derived EVs after stroke is increased in plasma when compared to a control group (Simak et al., 2006). Furthermore, the amount of endothelial cell-derived EVs correlated with the stroke lesion size and, thus, with a worse Barthel index (disability scale for daily activities) in patients at hospital discharge. Studies on neuron-derived EVs came to similar results. Interestingly, a lower concentration of neuron derived EVs in blood correlated with a worse functional outcome, while a higher concentration correlates with better Barthel index scores 6 months after stroke (Jödicke et al., 2021).

EVs can also be explored as new therapeutic tools. Webb *et al*. injected neuronal stem cell (NSC) derived EVs after occluding a cerebral artery in mice and neurological and sensorimotor tests were evaluated. The neurological deficit score at 2 days showed a significant decrease in neurological deficit and a motoric test was performed significantly better in NSC-EVs-treated mice compared to phosphate buffered saline (PBS)-treated mice or mesenchymal stem cell (MSC) derived EVs-treated mice. A decrease in tissue loss in NSC-EV treated mice compared to both controls was also uncovered. Injecting the isolated EVs definitely also impacted the whole body, including blood cell composition. Three days after stroke, NSC-EVs-treated mice showed a tendency of the macrophages towards an anti-inflammatory M2 phenotype, increased regulatory T cells and decreased pro-inflammatory Th17 cells. (Webb et al., 2018b).

Doeppner *et al*. found that MSC-derived EVs have an impact on post-ischemic outcomes when injected to stroke mice. They improved motoric coordination compared to PBS-treated mice, increased neuronal density, postischemic angiogenesis and drift peripheral immune cells towards anti-inflammatory responses (Doeppner et al., 2015).

Although many other studies have been made to characterize the effects of peripheral injections of EVs derived from mesenchymal and neuronal stem cells (Otero-Ortega et al., 2017, Shi et al., 2019, Webb et al., 2018a), it is still not known which specific cargo is responsible for the positive outcome of stem cell derived EVs in stroke. Nevertheless, this could be the start of a new therapy paradigm to reduce post-stroke neuroinflammation.

While protein or miRNA cargo in EVs altered by stroke conditions has been extensively researched in the past few years, there is little known about the mRNA's function in EVs after stroke. Recent studies in our lab found an increased abundance of full-length mRNAs

in EVs 72h after stroke, with putative roles in neuroprotection, synaptic plasticity, and the complement system (Bub et al., 2022).

2.6. Isolation of EVs: the density gradient ultracentrifugation

As definitions and methodologies across the published data about EVs and their cargo, were not uniform, the International Society for Extracellular Vesicles (ISEV) published a position statement in 2014 (Lötvall et al., 2014), which was revised and updated in 2018, the Minimal Information for Studies of Extracellular Vesicles (MISEV) (Théry et al., 2018, Witwer et al., 2021) and again in 2023 (Welsh et al., 2024). This minimal information states the various steps needed for characterizing EVs and describes what can be considered *bona fide* EVs. This characterization must include (I) the quantitatively described source and preparation of EVs, (II) at least three positive protein markers, one transmembrane (lipid-bound), one cytosolic and one negative marker, (III) characterization of single vesicles by electron microscopy and Nanoparticle Tracking Analysis and (VI) topology of the described components (Théry et al., 2018). Furthermore, another project focusing on exRNA, the NIH Common Found-supported Extracellular RNA Communication Consortium (ERCC), was launched in 2013. This project focuses on exRNA biology, exRNA species in body fluids, as disease biomarkers and in therapeutics (Das et al., 2019, Kügler, 2021).

Several problems occur when analyzing exRNA in EVs. Their concentration in biofluids and tissues is relatively low, they are susceptible to contamination with other exRNA carriers and different methodologies make existing data difficult to compare (Das et al., 2019). In order to analyze mRNAs in EVs, they need to be isolated. However, reproducible results with a specific isolation method remain a scientific challenge, because many isolation methods will always show slight contamination with other carriers of exRNA (Allen et al., 2018, Lässer et al., 2017, Murillo et al., 2019, Tauro et al., 2012). Density Gradient Ultracentrifugation (DGUC) is a commonly used method of isolating EVs based on their specific density. A biological fluid, like homogenized tissue in culture medium or body fluid, is first depleted from cells, cell debris and apoptotic bodies and then placed on top or at the bottom of a density gradient, which is formed using sucrose or a large polymer such as iodixanol. Iodixanol is an isosmotic and nonionic contrast agent, which is widely used for the isolation of EVs by ultracentrifugation (Vergauwen et al., 2017). Isolating sEVs by DGUC allows the separation of EVs by their ability to float at their equilibrium density.

During ultracentrifugation, the high g-forces push protein aggregates further to the bottom, while particles with a specific density will float (due to the lipidic composition) toward their equilibrium density (Colombo et al., 2014). This allows to isolate specific EV populations from protein aggregates and other vesicles with a higher or lower density (Duong et al., 2019, Turchinovich et al., 2019). The EVs can be loaded either at the top or bottom of an ultracentrifugation tube, resulting in EVs migrating downwards or upwards depending on their density. Thus, two principles can be differentiated: the top-down or bottom-up principle. Even higher purification can be acquired by including filtration and differential pelleting (Théry et al., 2018, Zhang et al., 2023).

In the past years, several other isolation methods have been developed or are currently being investigated. There are precipitation-, affinity-, size-, and density-based methods for isolating EVs from cell culture medium, body fluids or tissue (Théry et al., 2018). While not as prevalent as ultracentrifugation, size exclusion chromatography (SEC) has gained attention (Stam et al., 2021). The principle behind SEC is the elution of EVs based on their size. The sample is transported through porous material, which can be polymer or silica based. Since small particles have more access to smaller pores, they elute later than larger particles. SEC is simple to use and faster than ultracentrifugation-based isolation methods and it does not influence the EV integrity like ultracentrifugation, which pushes EVs to a surface, potentially harming EVs (Stam et al., 2021). A limitations of SEC is the reduced separation from proteins and lipoproteins when using plasma as sample (An et al., 2018). Precipitation-based techniques use hydrophilic polymers, which attach to EVs. Centrifugating the sample with low speed then pellets the EVs and polymers. There are multiple available kits, like ExoQuick^{TM} from System Bioscience or the Total Exosome Isolation Kit from Invitrogen. Despite being a cheap technique and not as time consuming as ultracentrifugation, it remains difficult to separate the EVs from the polymers used for isolation (Jia et al., 2022).

Although most of the literature defining different methods for isolating exosomes use a 200 nm filter or high-speed ultracentrifugation to purify them, as we already stated above, it is not a definition for exosomes and therefore with such isolation methods different EV populations, consisting of exosomes and small microvesicles, which are able to pass the filter, coisolate. The term sEVs, instead of exosomes, will be used in this study, referring to all EVs going through this step (Kowal et al., 2016a).

3. Material and Methods

3.1. Ethics statement

The animal experiments in this study have been executed in accordance with the guidelines of the UKE's (Universitätsklinikum Hamburg Eppendorf) animal facility and were previously approved by the local authorities (Behörde für Gesundheit und Verbraucherschutz, Veterinärwesen und Lebensmittelsicherheit of the Freie und Hansestadt Hamburg (project number 45/18).

3.2. Transient middle cerebral artery occlusion (tMCAO)

12-16 weeks old male C57/BL6 mice were used for all experiments. Mice were kept in a 12-hour day/night cycle and had continuous access to food and water in their cages (Typ II long, 540 cm^2 surface area). Temperature and humidity were controlled. For tMCAO operation, animals were anesthetized with 1,8% isoflurane in oxygen and tMCAO was performed using the intraluminal filament method, as described previously and practiced regularly in our lab (Bub et al., 2022). The filament (#602112PK5Re, Doccol) was inserted at the origin of the middle cerebral artery (MCA) and occlusion was performed for 50 min to cause a pan-hemispheric ischemia (Fig. 5). Sham mice, used as control, underwent the same procedure but cervical arteries were only visualized, no filament was inserted. Cerebral blood flow measurements via laser Doppler confirmed the occlusion (Gelderblom et al., 2009). At either 24 hours (24 h) or 7 days (7 d) after reperfusion, mice were euthanized using isoflurane, the brain was extracted, the cerebellum discarded and the brain hemispheres were stored separately at -80°C. Animals used to characterize sEVs of the new isolation protocol were not subjected to tMCAO.

The weight and a neurological deficit score were measured twice after the operation (at 2 h and 6 h) and once every day until euthanizing. Mice weighed between 22,4g and 32,4g and were scored on a scale from 0-5 (0: normal behavior; 1: mouse limps but can move straight; 2: circling; 3: few movements, reacts on external stimulus; 4: no movement, no reaction on external stimulus; 5: death). All operated mice (not shams) presented signs of stroke and had a score of either 1 or 2. An exclusion score was also documented, involving body weight,

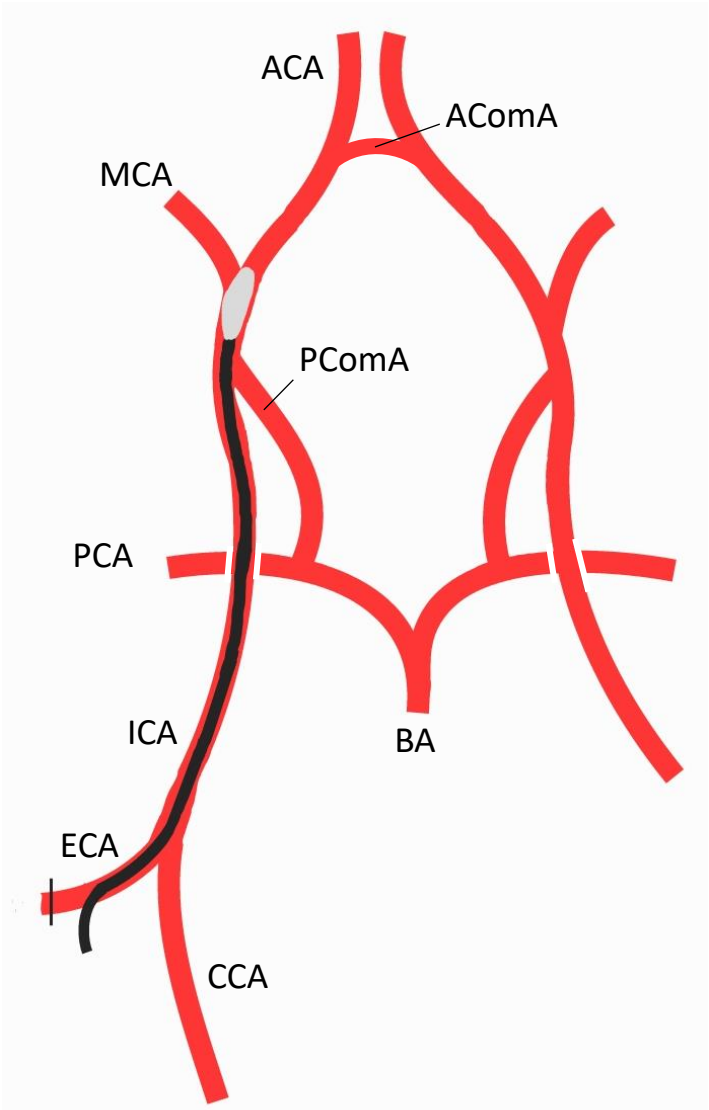

Figure 5: MCAO model. The brains arterial system is shown with the localization of the filament. It is inserted in the ECA, goes along the ICA until the basis of the MCA is occluded. Anterior cerebral artery (ACA), anterior communicating artery (AComA), middle cerebral artery (MCA), posterior communicating artery (PComA), posterior cerebral artery (PCA), basilar artery (BA), internal carotid artery (ICA), external carotid artery (ECA), common carotid artery (CCA).

general health, neurological function and wound infection. No mouse was excluded due to unethical body condition.

For the sEV characterization, single wild-type (wt) hemispheres were used. For mRNA experiments, the left tMCAO-mice hemispheres were used.

3.3. sEV isolation via iodixanol density gradient ultracentrifugation (DGUC)

To take a deeper look at the content of sEVs, they need to be separated from cells, subcellular particles and larger EVs. As stated in the introduction, there are several different techniques to enrich sEVs with high purity. DGUC is one of the current gold standards and was also

used in this approach (Shao et al., 2018, Théry et al., 2018). The protocol used in this study was adapted from Kowal *et al*. (Kowal et al., 2016a) and Vella *et al*. (Vella et al., 2017). Since establishing the new protocol according to the guidelines of MISEV2018 (Théry et al., 2018) was a significant part of this dissertation, the individual steps and development of the new protocol will be explained in the results.

3.3.1. Tissue preparation

The tissue preparation involved a digestion step in order to liberate the sEVs from the extracellular matrix. All the steps for the sEV isolation were performed on ice. The frozen brain hemispheres weighed between 160 and 220 mg.

First, the frozen brain was weighed and placed in a petri dish (#628160, Greiner bio-one) with 500 µl of Hibernate-E medium (#A1247601, ThermoFisher) containing 75 U/ml collagenase type III (CollIII; #LS004180, Worthington Biochemical Corporation) as the digestion enzyme. Once slightly thawed in this medium, the tissue was carefully cut into small pieces with a scalpel. The pieces were then transferred into a 15-ml falcon containing the rest of Hibernate-E (Hib-E)/ColIII in a ratio of 800 µl per 100 mg of brain tissue. For example, a brain that weighted 200 mg required 1600 µl of Hib-E/ColIII with 120U ColIII. Before use, ColIII was aliquoted to 2U/µl in Hib-E and stored at -20°C.

Afterwards, the falcon was placed in a water bath at 37°C for 20 min for the collagenase to work and to loosen the tissue. This moderate tissue manipulation is required to avoid EV damage and cell debris (Vella et al., 2017) and therefore to minimize contaminating and

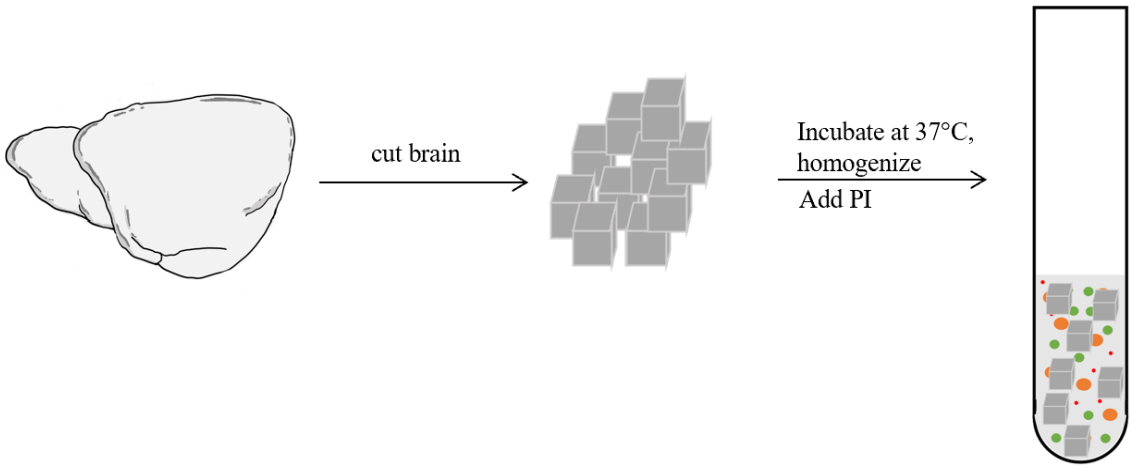

Figure 6: Tissue preparation.

altering the EV population. During incubation, the tissue was further homogenized using a 5 ml pipette every 15 min and gentle shaking every 5 min. Then, samples were placed immediately back on ice and protease-inhibitors (PI) (#11697498001, Sigma) were added to stop ColIII (Fig. 6).

3.3.2. Clearing sEV-population of larger particles

The next step in isolating sEVs is differential centrifugation. The sample was spun at 300*g* for 5 min (Eppendorf Centrifuge 5810R, Beckman Coulter), 2,000*g* for 10 min, and 10,000*g* for 30 min (Eppendorf Centrifuge 5424R, Beckman Coulter) at 4°C. Each time, the supernatant was filled in a fresh tube, and the pellet, containing larger particles and cell debris, was discarded. After the last centrifugation, the supernatant was filtered through a 0.2 µm filter (#10462200, GE Healthcare) for further isolation of particles with less than 200 nm (Fig. 7).

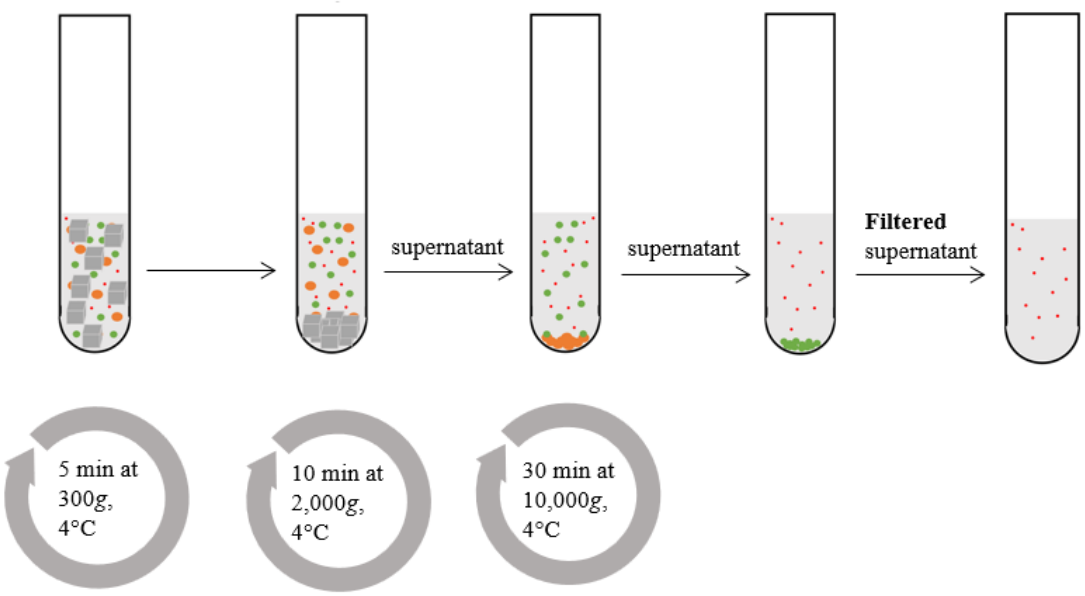

Figure 7: Differential centrifugation prior to DGUC.

Isolating sEVs without any contamination is unrealistic (Théry et al., 2018), but there are several methods to make the preparation as pure as possible. So, the differential ultracentrifugation should usually be combined with other steps to further purify EVs such as using devices for filtration, affinity isolation with antibodies or by density gradients. The DGUC uses layers of different densities. The highest density is at the bottom, while the lowest is at the top. Different concentrations of iodixanol (OptiPrep™, commercial name by Axis shield) in water were used as carrier solutions to create the gradient of densities.

Ultracentrifugation forces the sEVs to their specific density in the tube. Afterwards, the tube is divided into fractions to isolate sEVs from particles with other densities.

The first step was to prepare a working solution (WS) and homogenization medium (HM) needed to prepare the gradient. The WS contains 1 vol. of buffer (1.5 M sucrose, 60 mM Tris-HCl, 6 mM EDTA, pH 7.4) and 5 vol. iodixanol/OptiPrep™ (60% stock solution) (#1114542, Progen). The final concentration of the WS was 50% iodixanol, 0,25 M sucrose, 1mM EDTA and 10 mM Tris-HCl (pH 7.4). The HM consists of 0,25 M sucrose, 1mM EDTA and 10 mM Tris-HCl (pH 7.4). The WS and HM were prepared according to the OptiPrep™ product description (Internet reference 2: Serumwerk Bernburg AG, 2020a) to keep the concentration of EDTA, Tris-HCl and sucrose at the same level. EDTA, Tris-HCl and sucrose are necessary for stabilizing the EVs. After filtering, the sample was resuspended in buffer and water to the volume of 2.4 ml (final concentrations: 0.25 M sucrose, 1 mM EDTA and 10 mM Tris-HCl (pH 7.4)). The solution was mixed 6:4 with WS to reach a 30% iodixanol solution. Then, the buffered sample was transferred to a polypropylene ultracentrifugation tube (#331374, Beckman Coulter). 20% iodixanol (WS/HM volume ratio 4:6) following 10% iodixanol (WS/HM volume ratio 2:8) was layered on top (Fig. 8). Volume ratios were taken from the OptiPrep™ application sheet (Internet reference 2: Serumwerk Bernburg AG, 2020a).

In our study, the 30% iodixanol solution contained 2.4 ml buffered sample + 3.6 ml WS, the 20% iodixanol solution contained 1.2 ml WS and 1.8 ml HM, and the 10% iodixanol solution contained 0.6 ml WS and 2.4 ml HM.

The samples were centrifuged for 4 h at 217,000*g* (35,000rpm Rotor: SW40Ti, Settings: Acceleration (Acc): 5, Deceleration (Dec): 5) in a Beckman Coulter L-100XP centrifuge at 4°C. 10 fractions of 980 µl starting at the top were then collected and transferred to new tubes, diluted in Dubecco's phosphate-buffered saline (PBS) (#14190-094, ThermoFisher) and spun again for 1:10 h at 100,000*g* at 4°C (Acc: 5, Dec: 5) to pellet the isolated sEVs. Because only 6 tubes were fitting in the ultracentrifuge and we had 10 fractions, the first 6 fractions were first centrifuged while the other 4 were stored in PBS on ice for 1:10 h before ultracentrifugation.

Afterwards, the supernatant was discarded and the pellet was resuspended in 30 µl of PBS and PI (1x) for Nanoparticle Tracking Analysis (NTA) or for Western Blot.

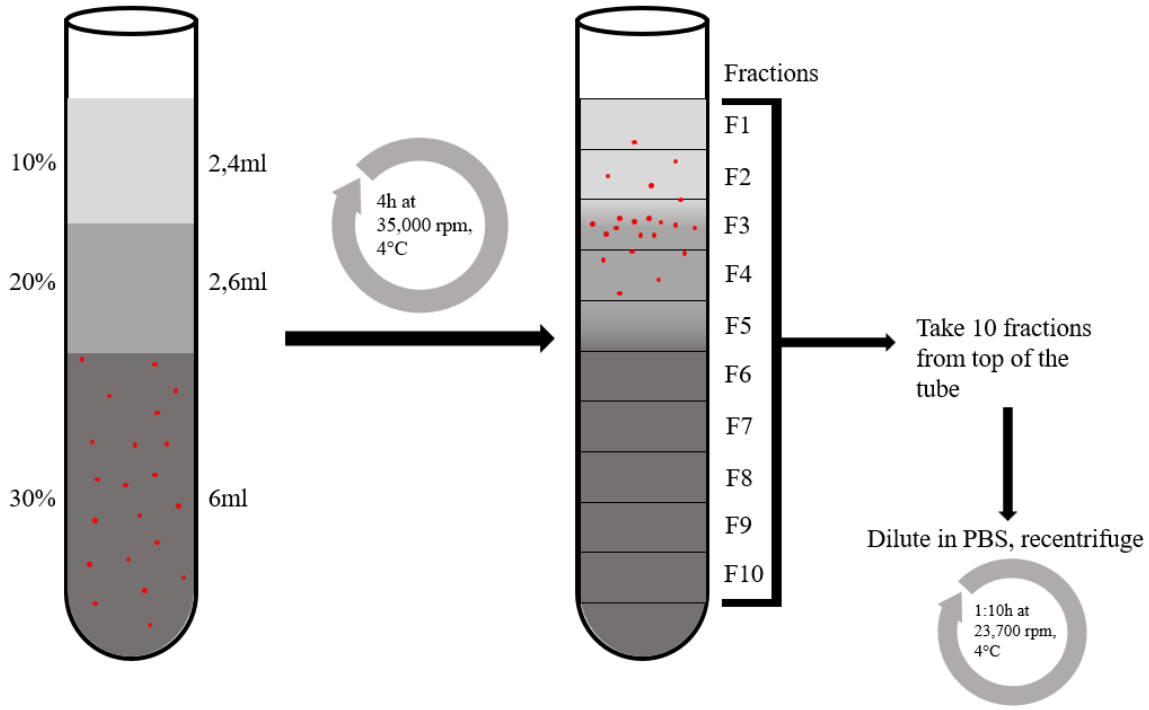

Figure 8: DGUC.

After assessing that fraction 1 an fraction 3 contained the majority of EVs, for further experiments, fraction 1 and fraction 3 were mixed after DGUC, then diluted 1:6 in 10 ml of PBS and pelleted together for 1:10 h at 100,000*g* at 4°C. Until further analysis, the tubes, containing the pelleted sEVs, were stored at -80°C.

3.4. sEVs characterization methods

To assess the results of the isolation method and to verify the protocol, several methods should be used for the characterization as stated by the MISEV 2018 and 2023, as described in the introduction. In this case, we checked the exact density for every fraction, and we performed western blot, NTA and electron microscopy assessment (Théry et al., 2018, Welsh et al., 2024).

3.4.1. Analysis of gradient density

To verify the density of iodixanol in each fraction after ultracentrifugation, the absorbance of each fraction was measured. The method is described in the OptiPrep™ application sheet (Internet reference 3: Serumwerk Bernburg AG, 2020b). Briefly, three blank samples without brain tissue were processed until after DGUC according to the protocol. 100 µl of each fraction were diluted with 100 µl H2O in duplicates in a 96-well plate and the

absorbance was measured at 340 nm. The base absorbance of 0.25 M sucrose was used as a background and was subtracted.

3.4.2. Western Blot

After thawing the samples slowly on ice, the DGUC-pelleted sEVs were lysed in radioimmunoprecipitation assay (RIPA) buffer (50 mM Tris base, 150 mM NaCl, 1% NP40, 0.5% Na-Deoxycholate, 0.1% sodium dodecyl sulfate (SDS), 1 mM phenylmethylsulfonyl fluoride (PMSF)). The samples were kept on ice for at least 10 minutes or frozen at -80 °C for later use. NuPAGE Sample Reducing Agent (10x) (#NP0009, Invitrogen) and LDS Sample Buffer (4x) (#NP0007, Invitrogen) were added to a final concentration of 1x. Digestion was performed for 10 minutes at 70°C. 15 µl of sample and 5 µl of PageRuler Plus Prestained Protein Ladder (#26619, Thermo Fisher) were loaded into a NuPAGE 10% Bis-Tris-Gel (1,5mm X 15 well) (#NP0316BOX, Invitrogen). 5 µg of protein from mouse brain homogenate, measured with Pierce BCA protein assay, were also loaded for comparison purposes. Electrophoresis was performed for approximately 1 h at 150 V prior to transferring the proteins to a Odyssey Nitrocellulose Membrane (#926-31092, Li-COR) for 1:20 h at 400 mA in a wet chamber (Mini-PROTEAN II cell (BIO-RAD)) with a transfer buffer containing 25 mM Tris base, 192 mM glycine and10% methanol. Total protein staining was performed with the Revert Total Protein Stain Kit (#926-11010, LI-COR) on the membrane for protein loading. Afterwards, the membranes were blocked with Roti-Block (#A151.2, Carl Roth) for 1 hour. Primary antibody labeling was done overnight at 4°C. The following antibodies were used: Purified Mouse Anti-GM130 (#610822, BD Bioscience), Purified Mouse Anti-Flotillin-1 (#610820, BD Bioscience), CD81 (D5O2Q) Rabbit mAb (Mouse Specific) (#10037S, Cell Signaling), ADAM10 (#EPR5622, Abcam), 14-3-3 (#sc-16-57, Santa Cruz). Next day, after washing the membranes with TBST (1:10; 100mM Tris Base, 140mM NaCl, pH 7.4, 0.1% Tween-20) 3x for 10 min, the membranes were incubated with the corresponding secondary antibodies (Anti-rabbit IgG, HRP-linked Antibody (#7074S, Cell Signaling), Anti-mouse IgG, HRP-linked Antibody (#7076S, Cell Signaling) at room temperature for 1 hour while shaking and washed again with TBST. The antibodies were diluted 1:1000. For developing the membrane, the SuperSignal West Femto Maximum Sensitivity Kit (#34095, Thermo Fisher) was used (approximately 0.1 ml Working Solution per cm^2). Membranes were incubated for 3 min and developed with a chemiDoc imaging station (BioRad). The software “Quantity One” was utilized for imaging

and further analysis. For each membrane, several antibodies were used; therefore, after rewashing the membrane with TBST, it was incubated with other primary antibodies.

3.4.3. Nanoparticle Tracking Analysis

NTA is a light-scattering technique to characterize the size and concentration distribution of a particle population (McNicholas and Michael, 2017). The NTA is provided with the NanoSight software and an accompanying microscope, which uses a laser beam to illuminate the particle's movement (Brownian motion) in a small chamber which is recorded by a camera as short videos. For quantification, all particles from all frames are related to the total volume of the chamber and the extrapolation results in the total concentration and size distribution of the particles (Shao et al., 2018). The NanoSight method is used in a variety of particle characterizations (Dragovic et al., 2011, Gardiner et al., 2013, Szatanek et al., 2017) and is one of the recommended techniques for characterization in MISEV2018 and MISEV 2023 (Théry et al., 2018, Welsh et al., 2024).

The microscope is placed on an antivibration mat on a separate table, where only the instrument and a computer are placed to minimize the influence of any vibration source (Gardiner et al., 2013).

The NTA machine used was the NanoSight LM10. Briefly, frozen isolated sEVs (-80°C) were thawed on ice prior to resuspending the pellet in 30 µl of PBS. 2 µl of the sample was mixed with 498 µl PBS (1:250 dilution), to reach the ideal particle concentration range where the software works best (2-20*10^8 / ml) (Szatanek et al., 2017). 500 µl of the diluted samples were flushed in the chamber with a 1 ml syringe. Before loading the chamber with a new sample, the chamber was cleaned with 10% ethanol.

Capture settings for obtaining a video were: screen gain = 2, camera level = 16. Process settings were: screen gain = 2, detection threshold = 6. 10 videos of 10 seconds were obtained and the temperature of the chamber was set to 23.5 °C. The mean particle concentration and size was calculated from these 10 videos. Transmission electron microscopy.

3.4.4. Transmission electron microscopy

For transmission electron microscopy (TEM), the sEVs were resuspended in PBS and fixed onto parafilm and carbon-coated copper meshed grids (Plano) for 5 min with 1%

glutaraldehyde (Roth). Afterwards, the grids were washed for 30 seconds 4 times. For negative contrast, 1% uranyl acetate was used. A Philips CM 100 TEM was used to analyze the air-dried grids.

The TEM experiments were performed by Valerie Oberüber and PD Dr. Oliver Kretz of the electron microscopy facility of the UKE.

3.5. mRNA analysis

3.5.1. BCA-assay

One of the advantages of the nCounter® panels from NanoString is that prior RNA isolation is not necessary, so it minimizes RNA losses due to extraction procedures. However, in order to be comparable, the same amount of sample should be loaded for every slot. Therefore, we decided to load the same amount of protein as a proxy for the same amount of RNA. EV protein amounts were assessed with the Micro BCA Protein Assay Kit (#23235, Thermo Scientific). Frozen EV pellets of 24 h and 7 d were gently thawed on ice and resuspended in 1:3 in RLT lysis buffer, taken from the RNA isolation kit Qiagen RNeasy Plus Micro Kit (#74034, Qiagen), in RNase-free H2O, as described before (Bub et al., 2022). 1 µl of sample was diluted with 149 µl of H2O and incubated with microBCA reagents for 2 h at 37°C. Absorbance was measured with a Tecan plate reader at 570 nm.

3.5.2. NanoString nCounter® panels

Three EV samples from three mice were used for each condition (24 h stroke/sham, 7 d stroke/sham), thus 12 samples in total (as the panel also contains 12 wells). Hybridization reactions were prepared by mixing 5 µl of sample, containing 3.12 µg of protein, 8 µl of Master Mix (hybridization buffer and Reporter CodeSet), and 2 µl of Capture ProbeSet. The tubes containing 15 µl were incubated for 16.5 h at 65°C for the hybridization of mRNA samples. Once the complexes were formed, the mix was cooled to 4 °C before adding 15 µl of RNase-free H20. The total volume of 30 µl per sample was loaded into the nCounter® SPRINT cartridge (#SPRINT-CAR-1.0, NanoString Technologies) which measured for approximately 6.5 h. The nCounter® instrument moved the samples onto a slide, where the capture probe bound to the surface through the biotin molecule at the end of each capture

probe. The specific color barcodes attached to the mRNAs via the reporter probe were counted and exported with 6 positive and 8 negative controls.

3.5.3. nSolver analysis, advanced analysis module and statistics

For data analysis, the NanoString nSolver™ 4.0 Analysis Software and its advanced analysis module were used in accordance with the user manuals (Internet reference 4: NanoString Technologies, Inc, 2018a, Internet reference 5: NanoString Technologies, Inc, 2018b). Prior to loading the raw mRNA counts into nSolver, they were submitted to quality control in Microsoft Excel. The criteria were similar positive control counts in each sample, highest positive control over 10,000 counts and binding density in an acceptable range, which is 0.1 to 1.8 fluorescent spots/μm^2. Furthermore, a background threshold was defined as the mean of all 8 negative controls plus two times the standard deviation. In nSolver, a two-step normalization of raw counts was also performed. First, the geometric mean of all positive controls in the corresponding sample was used for calculating a technical normalization factor, which helps to reduce the variability across samples due to differences in hybridization, binding density and imaging. The second normalization step was based on the housekeeping mRNAs included in the panel. The housekeeping genes with at least one sample not exceeding or being close to the background threshold were not used for normalization. Out of 13 housekeeping genes, 10 were selected for normalization, namely Aars, Ccdc127, Cnot10, Csnk2a2, Fam104a, Gusb, Lars, Tada2b, Tbp and Xpnpep1.

The two-step normalized data was then analyzed in the advanced analysis module of NanoString nSolver. Threshold counts were set to 30 and observation frequency to 0.6. For differential expression analysis, the calculating method was set to optimal and the p-value adjustment used the Benjamini-Hochberg method.

The cellular origin of the mRNAs was further analyzed with the Whole Cortex & Hippocampus—10X Genomics (2020) gene expression data set from the Allen mouse brain atlas (Lein et al., 2007).

GraphPad Prism and Microsoft Excel were additionally used for further analyses and to create figures. Non-parametric Mann-Whitney U test was used for comparing NTA results. Statistical significance was considered for $*p < 0.05$. Values for are given as mean ± standard error of the mean (SEM).

4. Results

4.1. Optimizing a protocol to isolate sEVs in accordance with MISEV2018

In MISEV2018, a guideline for publishing reliable results on EV studies (at the time of the experimental research presented in this thesis), which was further confirmed in MISEV2023 (Welsh et al., 2024), density gradient ultracentrifugation combined with previous differential centrifugation and filtration is defined as a method with low recovery but high specificity (Théry et al., 2018). It is also one of the most commonly used methods. In 2016, Kowal *et al.* published a paper regarding the benefits of an iodixanol-based density gradient ultracentrifugation instead of a sucrose-based one (Kowal et al., 2016a). Hence, the first part of this work was to combine the method of extracting sEVs from whole brain tissue (Vella et al., 2017) with the iodixanol-based centrifugation. For reference and solution preparation, the manufacturer's recommendations were followed (Internet reference 2: Serumwerk Bernburg AG, 2020a).

Centrifugation settings:

To adapt the protocol, we had to modify the run speed and run time variables. To generate comparable *g*-forces over a period of time, the k-factor of the rotor, which can be calculated on the Beckman-website (Internet reference 6: Beckman Coulter, 2024), was calculated from the SW55Ti (the used by Kowal *et al.*) to our rotor (SW40Ti). With a k-factor of 50, the SW55Ti is much more efficient than the SW40Ti used in this protocol. Nevertheless, setting the SW40Ti speed on 35,000 rpm (max. is 40,000 rpm) results in a run time of theoretical 215 min. Because of slow acceleration and deceleration time (5 and 5 respectively), the run time was set to 240 min (4 h) (Table 1).

Table 1: Rotor variable conversion using k-factors.

	Rotor name	
	SW55Ti	SW40Ti
Rotor speed	54,000 rpm	35,000 rpm
Max. rotor speed	55,000 rpm	40,000 rpm
g-force (avg.)	276.460 g	154.693 g
g-force (max)	354.352 g	217.874 g
Run Time	60 min	215 min (240 min)
k-factor	50	179

OPTIPREP™ gradient:

The recommendation of using a WS and HM to maintain the concentration of EDTA and Tris-HCl is from the OptiPrep™ product description (Internet reference 2: Serumwerk Bernburg AG, 2020a). OptiPrep™ itself is a 60% solution of iodixanol in water. Therefore, mixing the 60% iodixanol solution with buffer or sample to the percentages needed for DGUC will result in different concentrations of the buffer's components. Preparing a WS with 50% iodixanol and final concentrations equal to the concentrations of the HM solves this problem. The only recommendation that was not followed was the concentration of sucrose in the WS. According to the product description, the WS would contain different amounts of sucrose depending on the iodixanol concentration. Therefore, the 50% iodixanol WS contains only 0.0417 M sucrose (30%: 0.125 M, 20%: 0.667 M, 10%: 0.208 M). These different amounts of sucrose could affect DGUC in different ways. Sucrose is highly osmotic and changes in the osmotic pressure in the different gradients could potentially harm EVs moving from one gradient to another. Thus, the isolation protocol was adjusted, leading to the same concentration of sucrose, EDTA and Tris-HCl. The iodixanol concentration is the only variable that changed throughout the gradient.

4.2. Characterization of isolated sEVs

To verify the new isolation protocol, different characterization steps had to be performed in line with MISEV2018 (Théry et al., 2018).

4.2.1. Isolated sEVs are present at their predicted density

DGUC with an iodixanol gradient allows to separate sEVs depending on their density. Samples were mixed with 30% iodixanol and HM and placed at the bottom of the tube and the EVs went from the bottom of the gradient to where their density reached the equilibrium following the bottom-up method (Fig. 8).

After the ultracentrifugation, 10 fractions were taken and the density was measured. Fraction 1 showed a density of 1.078 ± 0.00084 g/ml and fraction 3 showed a density of 1.114 ± 0.0011 g/ml. Western blot and EM results, which will be displayed below, indicate that most of the sEVs are located in these two fractions. The densities of other fractions can be seen in Fig. 9c.

4.2.2. Western blot analysis show typical transmembrane and cytosolic markers in the isolated sEVs

To characterize EVs by Western blot, different protein markers have to be used. According to MISEV2018, at least one transmembrane or GPI-anchored protein, one cytosolic marker and one marker for showing contamination must be included in the characterization.

ADAM10 (a disintegrin and metalloproteinase domain-containing protein 10) is a transmembrane protein specific for sEVs (Kowal et al., 2016b, Lischnig et al., 2022). It is a sheddase of several proteins from the plasma membrane (Hansen et al., 2020). CD81 is also a membrane protein and a member of the tetraspanin family, which functions in exosome biogenesis and cargo selection (Gurung et al., 2021, Kowal et al., 2016b). Flotillins, present at the luminal face of the plasma membrane, are involved in trafficking protein cargo to the EV building site by interacting with a specific motive (Yeung et al., 2022). Flotillin-1 served as a cytosolic marker, as well as 14-3-3, which is a protein that functions in vesicle-mediated transport (Choi et al., 2015). The protein GM130 is generally used as a marker for contamination with intracellular organelles and is resident at the cis-Golgi matrix (Bub et al., 2022, Huang et al., 2021, Théry et al., 2018).

CD81 and Flotillin-1 show clear presence in fractions 1-5, with the most intense signal in fraction 3, while ADAM10 and 14-3-3 are only shown in fraction 3. GM130 was absent in any fraction, suggesting the absence of intracellular organelles (Fig. 9b).

Another commonly used cytosolic marker for EVs is the apoptosis-linked gene 2 (ALG-2)-Interacting protein X (Alix). It interacts with members of the ESCRT-family and takes part in exosome construction (Fabbiano et al., 2020). In our preparations, Alix was absent from all fractions but present in the TH, indicating amounts under the detection limit in our isolated EVs.

4.2.3. Fraction 1 and 3 show highest particle concentration of all fractions measured by NTA and EM

NTA is a widely used method for determining EV concentration and size. Here, we used the technique to characterize the 10 fractions obtained from DGUC.

Previous to the measure by NTA, the fractions of isolated sEVs from 3 wt-mice were diluted 1:250. Reliable results can be acquired with particle concentrations ranging from $2\text{-}20*10^8$

particles/ml after dilution (Szatanek et al., 2017), which was the case for fractions 1 and 3. The highest concentrations of sEVs were found in fractions 1 and 3. Fraction 1 had a mean concentration of $7.73*10^{10}$ particles/ml (undiluted) and fraction 3 had a mean concentration of $1.52*10^{11}$ particles/ml (undiluted). Fractions 2, 4 and 5 showed mean concentrations ranging from $2.2*10^{10}$ to $3.7*10^{10}$ particles/ml (Fig. 9c). Thus, only fractions 1 and 3 were found in the reliable concentration range. Fractions 6 to 10 had very few particle concentration. The EVs seem to group at the top of the tube (fraction 1) or between the 10% and 20% iodixanol-concentrations (fraction 3).

The size of sEVs varied from 30 nm to 500 nm, although most sEVs are below 200nm. The mean sEV size over all fractions was 168 nm and, in fraction 3, was of 163 nm with a standard deviation of 67 nm. An example of size calculation can be seen in Fig. 9d.

Additionally, the sEV sizes were confirmed by TEM. Low membrane contamination and high vesicle concentrations were observed in fractions 1 and 3 (Fig. 9e).

Since fractions 1 and 3 presented markers of EVs with a corresponding fitting size for sEVs, we decided to pool fractions 1 and 3 together for the mRNA analysis to gather all the possible information about the mRNA content on the sEV population

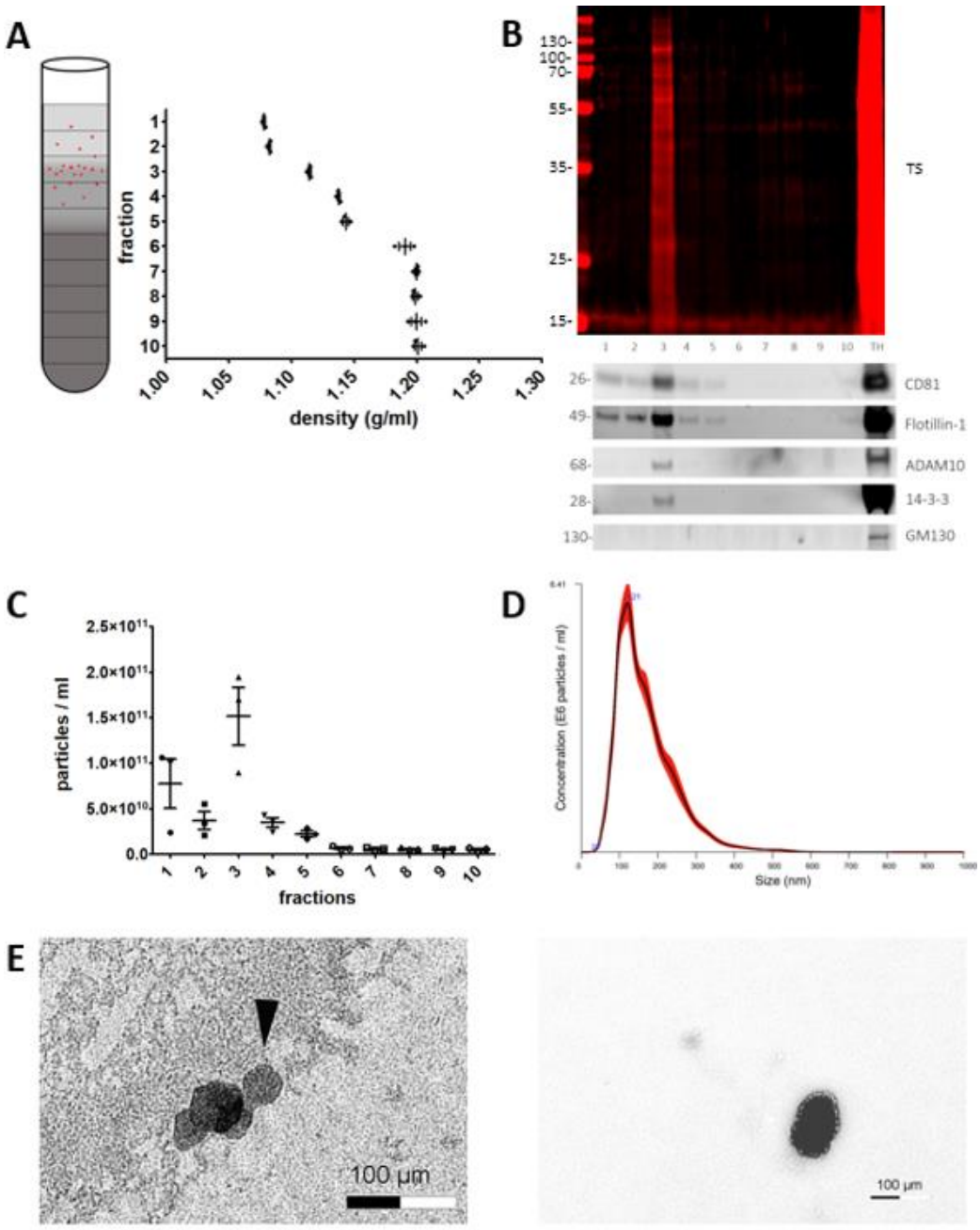

Figure 9: Summary of isolated sEV characterization. (A) *Scatter dot plot showing the different fractions densities after ultracentrifugation. The fractions are displayed on the y-axis while the density is shown on the x-axis. Mean and SEM are shown for each fraction (n=3). (B) Western blot of the 10 fractions acquired after DGUC. CD81 and ADAM10 are positive transmembrane markers, Flotillin-1 and 14-3-3 are positive cytosolic markers. GM130 is a negative marker. TH is a total brain homogenate of a WT-mouse, which served as positive control. (C) Scatter dot plot showing the particle concentration in the 10 fractions collected from the DGUC tube. The dots represent the different samples (n=3). Mean and SEM is shown additionally. (D) Example for size distribution in NTA. Here, one sample of fraction 3 is shown. X-axis shows the size in nm, y-axis shows the concentration (particles/ml). The black line shows the averaged concentration of EVs with their specific size. The red line is indicates +/- 1 SD from mean. The mode is 121 nm, 10th percentile is 90,1nm, 50th percentile is 149,4nm, 90th percentile is 268,2nm. (E) Electron microscopy of sEVs. The arrowhead points towards sEVs, the scale bar is 100 µm.*

4.3. sEVs in stroke

The third goal of this study was to get an overview of upregulated and downregulated mRNAs related to immunological pathways in sEVs in a stroke mouse model (tMCAO). For this, two timepoints, 24 h and 7 d after tMCAO representing the acute and the recovery phase after stroke were analyzed.

4.3.1. sEVs isolated from brain after 24 h and 7 d after tMCAO show no significant difference in particle concentration or size

The concentration and size of sEVs at the timepoints of 24 h and 7 d after tMCAO were analyzed with NTA. Regarding the first timepoint of 24 h, the mean concentration for tMCAO-sEVs was $3.73*10^{11} \pm 3.90*10^{10}$ particles/ml and for sham-sEVs $2.88*10^{11} \pm 3.38*10^{10}$ particles/ml. For 7 d, the mean concentration of tMCAO-sEVs was $6.47*10^{11} \pm 6.13*10^{10}$ particles/ml and for sham-sEVs $4.25*10^{11} \pm 3.03*10^{10}$ particles/ml (Fig. 10). The size varied between 160 nm and 180 nm and showed no significant difference between tMCAO and sham samples. 24 h and 7 d tMCAO samples had a higher concentration of sEVs than the sham samples, although the difference were not significant. Comparing the tMCAO samples of 24 h to the samples of 7 d, the latter showed a higher, but not significant, sEV concentration.

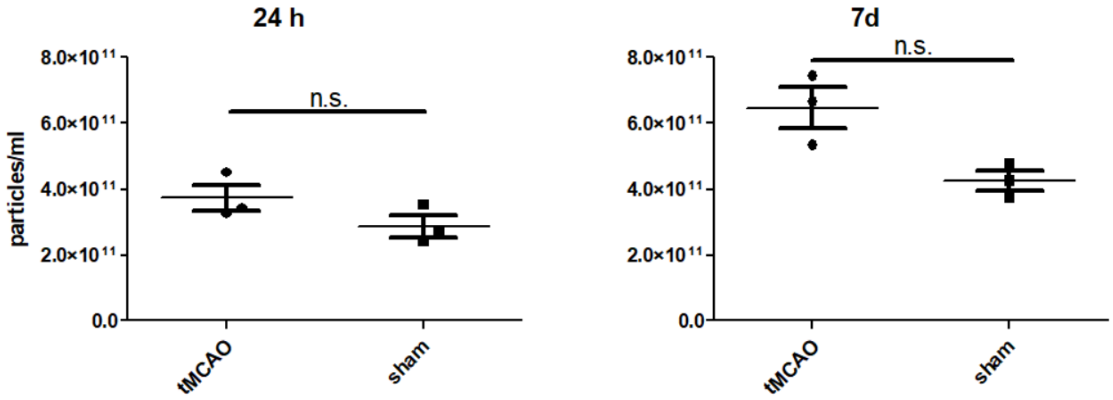

Figure 10: NTA of 24 h and 7 d sEVs. Scatter dot plots for 24 h (left) and 7 d (right) with mean and SEM (n=3). Exact values are given in the main text.

4.3.2. Robustness of the nCounter® neuroinflammation panel

Pooled fractions 1 and 3 of isolated sEVs either from stroke or sham brains at 24 h or 7 d after stroke (n = 3 for each condition) were used for mRNA analysis. mRNA was not isolated

prior to hybridizing the mRNA with the nCounter® neuroinflammation panel as previously done before (Bub et al, 2022). To load the same amount of sample, we guided us by the protein concentration measured by BCA. All samples were diluted to a protein concentration of 0,62 µg/µl, the highest possible protein concentration to load the same amount of each sample, and 5 µL (corresponding to 3.12µg) were used for the NanoString nCounter® panel.

The first milestone in analyzing the mRNA in sEVs was to confirm the reliability and robustness of the raw mRNA counts by calculating the background threshold. It varied between roughly 22 and 34 counts over all samples. Thus, the background threshold was set to 30 counts. Some highly upregulated mRNAs had high counts in the stroke samples, but low counts below the background threshold. To avoid discarding these highly interesting samples, only samples with at least one stroke and one sham sample below the background threshold were marked as not robust. 571 mRNAs were marked as robust 24 h after tMCAO and 586 mRNAs 7 d after tMCAO (Fig. 11).

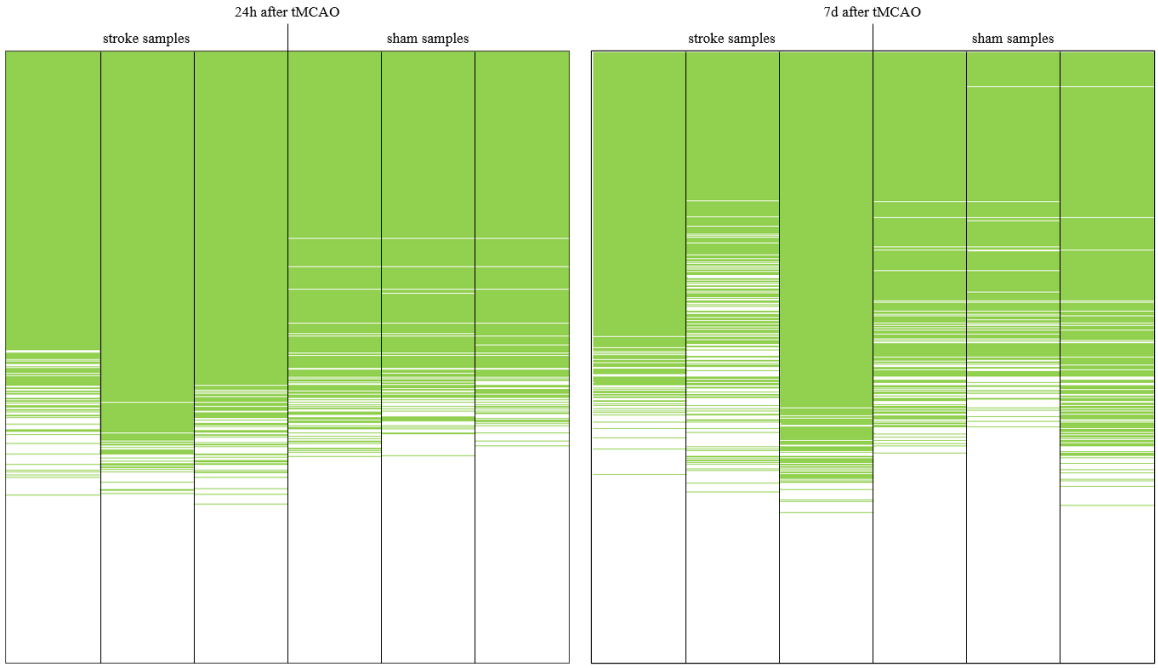

Figure 11: Robustness of raw mRNA counts. The figures show all 757 mRNAs in rows, 3 stroke and 3 sham samples in columns. The timepoint of 24 h after tMCAO is on the left, 7 d after tMCAO on the right. mRNAs are sorted with highest average count at the top and lowest average count at the bottom. Green means individual count to be above the threshold, white means below or at the threshold.

4.3.3. Principal component analysis and p-value distribution of mRNAs in sEVs 24 h and 7 d after tMCAO

Preprocessing the data to define a background threshold showed that the data set was usable for further analysis in NanoString nSolver. The whole data set was imported into the NanoString nSolver software. Discarding the mRNAs with low counts takes place in the advanced analysis tool, as explained before (part 3.5.3). The samples passed all quality control parameters, including imaging, binding density, positive control and limit of detection. One positive control (POS_F) was not used in any analysis because of its low count. The 2-step normalized data was then analyzed in the advanced analysis module.

First, a principal component analysis (PCA) for all variables (stroke/sham and 24 h/7 d after tMCAO) was performed. A PCA is a statistical method to simplify a large data set. This method can be used to identify the impact of different experimental variables. Here, the first four principal components, which can explain most of the variance in the data set, are plotted against each other (Fig. 12).

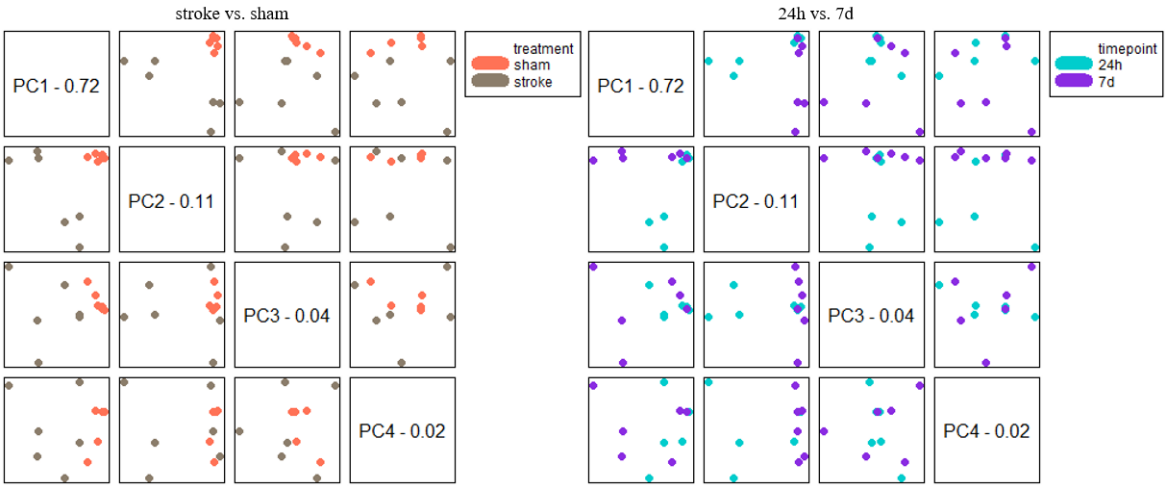

Figure 12: Principal component analysis (PCA). Plots show differential clustering of stroke and sham sEVs-mRNA. The first four principal components are plotted for the condition "treatment" (left) and "timepoint" (right). On the left plot, the orange dots show sham samples, brown dots show stroke samples and on the right plot, cyan dots show the 24 h timepoint while the violet dots show the 7 d timepoint.

The plot comparing PC1 to PC2, which are the most impactful, shows a clear cluster of the sham samples and two clear clusters for 24 h and 7 d after stroke, indicating differential expression of mRNAs in both settings stroke vs shams and 24 h vs. 7 d. Moreover, the p-value distribution for treatment (shams vs stroke) and timepoint (24h vs 7 days) show a clear tendency towards low p-values (Fig. 13).

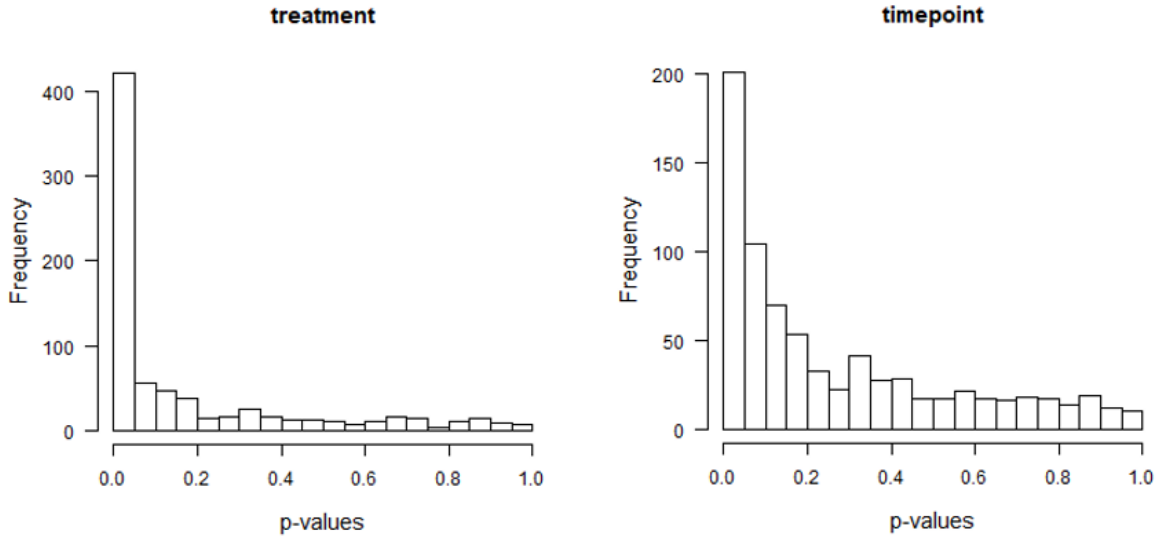

Figure 13: p-value distribution plots for the treatment and timepoint conditions. On the left, the p-values of the treatment condition (stroke vs. sham) and on the right side, the timepoint condition (24 h vs. 7 d) are displayed in histograms.

These results can show that not only the tMCAO changes the abundance of mRNAs in sEVs, but also that the mRNA population changes depending on the observed time point, indicating the activation of different pathways 24 h and 7 d after tMCAO or different cells actively producing different sEV-populations at different time points.

4.3.4. Differential expression of mRNAs

The NanoString nSolver program and its advanced analysis software analyzed individual mRNA counts' differential expression mRNAs were defined as differentially expressed by having a log2(fold change) (log2(FC)) of over 2 (upregulated) or below -2 (downregulated).

Several mRNAs were significantly upregulated (log2(FC) ≥ 2 after 24 h as well as 7 d after stroke. At 24 h after stroke, 11 mRNAs had a significant upregulation. The 5 most upregulated mRNAs were Hmox1, Hspb1, Slfn8, Emp1 and Spp1. Hmox1 had the highest log2(FC) of 5.4, equivalent to an 18.6-fold increase in stroke sEV-mRNA compared to sham sEV-mRNA (Table 2 and Fig. 14 and 15). For 7 d after tMCAO, 29 mRNAs showed a significant upregulation. The 5 most upregulated mRNAs were Spp1, Tnf, Mpeg1, C3ar1 and Trem2. Spp1 had a log2(FC) of 6.6 and was, therefore, 97.1 times higher in stroke compared to sham samples (Table 2). This time point showed a higher amount of differentially expressed mRNAs with the higher top fold changes compared to 24h. Significantly downregulated mRNAs did not present a log2(FC) ≤ -2 at either timepoint. When the cut off was set to log2(FC) ≤ -1, only Arc mRNA (log2(FC) = -1.17), was found

significantly downregulated at 24 h after tMCAO. At 7 d after tMCAO, when the cut off was set to log2(FC) ≤ -1, the most downregulated mRNAs were Rbfox3 (log2(FC) = -1.4), Egr1 (log2(FC) = -1.38), Mef2c (log2(FC) = -1.38), Vegfa (log2(FC) = -1.36) and Rab6b (log2(FC) = -1.33).

Table 2: Differentially expressed mRNAs at 24 h and 7 d after tMCAO. Mean counts of sham (sh), stroke (st), log2(FC), p-values and false discovery rate (FDR) adjusted p-value are provided for the observed timepoints. The log2(FC) was calculated using the differential expression algorithm provided in the advanced analysis module of NanoString nSolver. The complex algorithm includes the mean and dispersion of the background noise in each sample using the negative controls. Further information about the algorithm are given in the user manuals (Internet reference 4: NanoString Technologies, Inc, 2018a, Internet reference 5: NanoString Technologies, Inc, 2018b). For the timepoint of 24 h after tMCAO, all upregulated mRNAs (11 in total) are provided, while for the timepoint of 7 d after tMCAO, 20 mRNAs with the highest fold changes are provided.

24 after tMCAO						
mRNA	mean sh	mean st	linear FC	log2(FC)	p-value	FDR-adjusted p-value
Hmox1	26.9	428.66	42.1	5.4	0.000852	0.0454
Hspb1	22.5	278.27	39.9	5.32	0.000568	0.041
Slfn8	15.03	47.7	18.7	4.22	0.00501	0.0742
Emp1	21.88	97.6	12.8	3.67	1.74E-05	0.01
Spp1	51.23	387.26	10.1	3.34	0.000209	0.0284
Cxcl10	7.35	60.77	7.28	2.86	0.0052	0.0747
Tnfrsf12a	67.5	262.63	4.84	2.28	0.00122	0.0454
Cdkn1a	249.24	1,091.85	4.84	2.28	0.00282	0.0603
Gadd45g	78.49	276.48	4.29	2.1	0.00177	0.0512
S1pr3	132.04	506.38	4.22	2.08	0.000134	0.0258
Tnfrsf1a	116.1	420.31	4.05	2.02	0.000245	0.0284
7 d after tMCAO						
mRNA	mean sh	mean st	linear FC	log2(FC)	p-value	FDR-adjusted p-value
Spp1	50.6	3887.66	97.1	6.6	3.47E-05	0.00776
Tnf	9.61	74.09	39.8	5.31	1.54E-05	0.00776
Mpeg1	129.81	3,461.24	29.8	4.9	5.94E-05	0.00776
C3ar1	29.27	486.14	27.3	4.77	0.000332	0.0137
Trem2	39.53	711.62	24.4	4.61	0.000175	0.0109
Cd68	45.59	779.06	24.1	4.59	0.000512	0.0149
C1qc	115.27	1,936.75	19.8	4.31	0.000274	0.0129
Tyrobp	100.89	1,672.46	18.9	4.24	0.00014	0.0107
Grn	101.79	1,254.05	14.8	3.89	0.000554	0.0149
C1qa	65.49	775.52	14.4	3.85	0.00034	0.0137
Vim	153.44	1,680.24	14	3.81	0.0024	0.0275
Irf8	32.01	316.36	12.9	3.69	8.26E-05	0.00776
Ctss	60.45	646.33	12.8	3.68	8.23E-05	0.00776
Fcrls	48.84	475.37	12	3.59	0.000152	0.0107
C1qb	102.37	1,083.88	12	3.59	0.000473	0.0149
Tgfb1	73.12	520.91	8.49	3.09	0.000894	0.0177
Bcas1	177.87	886.73	7.48	2.9	0.0149	0.0674
Tnfrsf1a	68.73	419.64	7.43	2.89	0.00141	0.0206
Cx3cr1	424.65	2,585.26	6.28	2.65	7.26E-05	0.00776
Lgmn	170.83	914.44	6.06	2.6	0.00183	0.0239

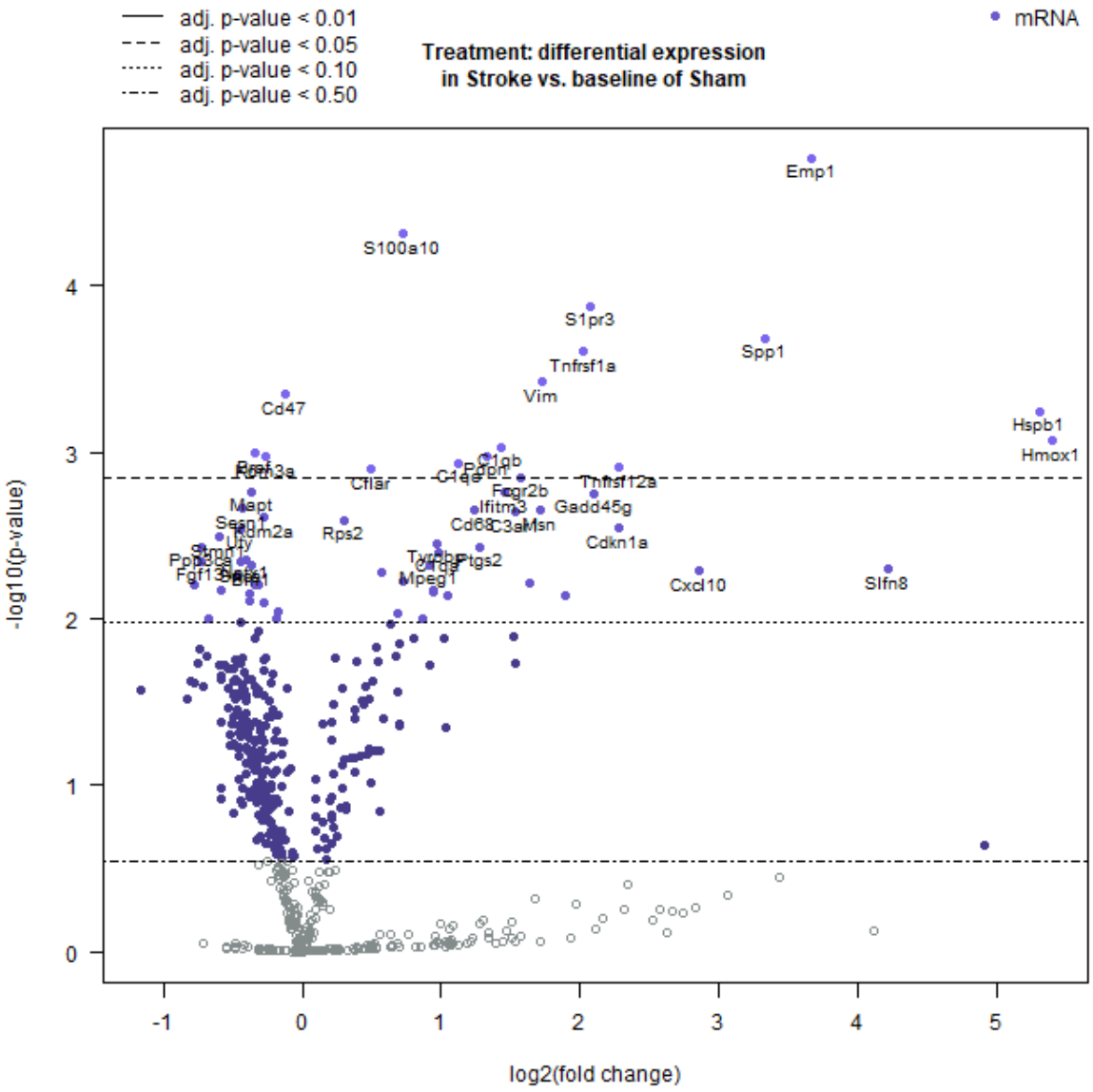

Figure 14: Vulcano plot of upregulated and downregulated mRNAs at 24 h after tMCAO. The x-axis shows the log2(FC) while the y-axis displays the -log10(p-value). The horizontal lines show 4 different thresholds of false-discovery-rate(FDR)-adjusted p-values. The names of the 40 most significant mRNAs are depicted on the plot.

When conducting multiple experiments, there is an increased probability of having false positive results. This is also the case for p-values. Using the Benjamini-Hochberg-method to calculate the false-discovery-rate (FDR) can indicate how many significantly upregulated mRNAs are false positives. An FDR-adjusted p-value of 0.05 means that 5% of the results are false positive.

At 24h after stroke, the mRNA counts even for the ones that presented the higher fold-change, are relatively low with only one mRNA (Cdkn1a) count over 1,000 (Table 3). In contrast, at 7 d after stroke, the mRNAs with highest fold change present higher counts as for example Spp1 had 3,888 counts, Mpeg1 had 3,461 counts and C1qc had 1,937 counts.

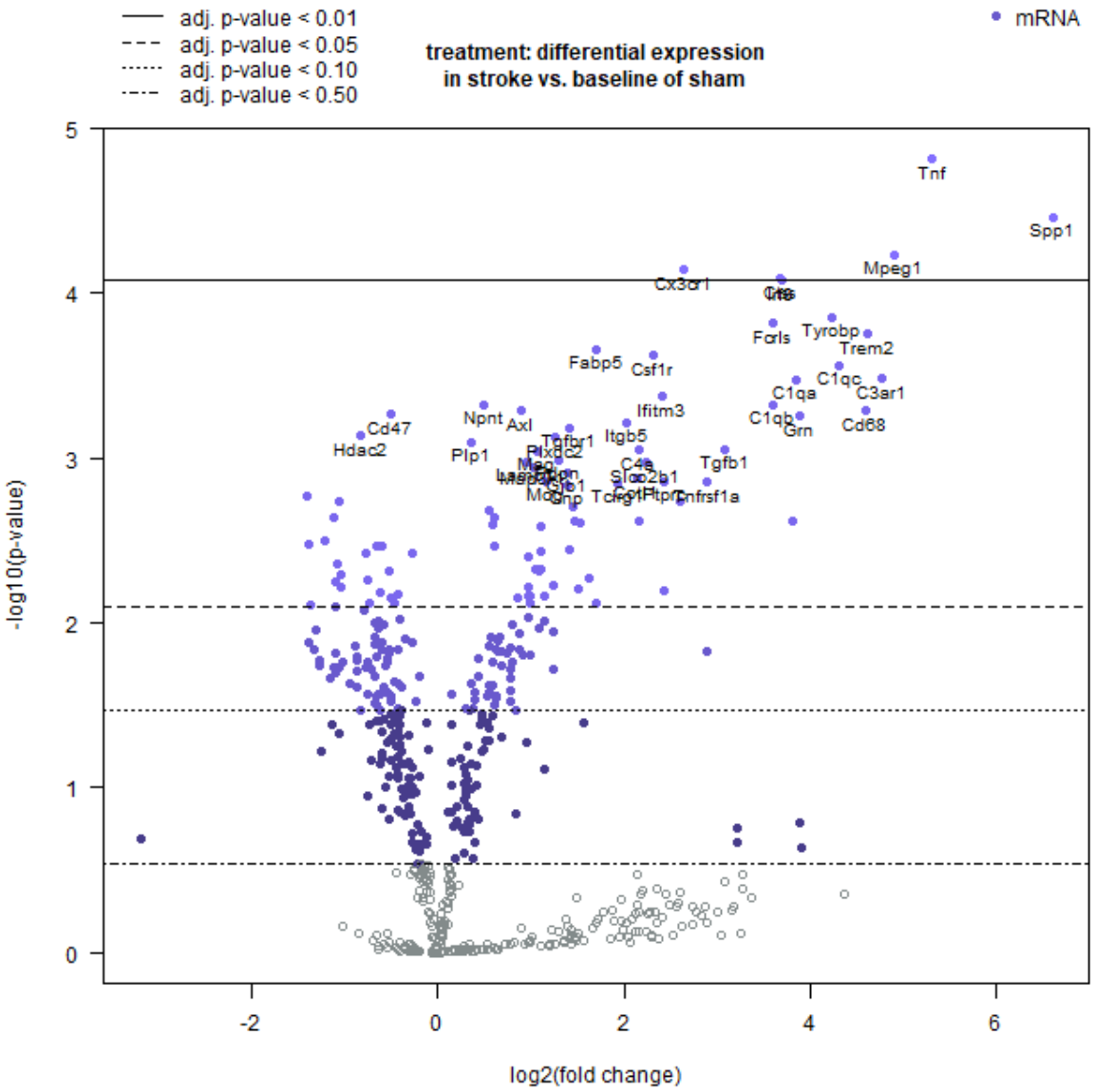

Figure 15: Vulcano plot of upregulated and downregulated mRNAs at 7 d after tMCAO. The x-axis shows the log2(FC) while the y-axis displays the -log10(p-value). The horizontal lines show 4 different thresholds of false-discovery-rate(FDR)-adjusted p-values. The FDR-adjustment used the Benjamini-Hochberg-method. The 40 most significant mRNAs are named in the plot.

Table 3: Top 25 most abundant mRNAs ranked after their absolute counts.

Most abundant mRNAs					
24 after tMCAO			7 d after tMCAO		
mRNA	mean sh	mean st	mRNA	mean sh	mean st
Prkar1a	10,577.9	7,591.98	Rps2	3,864.71	5,924.01
Ppp3r1	11,767.9	7,220.32	Prkar1a	7,787.71	5,006.79
Rps2	5,767.15	7,111.25	Dlg4	6,307.05	4,573.19
Dlg4	9,278.23	6,375.08	Plp1	3,362.01	4,329.28
Ppp3ca	10,207.2	6,149.59	Apoe	955.17	3,981.74
Pacsin1	7,344.49	5,552.64	Spp1	50.6	3,887.66
Mef2c	8,265.58	5,269.21	Eif1	3,340.54	3,718.1
Prkacb	7,717.94	5,169.68	Ppp3ca	7,355.98	3,502.38
Eif1	4,932.89	4,978.59	Ppp3r1	8,415.41	3,478.45
Pten	5,422.53	4,349.64	Mpeg1	129.81	3,461.24
Rab6b	5,748.07	4,150.49	Ptms	2,570.57	3,224.68
Slc1a3	4,643.65	3,855.71	Pacsin1	5,128.63	3,164.38
Ppp3cb	6,194.42	3,673.11	Rps9	1,355.6	3,124.46
Rac1	5,106.11	3,669.71	Prkacb	5,498.67	2,924.23
Shank3	3,957.04	3,036.33	Rac1	3,653.06	2,780.8
Stmn1	4,401.77	2,917.01	Cx3cr1	424.65	2,585.26
Mapk10	3,705.79	2,852.8	Stmn1	3,115.4	2,456.67
Ptms	3,702.86	2,771.23	Rpl29	1,345.41	2,389.56
Txnrd1	1,774.01	2,764.45	Ccni	2,289.98	2,348.18
Sqstm1	2,842.4	2,729.48	Pten	3,669.65	2,303.3
Pak1	3,461.73	2,646.84	Pink1	1,740.88	2,265.28
Sod2	3,433.07	2,627.41	Shank3	2,620.03	2,238.03
Plp1	4,601.97	2,614.95	Lamp1	1,134.57	2,201.09
Ccni	3,406.95	2,563.97	Nlgn2	1,950.94	2,182.63
Iqsec1	3,055.81	2,555.01	Ppp3cb	4,235.17	2,118.53

4.3.5. Upregulated mRNAs in sEVs after stroke have probably originated from microglia and PVMs

Next, we wanted to assess which cells were releasing these sEVs, as there is a differential cell population participation at different timepoints after stroke (Gelderblom et al., 2009). To address this question, the highest expressed mRNAs in stroke for each time point were analyzed in the Allen brain atlas transcriptomics explorer (Lein et al., 2007). We could show that many differentially expressed mRNAs from 24 h as well as 7 d such as C1qa, C1qb, C1qc, Tyrobp and Csf1r originated from microglia or perivascular macrophages (PVMs).

Moreover, we also analyzed the cell type profiling with the advanced analysis software from NanoString nSolver and obtained similar results. Thus, 24 h after tMCAO, the mRNAs specific for macrophages (CD68 and CD84) and microglia (Gpr84, Irf8, Ncf1 and Tnf) were significantly upregulated compared to the corresponding sham samples, while 7 d after tMCAO, the mRNAs specific for microglia (Irf8, Ncf1 and Tnf) were significantly upregulated. mRNAs specific for other cell types, such as astrocytes, oligodendrocytes or neurons, did not show significant data. This result imply that either the number of cells (in

this case, microglia and macrophages) are increased and therefore, more sEVs from these populations are found, or that more mRNA is sorted into the sEVs, thus accounting for an increased amount of mRNA.

4.3.6. Activated pathways by upregulated mRNAs

The NanoString nCounter® neuroinflammation panel includes mRNAs that can be ascribed to 23 biological pathways. The list can be downloaded from the website (Internet reference 7: NanoString Technologies, Inc., 2024). The advanced analysis module calculates a pathway score for each mRNAs annotated to each pathway, which allows to evaluate whether specific pathways are up or downregulated. An overview of these up- or downregulated pathways can be seen in Fig. 16.

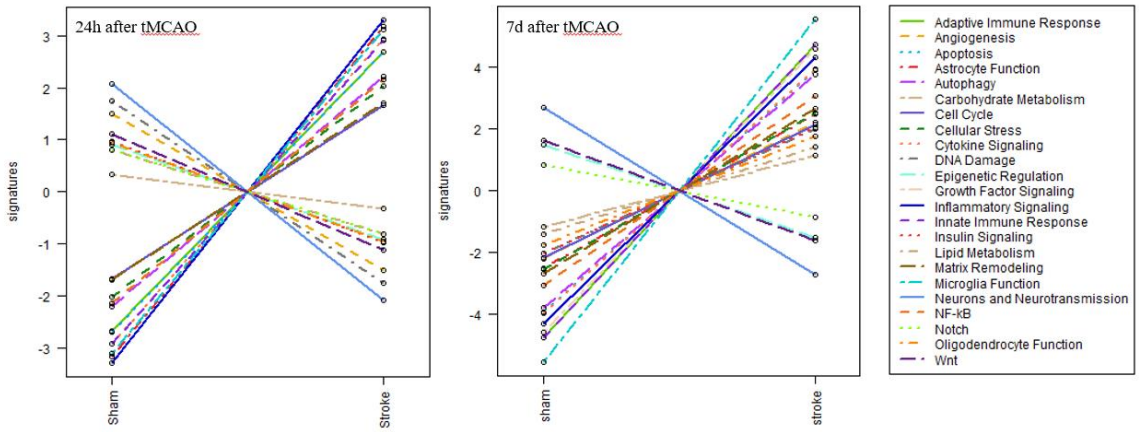

Figure 16: Pathway scores for each treatment. The left plot shows the up- and downregulated pathways 24 h after tMCAO while the right plot shows the same for the 7 d timepoint 23 pathways are plotted in different colors. Pathway scores are plotted against the two conditions, tMCAO and sham.

At 24 h after tMCAO, the most upregulated pathways were “Inflammatory Signaling”, “Astrocyte Function”, “Microglia function” and “Cytokine Signaling”, while “Neurons and Neurotransmission”-, “DNA Damage”- and “Angiogenesis”-pathways were downregulated. 7 d after tMCAO, more pathways were upregulated. At this time point, “Microglia Function”, “Innate Immune System” and “Adaptive Immune Response” were most upregulated, while “Neurons and Neurotransmission” were still downregulated.

Because the pathway scores might be confounded by the abundance of a specific cell type, these results must be interpreted cautiously. NanoString also provides a table with all mRNAs and the associated pathways (Internet reference 7, NanoString Technologies, Inc., 2024). A part of this table can be seen for the differentially upregulated mRNA in Table 4

and 5. “Astrocyte Function”, “Cellular Stress”, “Cytokine Signaling” and “Growth Factor Signaling” pathways were overrepresented at 24h after tMCAO. 7 d after tMCAO, “Adaptive Immune System”, “Cytokine Signaling”, “Growth Factor Signaling”, “Inflammatory Signaling”, “Innate Immune Response” and “Microglia Function” were overrepresented.

Table 4: Pathway annotations of differentially upregulated mRNAs 24 h after tMCAO. Rows show the 23 pathways given by NanoString and the columns show the differentially expressed mRNAs taken from table 3.

	Hmox1	Hspb1	Slfn8	Emp1	Spp1	Cxcl10	Tnfrsf12a	Cdkn1a	Gadd45g	S1pr3	Tnfrsf1a
Adaptive Immune Response	-	-	-	-	-	-	-	+	-	-	-
Angiogenesis	-	+	-	-	-	-	-	-	-	-	-
Apoptosis	-	-	-	-	-	-	-	-	-	-	+
Astrocyte Function	-	+	+	+	-	+	-	-	-	+	-
Autophagy	-	-	-	-	-	-	-	-	-	-	-
Carbohydrate Metabolism	-	-	-	-	-	-	-	-	-	-	-
Cell Cycle	-	-	-	-	-	-	-	+	+	-	-
Cellular Stress	+	+	-	-	-	-	-	+	-	-	-
Cytokine Signaling	-	-	-	-	-	+	+	+	-	-	+
DNA Damage	-	-	-	-	-	-	-	+	+	-	-
Epigenetic Regulation	-	-	-	-	-	-	-	-	-	-	-
Growth Factor Signaling	-	+	-	-	+	-	-	+	+	-	+
Inflammatory Signaling	-	-	-	-	-	+	+	-	-	-	-
Innate Immune Response	-	-	-	-	-	+	-	-	-	-	+
Insulin Signaling	-	-	-	-	-	-	-	-	-	-	-
Lipid Metabolism	-	-	-	-	-	-	-	-	-	-	-
Matrix Remodeling	-	-	-	-	+	-	-	-	-	-	-
Microglia Function	-	-	-	-	+	+	-	-	-	-	-
NF-kB	-	-	-	-	-	-	+	-	-	-	+
Neurons and Neurotransmission	-	-	-	-	-	-	-	-	-	+	-
Notch	-	-	-	-	-	-	-	-	-	-	-
Oligodendrocyte Function	-	-	-	-	-	-	-	-	-	-	-

Table 5: Pathway annotations of differentially upregulated mRNAs 7 d after tMCAO. Rows show the 23 pathways given by NanoString and the columns show 20 out of 29 differentially expressed mRNAs taken from table 3.

	Spp1	Tnf	Mpeg1	C3ar1	Trem2	Cd68	C1qc	Tyrobp	Grn	C1qa	Vim	Irf8	Ctss	Fcrls	C1qb	Tgfb1	Bcas1	Tnfrsf1a	Cx3cr1	Lgmn
Adaptive Immune Response	-	-	-	-	+	-	-	+	-	-	-	-	+	-	-	-	-	-	-	+
Angiogenesis	-	-	-	-	-	-	-	-	-	-	-	-	-	-	-	-	-	-	-	-
Apoptosis	-	+	-	-	-	-	-	-	-	-	+	-	-	-	-	-	-	+	-	-
Astrocyte Function	-	-	-	-	-	-	-	-	-	-	+	-	-	-	-	-	-	-	-	-
Autophagy	-	-	-	-	-	-	-	-	-	-	-	-	-	-	-	-	-	-	-	-
Carbohydrate Metabolism	-	-	-	-	-	-	-	-	-	-	-	-	-	-	-	-	-	-	-	-
Cell Cycle	-	-	-	-	-	-	-	-	-	-	-	-	-	-	-	+	-	-	-	-
Cellular Stress	-	+	-	-	-	-	-	-	-	-	-	-	-	-	-	-	-	-	-	-
Cytokine Signaling	-	+	-	-	-	-	-	-	-	-	-	-	-	-	-	+	-	+	+	-
DNA Damage	-	-	-	-	-	-	-	-	-	-	-	-	-	-	-	-	-	-	-	-
Epigenetic Regulation	-	-	-	-	-	-	-	-	-	-	-	-	-	-	-	-	-	-	-	-
Growth Factor Signaling	+	+	-	-	-	-	-	-	-	-	-	-	-	-	-	+	-	+	-	-
Inflammatory Signaling	-	+	+	-	+	-	-	-	-	-	-	+	-	-	-	-	-	-	-	-
Innate Immune Response	-	+	-	-	-	-	+	+	-	+	-	-	+	-	+	-	-	+	-	+
Insulin Signaling	-	-	-	-	-	-	-	-	-	-	-	-	-	-	-	-	-	-	-	-
Lipid Metabolism	-	-	-	-	-	-	-	-	-	-	-	-	-	-	-	-	-	-	-	-
Matrix Remodeling	+	-	-	-	-	-	-	-	-	-	-	-	+	-	-	+	-	-	-	-
Microglia Function	+	+	-	+	+	+	-	-	+	-	-	+	+	+	-	+	-	-	+	-
NF-kB	-	+	-	-	-	-	-	-	-	-	-	-	-	-	-	-	-	+	-	-
Neurons and Neurotransmission	-	-	-	+	-	-	-	-	-	-	-	-	-	-	-	-	-	-	-	-
Notch	-	-	-	-	-	-	-	-	-	-	-	-	-	-	-	-	-	-	-	-
Oligodendrocyte Function	-	-	-	-	-	-	-	-	-	-	-	-	-	-	-	-	+	-	-	-
Wnt	-	-	-	-	-	-	-	-	-	-	-	-	-	-	-	-	-	-	-	-

5. Discussion

The focal hypoxia and lack of nutrients in stroke cause several pathophysiological cascades. Neuroinflammation is one major contributor to the ongoing damage to neurons and other cells in the ischemic penumbra even days and weeks after the initial stroke (Iadecola et al., 2020). Several different cell populations are activated and infiltrate the ischemic tissue because of the release of various cytokines. The initial activation of microglia, astrocytes and macrophages can further damage the brain tissue, while the later polarization towards anti-inflammatory phenotypes, like the polarization of M1/M2 microglia, helps initiating beneficial pathways (Hu et al., 2012, Wen et al., 2020). sEVs can contribute to this complex intercellular communication system through their ability to transfer biological active information from donor cells to recipient cells (Russell et al., 2019). This study aimed to investigate the mRNA content of sEV populations 24 h and 7 d after tMCAO to determine whether beneficial or detrimental mRNAs are upregulated compared to sham controls. Thus, three purposes were defined. First, a new isolation protocol to isolate sEVs from whole brain tissue had to be created to reach the standard of MISEV2018. Second, the sEV population had to be characterized and third, the mRNAs associated with neuroinflammation had to be analyzed by the NanoString nCounter® technology.

5.1. Creating a new protocol to isolate sEVs

There are different techniques to isolate EVs from the cell culture medium, body fluids or tissues and they are precipitation-, affinity-, size-, or density-based. Each isolation method has its advantages and disadvantages. Combining different isolation methods usually results in higher purification with the cost of lower recovery (Théry et al., 2018). In 2017, Vella *et al*. created a protocol for isolating EVs from whole brain tissue using multiple centrifugation steps with ascending *g*-forces prior to an ultracentrifugation step with a sucrose gradient. Their sample was placed on top of the gradients. Thus, they used the top-down principle (Vella et al., 2017). A recent paper from our laboratory used this isolation protocol and, among other things, tested the effect of filtering the sample with a 0.2 µm filter before ultracentrifugation to purify sEVs further. Although the analysis of multiple mRNAs showed no significant difference in relative amount, the diameter of non-filtered EVs was higher. This copurification with larger EVs could also affect their protein or RNA population (Bub et al., 2022). According to Kowal *et al*., ultracentrifugation with sucrose could result

in high osmotic pressure, potentially destroying EVs in the isolation process. Instead of sucrose, they used iodixanol in the DGUC step with a bottom-up principle (Kowal et al., 2016a). These three publications were taken into account to create the new protocol. Many other protocols for isolating EVs from tissue have been created (Gallart-Palau et al., 2016, Hurwitz et al., 2019, Hurwitz et al., 2018). Here, the differences to published studies will be discussed.

Several recent papers have pointed out the importance of standardizing isolation methods by setting a new gold standard for future investigations and to minimize differences between them (Mateescu et al., 2017, Théry et al., 2018, Welsh et al., 2024). Since we used a different rotor and centrifuge than Kowal *et al*., the run time had to be prolonged from 60 min to 240 min. This change also resulted in a higher k-factor, which describes the pelleting efficiency of a rotor (Kowal et al., 2016a, Théry et al., 2018). Other studies have examined the influence of ultracentrifugation *g*-force and run time on the EV quantity and purity. Jeppensen *et al*. analysed the characteristics of exosomes from two different cell lines. The size, protein quantity and abundance of markers changed when isolating the vesicles with different *g*-forces. Furthermore, the optimal *g*-force for maximizing the purity of isolated exosomes is different for the two examined cell lines. HEK293 cells had an optimal *g*-force of 67,000*g* for exosome purity, while the optimal *g*-force for FL3 cells was 100,000*g*. Importantly, these results were obtained by pelleting EVs with an ultracentrifugation step, not DGUC (Jeppesen et al., 2014). Therefore, the results are only partially comparable to ours. However, the higher k-factor and higher run time in our isolation protocol might not indicate less efficiency. According to Jeppensen *et al*., the optimal isolation method for an EV population might be individual to a body fluid, tissue or condition (Jeppesen et al., 2014). Furthermore, other studies have demonstrated that long centrifugation times, notably not DGUC but pelleting ultracentrifugation, resulted in higher RNA and protein concentration compared to shorter centrifugation times, while the RNA was protected from RNase-dependent degradation even after 37 hours of ultracentrifugation and the RNA profile did not change (Cvjetkovic et al., 2014). Thus, establishing a general gold standard for the various EV populations, which can be isolated from diverse sources, remains challenging. Besides, this endorses the importance of including multiple characterization steps when publishing data about EVs to make it comparable to other studies.

Another critical point when isolating EVs from tissue is how to liberate the EVs from the extracellular matrix. Several studies have used proteolytic enzymes, like papain (Perez-

Gonzalez et al., 2012). Others have used mechanical homogenization methods (Gallart-Palau et al., 2016) or a combination of both (Hurwitz et al., 2019, Hurwitz et al., 2018, Muraoka et al., 2020). Homogenization could help collecting more EVs from tissue, which is crucial when working with small amounts of samples, like mouse brain hemispheres. However, it could reduce the EV purity by affecting the integrity of cell membranes and, thus, contaminating the EVs with intracellular organelles, like mitochondria or endosomes (Li et al., 2021a). We followed the protocol of Vella *et al*. by gently slicing the brain with a scalpel instead of mechanically homogenizing the tissue (Vella et al., 2017).

Related to the enzymatic digestion, the use of collagenase to dissociate cells and free EVs trapped in the extracellular matrix was already acknowledged by other studies (Crescitelli et al., 2021, Qin et al., 2021, Zhi et al., 2022) and by our group, as we have previously experienced poor EV recovery by using papain for the enzymatic digestion (unpublished results). Moreover, we have introduced a filtration step of the EV suspension which further separates sEVs from larger particles. As previously pointed out, sEVs carry the majority of mRNA associated with EVs (Bub et al., 2022, Crescitelli et al., 2021).

DGUC with an iodixanol-based gradient has been used in recent studies to isolate EVs from tissue (Crescitelli et al., 2021, D'Acunzo et al., 2022), body fluids (Iwai et al., 2016) or cell cultures (Zicari et al., 2018). Another possible reagent for DGUC is sucrose. Iodixanol has the advantage of a reduced osmolarity compared to sucrose, resulting in less osmotic stress for EVs passing through the gradient and preventing a change in EV shape and size (Crescitelli et al., 2021, Iwai et al., 2016). Compared to other isolation techniques like precipitation, membrane / phosphatidylserine affinity or SEC, Iodixanol-based DGUC has relatively low costs but needs experienced experimenters. On the other hand, the relatively long ultracentrifugation time required for DGUC, the EV- and gradient-preparation and the need for an ultracentrifuge are clear disadvantages (Veerman et al., 2021). Using the bottom-up principle, also adapted from Kowal *et al*., results in less contamination than the top-down principle (Hurwitz et al., 2018, Kowal et al., 2016a). An upcoming alternative for isolating EVs from brain tissue is SEC, which, compared to DGUC, is efficient in separating EVs with a decreased work time and relatively easy to perform (Huang et al., 2020).

Here, we used centrifugation- and filtration-steps prior to DGUC. The importance of combining different isolation techniques has been pointed out by MISEV2018 for recovering a specific subtype of EVs (Théry et al., 2018). A combination of DGUC with

other methods can have advantages for EV purification. For instance, the combination of DGUC followed by bind/elute chromatography, can separate EVs from lipoproteins and albumin present at the plasma with the disadvantage of less EV quantity (Onódi et al., 2018). Adding an SEC-step after DGUC reduces lipoprotein contamination in blood samples (Karimi et al., 2018). Several studies use an ultracentrifugation or centrifugation step before DGUC to remove cell debris or larger EVs or to concentrate EVs in a pellet when starting with a large sample volume (Crescitelli et al., 2021). Pelleting EVs could cause adverse effects, such as incomplete sedimentation and, thus, lower quantity of isolated EVs, or physical disruption and aggregation of vesicles (Duong et al., 2019, Linares et al., 2015). One approach to eliminate these negative effects is using a high-density iodixanol cushion, which is loaded in the bottom of a centrifugation tube to prevent pelleting the EVs on a surface (Li et al., 2018). Duong et al. showed an increase in the recovery rate of all nanoparticles from 30% in a standard ultracentrifugation step to 70% with a cushioned ultracentrifugation step (Duong et al., 2019).

In conclusion, the search for effective isolation methods continues and existing protocols can be further optimized. The use of DGUC with prior centrifugation steps has been validated and optimized in other studies (Crescitelli et al., 2021). Even though the optimal isolation method for EV populations might be individual to the analysed donor cell (Jeppesen et al., 2014), standardization is essential in the increasing environment of isolation methods and research groups working in EVs. Furthermore, as stated in MISEV2018, the individual characteristics of the isolated EV population must be obtained with a combination of different methods (Théry et al., 2018).

5.2. Characterization

The characterization of the isolated sEVs was a major purpose of this work. DGUC separated most of the sEVs in two fractions with densities of 1.078 g/ml (fraction 1) and 1.114 g/ml (fraction 3). These iodixanol fraction densities are partly in line with previous findings. An early study from 2009 from Théry *et al*. assigned exosomes the density of 1.13 – 1.19 g/ml in sucrose (Théry et al., 2009). However, more recent studies pointed out the variability in density of different EV populations when using sucrose as the gradient solution (Colombo et al., 2014). Kowal *et al*. found most of the analysed EVs in fractions with the density of 1.15 and 1.17 g/ml, while Vella *et al*. found EVs in all of their three fractions with

densities of 1.02 g/ml, 1.08 g/ml and 1.17 g/ml (Kowal et al., 2016a, Vella et al., 2017). Studies using an iodixanol-based DGUC method to isolate EVs from brain tissue accumulated in densities of 1.075 g/ml and 1.144 g/ml, which is comparable with our studies' densities (Hurwitz et al., 2019).

NTA showed a mean sEV concentration of 7.73 x 10^{10} particles/ml in fraction 1 and a mean size of 178 nm. Fraction 3 had a mean concentration of 1.52 x 10^{11} particles/ml and a slightly lower mean size of 163 nm. NTA is a reliable technique for single particles that can achieve reliable results with particle diameters as low as 30 nm. The protocol takes only a couple of minutes per sample and theoretically, the sample can be recovered after the analysis and used for further experiments (Szatanek et al., 2017), a procedure that was not done in our studies. NTA also exhibits certain limitations that we had to overcome. The optimal concentration for measurement is 2 – 20 x 10^{8} particles/ml. Therefore, the appropriate dilution factor must be found (Szatanek et al., 2017). With the dilution factor of 250, an optimal concentration was achieved for fraction 1 and fraction 3. The obtained concentrations were in the range of particle concentrations of other studies separating EVs from mouse brain hemispheres (Bub et al., 2022). Furthermore, TEM verified the size analysis of NTA, showing that the diameter of sEVs mainly fell below 200 nm.

The characterization of our sEVs included a detailed description of the single steps in the protocol, the iodixanol gradients' density, single particle analysis done by NTA, protein-based characterization by western blot and imaging single vesicles by TEM. The results verify the reliability of the isolation protocol by the guidelines for EVs, MISEV2018 and MISEV2023.

5.3. The NanoString nCounter® technology

We used the NanoString nCounter® technology to analyse the abundance of over 700 mRNAs in our sEVs to investigate their role in neuroimmunological pathways further. NanoString nCounter® technology has been demonstrated to be a powerful method for gene expression analysis in the past few years. There has been a noticeable increase of this method in the research of EVs, offering, like any methodology, both advantages and disadvantages. On the positive side, NanoString nCounter® allows the counting of up to 800 individual mRNAs and the counting procedure is suitable for very low and very high amounts of mRNA in a single sample. Other methods of transcriptomic analysis, like quantitative real-

time PCR (qRT-PCR), is only suitable for a limited number of genes (Bracht et al., 2021). Microarrays, which are used to analyse multiple transcripts and their expression profile, have a lack of reproducibility and are expensive (Veldman-Jones et al., 2015). They are also less sensitive than NanoString nCounter® (Geiss et al., 2008). Compared to these methods, it also requires less processing time and works with a more straightforward protocol (Dong et al., 2021). Furthermore, when comparing samples with a RNA isolation step and samples with no RNA isolation the RNA profiles where very similar with the NanoString nCounter®. This has the advantage that a prior RNA isolation, which could result in mRNA loss, is not obligate (Bub et al., 2022).

While the NanoString nCounter® system offers several advantages in analysing gene expression, it is essential to critically examine its limitations, especially when working with EVs. As mentioned before, an RNA isolation step prior to loading the sample into the NanoString nCounter® cartridge, is unnecessary. Even though this diminishes the problem of destroying EVs in the process, which holds the risk of RNA degradation, we do not know whether the input of mRNA in all the samples was the same as we could not measure it. We speculated that the amount of EVs (here measured by protein concentration) would contain similar amounts of RNA and therefore the samples were loaded by similar protein concentration measured by BCA. On the other hand, in the analysis of Bracht *et al*., where RNA was isolated prior to the NanoString nCounter® analysis, the problem was that the original RNA amount was too low for direct quantification so the solution was to amplify the RNA in a 10-cycle PCR before measurement. The group worked with plasma from cancer patients, thus, genomic DNA was also found in their EVs and was amplified in the PCR. Since the NanoString probes could attach to this genomic DNA, further DNase treatment was needed. Following purification steps to remove the DNase resulted in EV-RNA loss (Bracht et al., 2021). Hence, this method also presents several disadvantages, particularly when working with low starting amounts of mRNA.

To achieve suitable results with the NanoString nCounter® system, its analysis software includes a normalization process consisting of a positive control normalization and a housekeeping normalization. The first one adjusts the mRNA counts considering technical differences while the latter normalizes for the differences in the content's abundance or quality (Internet reference 4: NanoString Technologies, Inc., 2018). This step is critical in ensuring the reliability of the gene expression data and, thus, making significant biological comparisons. NanoString includes multiple housekeeping genes in its panels. They are

chosen depending on their low variability across treatments, tissues or conditions. Since the mRNA profile in EVs can be distinctly different from the mRNA profile of the donor cell (Dong et al., 2021, Kim et al., 2017), and since there are passive and active sorting machineries regulating the RNA loading process into EVs (Rädler et al., 2023), it is not generally agreed that housekeeping genes commonly used for normalization of intracellular mRNA can also be applied to EV mRNA content normalization, as indicated by several other studies (Bracht et al., 2021, Dong et al., 2021, Gouin et al., 2017, Waggott et al., 2012). Therefore, Gouin *et al*. investigated the potential of miRNAs as appropriate reference genes for normalizing gene expression data. They found the mean of three different miRNAs analyzed by RT-qPCR to be the most stable normalization strategy. However, one limitation of their study is the use of only one specific cell line of cardiosphere-derived cells (Gouin et al., 2017) whereas in our study we investigated the mRNA population of tissue-derived EVs, which is more complex than from cell culture derived EVs (Gouin et al., 2017). Many other approaches have been developed, such as NanoStringNorm (Waggott et al., 2012), NanoStringDiff (Wang et al., 2016) or RCRnorm (Jia et al., 2019). NanoStringNorm is an open-source R package. It provides steps for pre-processing gene expression data before analyzing it with NanoString nSolver. For sample content normalization, they suggest using all genes or a set of highly expressed genes to calculate a normalization factor (Waggott et al., 2012). It has to be pointed out that none of the normalization approaches outlined in the existing literature addresses their suitability for EVs. Then again, using the total counts of each sample to normalize the NanoString data, as suggested by NanoStringNorm, has been applied in other studies (Bracht et al., 2021) and has also been used in the analysis of EVs (Dong et al., 2021, Herrero et al., 2023, Zieren et al., 2021). In our approach, we decided to use the accompanying reference genes for normalizing our samples, as this approach provided applicable data in our laboratory before (Bub et al., 2022) and in other studies on EVs miRNA (Lo et al., 2021).

In summary, NanoString nCounter® is a reproducible method for detecting sEV-mRNA derived from ischemic brain tissue. However, the need for a suitable normalization strategy is challenging when working with mRNAs in EVs. Possible mRNA candidates with high fold changes could still be detected when skipping the housekeeping normalization step. Furthermore, analyzing the expression of high-fold-change-mRNAs obtained in NanoString nCounter® can be validated by combining it with another quantitative gene expression methods, like RT-qPCR (Bub et al., 2022).

5.4. sEVs mRNA in stroke

We used the NanoString nCounter® neuroinflammation panel to study the changes in sEV-mRNA abundance at 24 h and 7 d after tMCAO compared to shams. By taking specific clusters of upregulated mRNAs or high expression of single mRNAs into consideration, we got an insight into the activated pathways at these two time points after stroke, and an idea of which brain cells were releasing this RNA. However, because the NanoString nCounter® technology uses probes with a length of approximately 50 nucleotides, the counted mRNAs in EVs could be fragmented, as indicated by previous studies where they found that mRNAs of over 1000 nucleotides are mostly fragmented and that UTRs were enriched compared to the coding region of mRNAs (Wei et al., 2017). . However, our laboratory recently provided evidence of at least six full-length mRNAs in EVs at 72 h after tMCAO (Bub et al., 2022). Another study found that over 20% of mRNAs in EVs were full-length with an average of 2799 nucleotides (Li et al., 2019). These studies emphasize the significance of mRNAs in sEVs and indicate that functional mRNAs could be transported to the recipient cells where they may be translated into functional proteins.

When looking at the most upregulated mRNAs at 24 h and 7 d after tMCAO and their absolute counts, some candidates, such as Spp1, C1q, Mpeg1 and Hmox1, were highlighted. The **Spp1**-mRNA can be translated into the secreted protein phosphoprotein-1/osteopontin (OPN), a phosphorylated extracellular matrix glycoprotein, that can directly interact with other extracellular matrix proteins like fibronectin and collagen type I, as well as cell surface receptors, including integrins and CD44 (Lund et al., 2009, Weber et al., 1996, Zhou et al., 2020).

Various effects have been attributed to OPN in inflammation. It can function as a chemotactic protein, facilitating the migration of immune cells or as a proinflammatory cytokine, inducing maturation and differentiation of immune cells, especially macrophages. While circulating nonactivated monocytes lack the expression of OPN, several inflammatory cytokines, like TNF-α and IL-1β, which are also upregulated in early stages of neuroinflammation after stroke, induce the expression of OPN, which then acts in regulating migration, survival, phagocytosis and macrophage cytokine production (Lund et al., 2009).

In the CNS, OPN is weakly expressed in physiological conditions, but many pathological effects trigger its upregulation (Spitzer et al., 2022) and it has been reported to be

upregulated in Alzheimer's disease, Parkinson's disease, multiple sclerosis and stroke. (Zhou et al., 2020). Activated microglia, macrophages and astrocytes are mainly responsible for OPN upregulation in acute brain injuries (Kang et al., 2008). OPN then interacts with its receptors αvβ3 integrin and CD44 to further activate and polarize additional immune cells towards the antiinflammatory phenotype. Interestingly, αvβ3, one integrin receptor of OPN, is also upregulated on astrocytes after stroke (Ellison et al., 1998). This could imply an OPN-dependent activation of astrocytes after stroke. Via integrin-β1, OPN is able to inhibit the JAK1/STAT-pathway, downregulating the secretion of NO and MMP-9, leading to to reduced BBB disruption (Xin et al., 2021, Zhou et al., 2020). Single-cell transcriptomic analysis also identified OPN expressing microglia and macrophages 24h after MCAO in mice, while OPN-receptors (CD44 and integrin receptor α4β1) were expressed in various other primary and infiltrating brain cells. (Zheng et al., 2022a). This could indicate diverse effects of OPN on multiple cell types.

Related to neuroinflammation, previous studies have proposed a role for OPN in the microglia phenotype change from the proinflammatory M1 to the antiinflammatory M2 phenotype, the suppression of inducible NO synthase (iNOS), and the increase of vascularization in the ischemic area in OPN-treated mice after stroke in a focal photothrombotic stroke model (Ladwig et al., 2017). Furthermore, infiltrating regulatory T-cells can activate microglia by releasing OPN even weeks after stroke, which influences oligodendrogenesis, white matter repair and functional recovery (Shi et al., 2021). Along with these positive effects, it has also been shown that OPN secreted by hematogenous macrophages contributes to the NVU- and BBB-repair in a photothrombotic stroke model (Gliem et al., 2015). Other studies also observed an increase in OPN at capillary endothelial cells and astrocytes during the BBB-repair-phase 72 h after stroke, indicating a substantial role in the restoration of NVU after ischemia (Zhou et al., 2020). One mechanism behind this might be the suppression of vascular endothelial growth factor A (VEGF-A), which consequently reduces vascular permeability (Suzuki et al., 2010). However, other experiments have shown the contrary. Thus, Spitzer *et al*., showed that antibody neutralization of OPN at early time points after stroke in mice leads to preservation of BBB-integrity through a higher expression of adherent proteins and tight junctions on the surface of endothelial cells and, thus, reduced vascular leakage and decreased edema volume after stroke (Spitzer et al., 2022). This would fit with what is found in patients, where high serum levels of OPN correlate with increased lesion size and worse neurological scores, which

could be explained by increased BBB disruption and therefore higher OPN leakage into the vascular system (Carbone et al., 2015). In summary, these experiments suggest the involvement of several factors in the role of OPN, with the temporal component being one of them.

Our studies have observed a 10-fold increase of Spp1-mRNA 24 h after stroke and a dramatically higher, almost 100-fold increase 7 d after tMCAO. A similar temporal pattern was obtained by Wang *et al*. They observed increased Spp1-expression in ischemic cortices with increased expression of Spp1-mRNA starting at approximately 12 h after stroke and peaked at 5 d with a 40-fold increase (Wang et al., 1998). Interestingly, serum levels of OPN also peaked at 7 d in another study (Carbone et al., 2015), indicating potential leakage through the damaged BBB barrier into the vascular system. Other studies used this observation to analyze the temporal pattern of OPN at different time-points after stroke as a potential biomarker to predict poor outcome. However, sensitivity and specificity were not very high (Zhou et al., 2020).

Since all these observations were made when investigating the protein product of Spp1-mRNA or the Spp1-mRNA in cells but not in sEVs, the comparability of our results with others is limited. Kowalski *et al*. recently found OPN, among other proteins, to be elevated in blood-derived EVs in the first hours after stroke (Kowalski et al., 2023) and associated with neuroprotection. OPN has also been identified in EVs derived from other cells, such as dendritic (Silva et al., 2017) and cancer stem cells (Lindoso et al., 2015), but to date, there has not been any investigation related to the presence or effect of Spp1-mRNA in EVs. Of note, in our sEVs we could not find the presence of osteopontin, only the Spp1-mRNA (data not shown).

C1q initiates the classical pathway of the complement system and consists of three subunits: C1qa, C1qb and C1qc (Lu et al., 2008). We found their mRNA upregulated in EVs 7 d after tMCAO with a fold change of 10 to 20 compared to shams. No significant upregulation was observed 24 h after tMCAO. But from previous studies in our laboratory, we know that at 72 h after tMCAO there is already an 8-fold increase of all three subunits mRNA, notably full-length and not fragmented (Bub et al., 2022). The complement system is essential for various homeostatic functions, such as dead cell clearance and immune complex opsonization (Alawieh et al., 2015). C1q plays a crucial role in eliminating weak neuronal synapses (Chu et al., 2010). After stroke, the initiation of many pathways also includes the

activation of the complement system. Notably, C1q-mRNA was dramatically upregulated in microglia, but not in astrocytes or neurons in a rat model of ischemic stroke (Schäfer et al., 2000). However, *in-vitro* models have also shown that neuronal cells express C1q-mRNA and the protein after hypoxia (Tohgi et al., 2000). The findings on the upregulation of C1q in different cells may be explained by the transfer of C1q-mRNA from one cell to another via sEVs.

Mpeg1 is an intracellular protein present in phagosomes of macrophages (Bayly-Jones et al., 2020). There is a lack of research regarding Mpeg1 and its association with EVs, necessitating further exploration to unravel our finding of Mpeg1-mRNA being almost 30-fold upregulated in sEVs along with a very high absolute mRNA count in 7 d post tMCAO brains. It could be hypothesized that in the peripheral macrophages and PVMs into the ischemic area are the origin of these EVs. However, Mpeg1 expression can be induced in many other cells, such as endothelial cells as an answer to proinflammatory signals (Bayly-Jones et al., 2020, Buga et al., 2014).

Hmox1 is the gene encoding heme oxygenase 1 (HO1) (Bereczki et al., 2018). It can be induced through the nuclear factor erythroid 2 related factor 2 (Nrf2), leading to various defense mechanisms against oxidative stress, a crucial mechanism against further cell death in the ischemic region after stroke. HO1 exerts antioxidant, antiapoptotic, anti-inflammatory and vasorelaxant effects (Bereczki et al., 2018). We found the Hmox1-mRNA upregulated in sEVs 24 h after stroke (42-fold increase). At 7 d after tMCAO, there was not a significant upregulation. Upregulation of Hmox1-mRNA in sEVs like C1q, were already observed at 72h after tMCAO with an approximate fold change of 8 when compared to sham mice (Bub et al., 2022). Cressati *et al*. found HO1-loaded EVs derived from astrocytes and neurons in different biofluids (Cressatti et al., 2021). These studies are pioneer in the description of HO1 or Hmox1-mRNA in EVs and therefore more research has to be done to pinpoint their relevance in stroke pathology.

To understand the physiological/pathological role of mRNAs in EVs, it is important that the total counts of mRNAs in sEVs are taken into account. In our study, the highest absolute counts were in the range of 3,000 to 10,000 and notably, only two mRNAs with high fold changes, namely Spp1 and Mpeg1, could achieve these numbers 7 d after tMCAO. In another study analyzing EVs from glioblastoma cells, the authors found a relatively low ratio between the amount of EVs and different RNAs in their samples. The highest ratio was

achieved by rRNA- or tRNA-fragments or full-length miRNA with one or more copies per EV, while the most abundant mRNA was found with a ratio of 1 in 100,000 EVs, and other mRNAs with a ratio of 1:1,000,000 EVs (Wei et al., 2017). When taking the results from nCounter® and NTA together, roughly, a ratio of 1 copy of Spp1 per 1,000,000 EVs can be calculated. This raises the question of whether this relatively low ratio of mRNA to EVs, even for the mRNA with the highest fold change, has relevance for the recipient cell. Wei *et al*. have shown that a miRNA with a ratio of 1:10 EVs (miR-21) has a functional effect in recipient cells by suppressing its mRNA targets (Wei et al., 2017). However, EV-mRNA secreted by cancer cells can be taken up by other malignant cells and provoke phenotypic changes despite of the mRNA amount in EVs (Zomer et al., 2015). Previous studies in our laboratory had similar ratios of 1:1,000,000 and translated proteins could not be detected by confocal immunohistochemistry, a technique probably not sensitive enough (Bub et al., 2022).

To summarize, several studies have indicated that the translated protein of the here described mRNAs could have a possible role in pathophysiological steps in the ischemic area after a stroke event. However, the possible effect (positive or negative) cannot be anticipated as it is very dependent on many factors. Notably, very little is known about upregulated mRNA in sEVs after stroke. Most research groups have focused on the abundance or effect of proteins in EVs in a stroke model, as RNA is prone to fragmentation via RNases or degradation in the recipient cell (O'Brien et al., 2020). Several studies have indicated that mRNA in EVs can be full-length (Bub et al., 2022, Li et al., 2019, O'Brien et al., 2020, Wei et al., 2017) and EVs also carry parts of the translation machinery such as tRNA (Huang et al., 2023). Thus, it can be hypothesized that our upregulated mRNA could elicit a response in the recipient cells.

5.5. Origin of sEVs

Since we analyzed sEVs from brain tissue, our sEV population most probably originates from multiple cells, including the resident brain cells and the infiltrating peripheral cells into the ischemic region upon stroke. The most upregulated mRNAs, such as Spp1-mRNA, C1qa/C1qb/C1qc-mRNA and Mpeg1-mRNA, indicate that microglia and macrophages release EVs containing these mRNAs as assessed by the Allen brain Atlas Transcriptomics Explorer and the Cell Type Profiling in the advanced analysis software from NanoString

nSolver. However, as these mRNAs are not specific to one cell type, our experiments cannot assess the exact origin of the most upregulated mRNAs.

The upregulation of mRNA species in sEVs presumably of microglia and macrophages origin, described in this thesis may have several explanations. First, the production specific mRNAs into sEVs could be upregulated in the donor cell. For instance, the Spp1-mRNA was upregulated in microglia in a MCAO mouse model (Zheng et al., 2022a) and therefore, probably more mRNA was also directed to EVs (although not specifically investigated in this study). Second, the increased amounts of specific mRNAs in our sEVs could indicate simply increased proliferation of microglia and infiltration of macrophages in the ischemic brain (Gelderblom et al., 2009). A third option would be that microglia and PVM increase the number of released EVs as demonstrated by Yang *et al*. They analyzed the effect that neuroinflammation triggers on microglia-derived EV characteristics. They found a 30-fold increase in the quantity of EVs derived from microglia when activated by lipopolysaccharide, compared to the amount of microglia-derived EVs released when microglial activation was inhibited (Yang et al., 2018).

5.6. Outlook

The results of the NanoString nCounter® neuroinflammation panel presented in this thesis open multiple lines of investigation for follow up experiments. To demonstrate that for example Spp1-mRNA or Mpeg1-mRNA (just to mention the two most upregulated) in EVs has an effect after stroke, several steps have to be fulfilled. First it has to confirmed whether these mRNAs are full-length (for example by assessing the mRNA with specific primers in PCR). Second, it has to be demonstrated that the mRNAs reach the cytosol of the recipient cells, where they will be translated. Reaching this compartment from the extracellular space is possible either by direct fusion with the plasma membrane or through endocytosis and endosomal escape. When EVs enter into the recipient cell by endocytosis, the usual final fate is fusion with lysosomes and degradation of the sEVs cargo. Escaping the endosomal system is pivotal for the delivered mRNAs to be translated into proteins (O'Brien et al., 2020). To address this, *in vitro* experiments with Spp1-knock-out cells could be established, in which the cells are treated with 7 d post-tMCAO sEVs. Afterwards, Spp1 mRNA could be detected in the recipient cells by qPCR and, if the mRNA is functional, the OPN should

be detectable via immunohistochemistry or western blot. Then, a possible effect of it could be analyzed by subjecting recipient cells to ODG experiments.

Apart from downstream experiments referring to a possible function of upregulated mRNAs in sEVs following tMCAO, further technical advancements in EVs isolation from brain could be made. The already explained cushioned ultracentrifugation step could be implemented in our protocol to prevent damage to the EVs (Duong et al., 2019). Furthermore, as proposed by Crescitelli *et al*., differential centrifugation steps before DGUC could separate large and small vesicles. So, distinct experiments on the subpopulations of large and small EVs could be performed (Crescitelli et al., 2021).

Overall, our studies identified several different mRNAs in sEVs to be upregulated at 24 h and 7 d after tMCAO. The most upregulated single mRNAs, the potentially upregulated pathways, the temporal differences on both time points and the analysis of the origin cell type of our sEVs indicate a possible role of sEV mRNA in neuroinflammation. This is an essential finding in understanding the pathophysiology following a stroke event. However, more investigations are required to validate the assumptions that can be drawn from this study.

6. Summary

Ischemic stroke is a leading cause of death in the world (Internet reference 1: WHO, 2020) and understanding its pathophysiology is crucial to the establishment of new therapeutical options to improve the outcome after a stroke event. Various studies have investigated EVs in the pathophysiological landscape of stroke. However, so far, only one previous study from our laboratory has focused on mRNAs being transported by EVs and their effect on different cells in the ischemic penumbra. We hypothesized that the mRNA population in sEVs changes following tMCAO. To assess this, we set up a new isolation protocol for isolating sEVs from whole brain tissue, consisting on homogenization, differential centrifugation and filtration to separate sEVs from cells, debris, and larger EVs. This was followed by a bottom-up iodixanol-based DGUC, the current gold standard for isolating EVs (Zhang et al., 2023) that further purified the sEVs based on their density. Next, we characterized our isolated sEVs by western blot, NTA and EM according with the MISEV2018 (Théry et al., 2018). Then, we analyzed the differential expression of 757 different mRNAs associated with neuroinflammation with the NanoString nCounter® technology at 24 h and 7 d after tMCAO. Of note, the NTA assay which analyzes the size and quantity of EVs showed no significant difference at both time points between tMCAO and shams.

At both time points, several mRNAs were significantly upregulated. From all analyzed mRNAs, Spp1-mRNA was revealed as a potential candidate for further analysis, mainly because of its high fold change of approximately 100 times increase in tMCAO compared to sham sEVs. The nSolver cell type profiling and open-source transcriptome atlases indicated that microglia and macrophages were the main source of the differentially expressed mRNAs. Furthermore, multiple pathways could be ascribed to the upregulated mRNAs. Although the functionality of the mRNAs and their translation to proteins could not be assessed in this thesis, it provides a solid starting point for further investigations of the role on mRNA in EVs in stroke.

7. Zusammenfassung

Der ischämische Schlaganfall ist einer der häufigsten Todesursachen weltweit (Internetreferenz 1). Um neue Therapiekonzepte zu entwickeln und die Prognose nach einem Schlaganfall zu verbessern, ist es von fundamentaler Bedeutung, die pathophysiologischen Prozesse innerhalb der ischämischen Penumbra vollständig zu verstehen. Viele Studien haben die Rolle von EVs untersucht, allerdings wurden nur wenige Untersuchungen über die Bedeutung von mRNA in EVs angestellt. Da aus vorangegangenen Untersuchungen klar war, dass ein Schlaganfall die EV Population und deren Inhalt beeinflusst, wurde die Hypothese aufgestellt, dass auch die mRNA in sEVs beeinflusst wird. Um dies zu untersuchen, haben wir ein neues Protokoll zur Isolation von EVs aus Gewebe erstellt. Dieses umfasst eine Homogenisierung, Zentrifugationsschritte und eine Filtration um die sEVs von Zellen, extrazellulärem Gewebe und größeren Partikeln zu befreien. Anschließend führten wir eine DGUC mit Iodixanol als Träger-Medium durch. Dies hat die sEV-Population weiter nach ihrer Dichte aufgeteilt und ist der aktuelle Goldstandard der EV-Isolationsmethoden (Zhang et al., 2023). Die durch das neue Protokoll isolierten sEVs wurden mit Hilfe von Western Blots, NTA und EM auf der Basis von MISEV2018 (Théry et al., 2018) weiter charakterisiert. Anhand des validierten Protokolls wurden sEVs aus Mausgehirnen 24 Stunden und 7 Tage nach experimentellem Schlaganfall und aus den Kontrollen isoliert. Mit der NanoString nCounter® Technik wurden dann 757 mRNAs aus diesen sEVs quantitativ untersucht, welche einen Zusammenhang zu Neuroinflammation haben.

Zu beiden Zeitpunkten war die Anzahl mehrerer mRNAs signifikant erhöht. Die Spp1-mRNA, welche nach 7 Tagen ca. um den Faktor 100 anstieg, ist einer der besten Kandidaten für weitere Analysen bezüglich dessen Funktion. Unter Benutzung der nSolver Zelltypisierung und Transkript-Atlanten konnte gezeigt werden, dass Mikroglia and Makrophagen höchstwahrscheinlich an der Hochregulation der mRNAs in sEVs beteiligt sind. Eine NTA-Analyse der sEVs ergab keinen signifikanten Unterschied in Anzahl und Größe der sEVs 24 h und 7 d nach Schlaganfall im Vergleich zu deren gesunden Kontrollen. Somit bietet diese Arbeit einen soliden Ausganspunkt für weitere Analysen bezüglich der Rolle von mRNAs in sEVs im Schlaganfallmodel.

8. Figure index

9. Table index

10. References

ABELS, E. R. & BREAKEFIELD, X. O. 2016. Introduction to Extracellular Vesicles: Biogenesis, RNA Cargo Selection, Content, Release, and Uptake. *Cell Mol Neurobiol,* 36**,** 301-12.

ADIBHATLA, R. M. & HATCHER, J. F. 2010. Lipid oxidation and peroxidation in CNS health and disease: from molecular mechanisms to therapeutic opportunities. *Antioxid Redox Signal,* 12**,** 125-69.

ALAWIEH, A., ELVINGTON, A. & TOMLINSON, S. 2015. Complement in the Homeostatic and Ischemic Brain. *Front Immunol,* 6**,** 417.

ALLEN, R. M., ZHAO, S., RAMIREZ SOLANO, M. A., ZHU, W., MICHELL, D. L., WANG, Y., SHYR, Y., SETHUPATHY, P., LINTON, M. F., GRAF, G. A., SHENG, Q. & VICKERS, K. C. 2018. Bioinformatic analysis of endogenous and exogenous small RNAs on lipoproteins. *J Extracell Vesicles,* 7**,** 1506198.

AMANTEA, D., MICIELI, G., TASSORELLI, C., CUARTERO, M. I., BALLESTEROS, I., CERTO, M., MORO, M. A., LIZASOAIN, I. & BAGETTA, G. 2015. Rational modulation of the innate immune system for neuroprotection in ischemic stroke. *Front Neurosci,* 9**,** 147.

AN, M., WU, J., ZHU, J. & LUBMAN, D. M. 2018. Comparison of an Optimized Ultracentrifugation Method versus Size-Exclusion Chromatography for Isolation of Exosomes from Human Serum. *J Proteome Res,* 17**,** 3599-3605.

ANDERSON, H. C. 1969. Vesicles associated with calcification in the matrix of epiphyseal cartilage. *J Cell Biol,* 41**,** 59-72.

ANRATHER, J. & IADECOLA, C. 2016. Inflammation and Stroke: An Overview. *Neurotherapeutics,* 13**,** 661-670.

ARROYO, J. D., CHEVILLET, J. R., KROH, E. M., RUF, I. K., PRITCHARD, C. C., GIBSON, D. F., MITCHELL, P. S., BENNETT, C. F., POGOSOVA-AGADJANYAN, E. L., STIREWALT, D. L., TAIT, J. F. & TEWARI, M. 2011. Argonaute2 complexes carry a population of circulating microRNAs independent of vesicles in human plasma. *Proc Natl Acad Sci U S A,* 108**,** 5003-8.

ARYA, S. B., COLLIE, S. P. & PARENT, C. A. 2024. The ins-and-outs of exosome biogenesis, secretion, and internalization. *Trends in Cell Biology,* 34**,** 90-108.

BARON, J. C. 2018. Protecting the ischaemic penumbra as an adjunct to thrombectomy for acute stroke. *Nat Rev Neurol,* 14**,** 325-337.

BATAGOV, A. O. & KUROCHKIN, I. V. 2013. Exosomes secreted by human cells transport largely mRNA fragments that are enriched in the 3'-untranslated regions. *Biol Direct,* 8**,** 12.

BAYLY-JONES, C., PANG, S. S., SPICER, B. A., WHISSTOCK, J. C. & DUNSTONE, M. A. 2020. Ancient but Not Forgotten: New Insights Into MPEG1, a Macrophage Perforin-Like Immune Effector. *Front Immunol,* 11**,** 581906.

BERECZKI, D., JR., BALLA, J. & BERECZKI, D. 2018. Heme Oxygenase-1: Clinical Relevance in Ischemic Stroke. *Curr Pharm Des,* 24**,** 2229-2235.

BRACHT, J. W. P., GIMENEZ-CAPITAN, A., HUANG, C. Y., POTIE, N., PEDRAZ-VALDUNCIEL, C., WARREN, S., ROSELL, R. & MOLINA-VILA, M. A. 2021. Analysis of extracellular vesicle mRNA derived from plasma using the nCounter platform. *Sci Rep,* 11**,** 3712.

BRENNAN, A. M., SUH, S. W., WON, S. J., NARASIMHAN, P., KAUPPINEN, T. M., LEE, H., EDLING, Y., CHAN, P. H. & SWANSON, R. A. 2009. NADPH oxidase

is the primary source of superoxide induced by NMDA receptor activation. *Nat Neurosci,* 12**,** 857-63.
BRIYAL, S., RANJAN, A. K. & GULATI, A. 2023. Oxidative stress: A target to treat Alzheimer's disease and stroke. *Neurochem Int,* 165**,** 105509.
BROSIUS, J. & RAABE, C. A. 2016. What is an RNA? A top layer for RNA classification. *RNA Biol,* 13**,** 140-4.
BUB, A., BRENNA, S., ALAWI, M., KÜGLER, P., GUI, Y., KRETZ, O., ALTMEPPEN, H., MAGNUS, T. & PUIG, B. 2022. Multiplexed mRNA analysis of brain-derived extracellular vesicles upon experimental stroke in mice reveals increased mRNA content with potential relevance to inflammation and recovery processes. *Cell Mol Life Sci,* 79**,** 329.
BUDNIK, V., RUIZ-CANADA, C. & WENDLER, F. 2016. Extracellular vesicles round off communication in the nervous system. *Nat Rev Neurosci,* 17**,** 160-72.
BUGA, A. M., MARGARITESCU, C., SCHOLZ, C. J., RADU, E., ZELENAK, C. & POPA-WAGNER, A. 2014. Transcriptomics of post-stroke angiogenesis in the aged brain. *Front Aging Neurosci,* 6**,** 44.
BUSCH, M. R. & KUHNERT, R. 2017. 12-Monats-Prävalenz von Schlaganfall oder chronischen Beschwerden infolge eines Schlaganfalls in Deutschland. *Journal of Health Monitoring,* 2**,** 70-76.
CAI, W., LIU, S., HU, M., HUANG, F., ZHU, Q., QIU, W., HU, X., COLELLO, J., ZHENG, S. G. & LU, Z. 2020. Functional Dynamics of Neutrophils After Ischemic Stroke. *Transl Stroke Res,* 11**,** 108-121.
CAMPBELL, B. C. V., DE SILVA, D. A., MACLEOD, M. R., COUTTS, S. B., SCHWAMM, L. H., DAVIS, S. M. & DONNAN, G. A. 2019. Ischaemic stroke. *Nat Rev Dis Primers,* 5**,** 70.
CANDELARIO-JALIL, E., DIJKHUIZEN, R. M. & MAGNUS, T. 2022. Neuroinflammation, Stroke, Blood-Brain Barrier Dysfunction, and Imaging Modalities. *Stroke,* 53**,** 1473-1486.
CARBONE, F., VUILLEUMIER, N., BURGER, F., ROVERSI, G., TAMBORINO, C., CASETTA, I., SERACENI, S., TRENTINI, A., PADRONI, M., DALLEGRI, F., MACH, F., FAINARDI, E. & MONTECUCCO, F. 2015. Serum osteopontin levels are upregulated and predict disability after an ischaemic stroke. *Eur J Clin Invest,* 45**,** 579-86.
CHEN, H., HE, Y., CHEN, S., QI, S. & SHEN, J. 2020. Therapeutic targets of oxidative/nitrosative stress and neuroinflammation in ischemic stroke: Applications for natural product efficacy with omics and systemic biology. *Pharmacol Res,* 158**,** 104877.
CHITTI, S. V., GUMMADI, S., KANG, T., SHAHI, S., MARZAN, A. L., NEDEVA, C., SANWLANI, R., BRAMICH, K., STEWART, S., PETROVSKA, M., SEN, B., OZKAN, A., AKINFENWA, M., FONSEKA, P. & MATHIVANAN, S. 2023. Vesiclepedia 2024: an extracellular vesicles and extracellular particles repository. *Nucleic Acids Res*.
CHOI, D. S., KIM, D. K., KIM, Y. K. & GHO, Y. S. 2015. Proteomics of extracellular vesicles: Exosomes and ectosomes. *Mass Spectrom Rev,* 34**,** 474-90.
CHU, Y., JIN, X., PARADA, I., PESIC, A., STEVENS, B., BARRES, B. & PRINCE, D. A. 2010. Enhanced synaptic connectivity and epilepsy in C1q knockout mice. *Proc Natl Acad Sci U S A,* 107**,** 7975-80.
CLANCY, J. W., SCHMIDTMANN, M. & D'SOUZA-SCHOREY, C. 2021. The ins and outs of microvesicles. *FASEB Bioadv,* 3**,** 399-406.

COLOMBO, M., RAPOSO, G. & THERY, C. 2014. Biogenesis, secretion, and intercellular interactions of exosomes and other extracellular vesicles. *Annu Rev Cell Dev Biol,* 30**,** 255-89.

COLONNA, M. & BUTOVSKY, O. 2017. Microglia Function in the Central Nervous System During Health and Neurodegeneration. *Annu Rev Immunol,* 35**,** 441-468.

COUCH, Y., AKBAR, N., DAVIS, S., FISCHER, R., DICKENS, A. M., NEUHAUS, A. A., BURGESS, A. I., ROTHWELL, P. M. & BUCHAN, A. M. 2017. Inflammatory Stroke Extracellular Vesicles Induce Macrophage Activation. *Stroke,* 48**,** 2292-2296.

COUCH, Y., BUZÀS, E. I., DI VIZIO, D., GHO, Y. S., HARRISON, P., HILL, A. F., LÖTVALL, J., RAPOSO, G., STAHL, P. D., THÉRY, C., WITWER, K. W. & CARTER, D. R. F. 2021. A brief history of nearly EV-erything – The rise and rise of extracellular vesicles. *Journal of Extracellular Vesicles,* 10**,** e12144.

COUPLAND, A. P., THAPAR, A., QURESHI, M. I., JENKINS, H. & DAVIES, A. H. 2017. The definition of stroke. *J R Soc Med,* 110**,** 9-12.

CRESCITELLI, R., LÄSSER, C. & LÖTVALL, J. 2021. Isolation and characterization of extracellular vesicle subpopulations from tissues. *Nat Protoc,* 16**,** 1548-1580.

CRESSATTI, M., GALINDEZ, J. M., JUWARA, L., ORLOVETSKIE, N., VELLY, A. M., EINTRACHT, S., LIBERMAN, A., GORNITSKY, M. & SCHIPPER, H. M. 2021. Characterization and heme oxygenase-1 content of extracellular vesicles in human biofluids. *J Neurochem,* 157**,** 2195-2209.

CVJETKOVIC, A., LÖTVALL, J. & LÄSSER, C. 2014. The influence of rotor type and centrifugation time on the yield and purity of extracellular vesicles. *J Extracell Vesicles,* 3.

D'ACUNZO, P., KIM, Y., UNGANIA, J. M., PÉREZ-GONZÁLEZ, R., GOULBOURNE, C. N. & LEVY, E. 2022. Isolation of mitochondria-derived mitovesicles and subpopulations of microvesicles and exosomes from brain tissues. *Nat Protoc,* 17**,** 2517-2549.

DAS, S., ANSEL, K. M., BITZER, M., BREAKEFIELD, X. O., CHAREST, A., GALAS, D. J., GERSTEIN, M. B., GUPTA, M., MILOSAVLJEVIC, A., MCMANUS, M. T., PATEL, T., RAFFAI, R. L., ROZOWSKY, J., ROTH, M. E., SAUGSTAD, J. A., VAN KEUREN-JENSEN, K., WEAVER, A. M. & LAURENT, L. C. 2019. The Extracellular RNA Communication Consortium: Establishing Foundational Knowledge and Technologies for Extracellular RNA Research. *Cell,* 177**,** 231-242.

DIRNAGL, U., IADECOLA, C. & MOSKOWITZ, M. A. 1999. Pathobiology of ischaemic stroke: an integrated view. *Trends Neurosci,* 22**,** 391-7.

DISSING-OLESEN, L., LEDUE, J. M., RUNGTA, R. L., HEFENDEHL, J. K., CHOI, H. B. & MACVICAR, B. A. 2014. Activation of neuronal NMDA receptors triggers transient ATP-mediated microglial process outgrowth. *J Neurosci,* 34**,** 10511-27.

DOEPPNER, T. R., HERZ, J., GÖRGENS, A., SCHLECHTER, J., LUDWIG, A. K., RADTKE, S., DE MIROSCHEDJI, K., HORN, P. A., GIEBEL, B. & HERMANN, D. M. 2015. Extracellular Vesicles Improve Post-Stroke Neuroregeneration and Prevent Postischemic Immunosuppression. *Stem Cells Transl Med,* 4**,** 1131-43.

DONG, L., HUANG, C. Y., JOHNSON, E. J., YANG, L., ZIEREN, R. C., HORIE, K., KIM, C. J., WARREN, S., AMEND, S. R., XUE, W. & PIENTA, K. J. 2021. High-Throughput Simultaneous mRNA Profiling Using nCounter Technology Demonstrates That Extracellular Vesicles Contain Different mRNA Transcripts Than Their Parental Prostate Cancer Cells. *Anal Chem,* 93**,** 3717-3725.

DRAGOVIC, R. A., GARDINER, C., BROOKS, A. S., TANNETTA, D. S., FERGUSON, D. J., HOLE, P., CARR, B., REDMAN, C. W., HARRIS, A. L., DOBSON, P. J.,

HARRISON, P. & SARGENT, I. L. 2011. Sizing and phenotyping of cellular vesicles using Nanoparticle Tracking Analysis. *Nanomedicine,* 7**,** 780-8.
DUONG, P., CHUNG, A., BOUCHAREYCHAS, L. & RAFFAI, R. L. 2019. Cushioned-Density Gradient Ultracentrifugation (C-DGUC) improves the isolation efficiency of extracellular vesicles. *PLoS One,* 14**,** e0215324.
ELLISON, J. A., VELIER, J. J., SPERA, P., JONAK, Z. L., WANG, X., BARONE, F. C. & FEUERSTEIN, G. Z. 1998. Osteopontin and its integrin receptor alpha(v)beta3 are upregulated during formation of the glial scar after focal stroke. *Stroke,* 29**,** 1698-706; discussion 1707.
ELSHARKASY, O. M., NORDIN, J. Z., HAGEY, D. W., DE JONG, O. G., SCHIFFELERS, R. M., ANDALOUSSI, S. E. & VADER, P. 2020. Extracellular vesicles as drug delivery systems: Why and how? *Adv Drug Deliv Rev,* 159**,** 332-343.
ELZANOWSKA, J., SEMIRA, C. & COSTA-SILVA, B. 2021. DNA in extracellular vesicles: biological and clinical aspects. *Mol Oncol,* 15**,** 1701-1714.
EVERAERT, C., HELSMOORTEL, H., DECOCK, A., HULSTAERT, E., VAN PAEMEL, R., VERNIERS, K., NUYTENS, J., ANCKAERT, J., NIJS, N., TULKENS, J., DHONDT, B., HENDRIX, A., MESTDAGH, P. & VANDESOMPELE, J. 2019. Performance assessment of total RNA sequencing of human biofluids and extracellular vesicles. *Sci Rep,* 9**,** 17574.
FABBIANO, F., CORSI, J., GURRIERI, E., TREVISAN, C., NOTARANGELO, M. & D'AGOSTINO, V. G. 2020. RNA packaging into extracellular vesicles: An orchestra of RNA-binding proteins? *J Extracell Vesicles,* 10**,** e12043.
FEIGIN, V. L., BRAININ, M., NORRVING, B., MARTINS, S., SACCO, R. L., HACKE, W., FISHER, M., PANDIAN, J. & LINDSAY, P. 2022. World Stroke Organization (WSO): Global Stroke Fact Sheet 2022. *Int J Stroke,* 17**,** 18-29.
FRENGUELLI, B. G. 2019. The Purine Salvage Pathway and the Restoration of Cerebral ATP: Implications for Brain Slice Physiology and Brain Injury. *Neurochem Res,* 44**,** 661-675.
FROHLICH, D., KUO, W. P., FRUHBEIS, C., SUN, J. J., ZEHENDNER, C. M., LUHMANN, H. J., PINTO, S., TOEDLING, J., TROTTER, J. & KRAMER-ALBERS, E. M. 2014. Multifaceted effects of oligodendroglial exosomes on neurons: impact on neuronal firing rate, signal transduction and gene regulation. *Philos Trans R Soc Lond B Biol Sci*, 369.
GALLART-PALAU, X., SERRA, A. & SZE, S. K. 2016. Enrichment of extracellular vesicles from tissues of the central nervous system by PROSPR. *Mol Neurodegener,* 11**,** 41.
GALVANIN, A., DOSTERT, G., AYADI, L., MARCHAND, V., VELOT, É. & MOTORIN, Y. 2019. Diversity and heterogeneity of extracellular RNA in human plasma. *Biochimie,* 164**,** 22-36.
GARDINER, C., FERREIRA, Y. J., DRAGOVIC, R. A., REDMAN, C. W. & SARGENT, I. L. 2013. Extracellular vesicle sizing and enumeration by nanoparticle tracking analysis. *J Extracell Vesicles,* 2.
GBD 2019 STOKE COLLABORATORS 2021. Global, regional, and national burden of stroke and its risk factors, 1990-2019: a systematic analysis for the Global Burden of Disease Study 2019. *Lancet Neurol,* 20**,** 795-820.
GEBETSBERGER, J. & POLACEK, N. 2013. Slicing tRNAs to boost functional ncRNA diversity. *RNA Biol,* 10**,** 1798-806.
GEISS, G. K., BUMGARNER, R. E., BIRDITT, B., DAHL, T., DOWIDAR, N., DUNAWAY, D. L., FELL, H. P., FERREE, S., GEORGE, R. D., GROGAN, T.,

JAMES, J. J., MAYSURIA, M., MITTON, J. D., OLIVERI, P., OSBORN, J. L., PENG, T., RATCLIFFE, A. L., WEBSTER, P. J., DAVIDSON, E. H., HOOD, L. & DIMITROV, K. 2008. Direct multiplexed measurement of gene expression with color-coded probe pairs. *Nat Biotechnol,* 26**,** 317-25.

GELDERBLOM, M., LEYPOLDT, F., STEINBACH, K., BEHRENS, D., CHOE, C. U., SILER, D. A., ARUMUGAM, T. V., ORTHEY, E., GERLOFF, C., TOLOSA, E. & MAGNUS, T. 2009. Temporal and spatial dynamics of cerebral immune cell accumulation in stroke. *Stroke,* 40**,** 1849-57.

GEORGE, J. N., THOI, L. L., MCMANUS, L. M. & REIMANN, T. A. 1982. Isolation of human platelet membrane microparticles from plasma and serum. *Blood,* 60**,** 834-40.

GLIEM, M., KRAMMES, K., LIAW, L., VAN ROOIJEN, N., HARTUNG, H. P. & JANDER, S. 2015. Macrophage-derived osteopontin induces reactive astrocyte polarization and promotes re-establishment of the blood brain barrier after ischemic stroke. *Glia,* 63**,** 2198-207.

GORDON, G. R., MULLIGAN, S. J. & MACVICAR, B. A. 2007. Astrocyte control of the cerebrovasculature. *Glia,* 55**,** 1214-21.

GOUIN, K., PECK, K., ANTES, T., JOHNSON, J. L., LI, C., VATURI, S. D., MIDDLETON, R., DE COUTO, G., WALRAVENS, A. S., RODRIGUEZ-BORLADO, L., SMITH, R. R., MARBÁN, L., MARBÁN, E. & IBRAHIM, A. G. 2017. A comprehensive method for identification of suitable reference genes in extracellular vesicles. *J Extracell Vesicles,* 6**,** 1347019.

GOULD, S. J. & RAPOSO, G. 2013. As we wait: coping with an imperfect nomenclature for extracellular vesicles. *J Extracell Vesicles,* 2.

GURUNG, S., PEROCHEAU, D., TOURAMANIDOU, L. & BARUTEAU, J. 2021. The exosome journey: from biogenesis to uptake and intracellular signalling. *Cell Commun Signal,* 19**,** 47.

HANKEY, G. J. 2017. Stroke. *Lancet,* 389**,** 641-654.

HANSEN, H. P., PAES LEME, A. F. & HALLEK, M. 2020. Role of ADAM10 as a CD30 Sheddase in Classical Hodgkin Lymphoma. *Front Immunol,* 11**,** 398.

HARDING, C., HEUSER, J. & STAHL, P. 1983. Receptor-mediated endocytosis of transferrin and recycling of the transferrin receptor in rat reticulocytes. *J Cell Biol,* 97**,** 329-39.

HERRERO, C., FERREIRÓS, A., PÉREZ-FENTES, D., LEÓN-MATEOS, L., LÓPEZ-LÓPEZ, R., ABAL, M. & ALONSO-ALCONADA, L. 2023. Extracellular Vesicles' Genetic Cargo as Noninvasive Biomarkers in Cancer: A Pilot Study Using ExoGAG Technology. *Biomedicines,* 11.

HOMBACH, S. & KRETZ, M. 2016. Non-coding RNAs: Classification, Biology and Functioning. *Adv Exp Med Biol,* 937**,** 3-17.

HU, X., LEAK, R. K., SHI, Y., SUENAGA, J., GAO, Y., ZHENG, P. & CHEN, J. 2015. Microglial and macrophage polarization—new prospects for brain repair. *Nat Rev Neurol,* 11**,** 56-64.

HU, X., LI, P., GUO, Y., WANG, H., LEAK, R. K., CHEN, S., GAO, Y. & CHEN, J. 2012. Microglia/macrophage polarization dynamics reveal novel mechanism of injury expansion after focal cerebral ischemia. *Stroke,* 43**,** 3063-70.

HUANG, B., LI, X. & ZHU, X. 2021. The Role of GM130 in Nervous System Diseases. *Front Neurol,* 12**,** 743787.

HUANG, Y., CHENG, L., TURCHINOVICH, A., MAHAIRAKI, V., TRONCOSO, J. C., PLETNIKOVÁ, O., HAUGHEY, N. J., VELLA, L. J., HILL, A. F., ZHENG, L. & WITWER, K. W. 2020. Influence of species and processing parameters on recovery

and content of brain tissue-derived extracellular vesicles. *J Extracell Vesicles,* 9**,** 1785746.

HUANG, Y., DRIEDONKS, T. A. P., CHENG, L., TURCHINOVICH, A., PLETNIKOVÁ, O., REDDING-OCHOA, J., TRONCOSO, J. C., HILL, A. F., MAHAIRAKI, V., ZHENG, L. & WITWER, K. W. 2023. Small RNA Profiles of Brain Tissue-Derived Extracellular Vesicles in Alzheimer's Disease. *J Alzheimers Dis*.

HUNG, M. E. & LEONARD, J. N. 2016. A platform for actively loading cargo RNA to elucidate limiting steps in EV-mediated delivery. *J Extracell Vesicles,* 5**,** 31027.

HUNTZINGER, E. & IZAURRALDE, E. 2011. Gene silencing by microRNAs: contributions of translational repression and mRNA decay. *Nat Rev Genet,* 12**,** 99-110.

HURWITZ, S. N., OLCESE, J. M. & MECKES, D. G., JR. 2019. Extraction of Extracellular Vesicles from Whole Tissue. *J Vis Exp*.

HURWITZ, S. N., SUN, L., COLE, K. Y., FORD, C. R., 3RD, OLCESE, J. M. & MECKES, D. G., JR. 2018. An optimized method for enrichment of whole brain-derived extracellular vesicles reveals insight into neurodegenerative processes in a mouse model of Alzheimer's disease. *J Neurosci Methods,* 307**,** 210-220.

IADECOLA, C. 2017. The Neurovascular Unit Coming of Age: A Journey through Neurovascular Coupling in Health and Disease. *Neuron,* 96**,** 17-42.

IADECOLA, C. & ANRATHER, J. 2011. The immunology of stroke: from mechanisms to translation. *Nat Med,* 17**,** 796-808.

IADECOLA, C., BUCKWALTER, M. S. & ANRATHER, J. 2020. Immune responses to stroke: mechanisms, modulation, and therapeutic potential. *J Clin Invest,* 130**,** 2777-2788.

IWAI, K., MINAMISAWA, T., SUGA, K., YAJIMA, Y. & SHIBA, K. 2016. Isolation of human salivary extracellular vesicles by iodixanol density gradient ultracentrifugation and their characterizations. *J Extracell Vesicles,* 5**,** 30829.

JANKOVIČOVÁ, J., SEČOVÁ, P., MICHALKOVÁ, K. & ANTALÍKOVÁ, J. 2020. Tetraspanins, More than Markers of Extracellular Vesicles in Reproduction. *Int J Mol Sci,* 21.

JEPPESEN, D. K., FENIX, A. M., FRANKLIN, J. L., HIGGINBOTHAM, J. N., ZHANG, Q., ZIMMERMAN, L. J., LIEBLER, D. C., PING, J., LIU, Q., EVANS, R., FISSELL, W. H., PATTON, J. G., ROME, L. H., BURNETTE, D. T. & COFFEY, R. J. 2019. Reassessment of Exosome Composition. *Cell,* 177**,** 428-445.e18.

JEPPESEN, D. K., HVAM, M. L., PRIMDAHL-BENGTSON, B., BOYSEN, A. T., WHITEHEAD, B., DYRSKJØT, L., ORNTOFT, T. F., HOWARD, K. A. & OSTENFELD, M. S. 2014. Comparative analysis of discrete exosome fractions obtained by differential centrifugation. *J Extracell Vesicles,* 3**,** 25011.

JIA, G., WANG, X., LI, Q., LU, W., TANG, X., WISTUBA, I. & XIE, Y. 2019. RCRnorm: An integrated system of random-coefficient hierarchical regression models for normalizing NanoString nCounter data. *Ann Appl Stat,* 13**,** 1617-1647.

JIA, Y., YU, L., MA, T., XU, W., QIAN, H., SUN, Y. & SHI, H. 2022. Small extracellular vesicles isolation and separation: Current techniques, pending questions and clinical applications. *Theranostics,* 12**,** 6548-6575.

JIN, Y., MA, L., ZHANG, W., YANG, W., FENG, Q. & WANG, H. 2022. Extracellular signals regulate the biogenesis of extracellular vesicles. *Biol Res,* 55**,** 35.

JÖDICKE, R. A., HUO, S., KRÄNKEL, N., PIPER, S. K., EBINGER, M., LANDMESSER, U., FLÖEL, A., ENDRES, M. & NAVE, A. H. 2021. The Dynamic of Extracellular Vesicles in Patients With Subacute Stroke: Results of the "Biomarkers and

Perfusion-Training-Induced Changes After Stroke" (BAPTISe) Study. *Front Neurol,* 12**,** 731013.

JOHNSTONE, R. M., ADAM, M., HAMMOND, J. R., ORR, L. & TURBIDE, C. 1987. Vesicle formation during reticulocyte maturation. Association of plasma membrane activities with released vesicles (exosomes). *J Biol Chem,* 262**,** 9412-20.

JOSHI, B. S., DE BEER, M. A., GIEPMANS, B. N. G. & ZUHORN, I. S. 2020. Endocytosis of Extracellular Vesicles and Release of Their Cargo from Endosomes. *ACS Nano,* 14**,** 4444-4455.

KAHLERT, C., MELO, S. A., PROTOPOPOV, A., TANG, J., SETH, S., KOCH, M., ZHANG, J., WEITZ, J., CHIN, L., FUTREAL, A. & KALLURI, R. 2014. Identification of double-stranded genomic DNA spanning all chromosomes with mutated KRAS and p53 DNA in the serum exosomes of patients with pancreatic cancer. *J Biol Chem,* 289**,** 3869-75.

KALLURI, R. & LEBLEU, V. S. 2020. The biology, function, and biomedical applications of exosomes. *Science,* 367.

KANG, W. S., CHOI, J. S., SHIN, Y. J., KIM, H. Y., CHA, J. H., LEE, J. Y., CHUN, M. H. & LEE, M. Y. 2008. Differential regulation of osteopontin receptors, CD44 and the alpha(v) and beta(3) integrin subunits, in the rat hippocampus following transient forebrain ischemia. *Brain Res,* 1228**,** 208-16.

KARIMI, N., CVJETKOVIC, A., JANG, S. C., CRESCITELLI, R., HOSSEINPOUR FEIZI, M. A., NIEUWLAND, R., LÖTVALL, J. & LÄSSER, C. 2018. Detailed analysis of the plasma extracellular vesicle proteome after separation from lipoproteins. *Cell Mol Life Sci,* 75**,** 2873-2886.

KATO, G., INADA, H., WAKE, H., AKIYOSHI, R., MIYAMOTO, A., ETO, K., ISHIKAWA, T., MOORHOUSE, A. J., STRASSMAN, A. M. & NABEKURA, J. 2016. Microglial Contact Prevents Excess Depolarization and Rescues Neurons from Excitotoxicity. *eNeuro,* 3.

KEERTHIKUMAR, S., CHISANGA, D., ARIYARATNE, D., AL SAFFAR, H., ANAND, S., ZHAO, K., SAMUEL, M., PATHAN, M., JOIS, M., CHILAMKURTI, N., GANGODA, L. & MATHIVANAN, S. 2016. ExoCarta: A Web-Based Compendium of Exosomal Cargo. *J Mol Biol,* 428**,** 688-692.

KHOSHNAM, S. E., WINLOW, W., FARZANEH, M., FARBOOD, Y. & MOGHADDAM, H. F. 2017. Pathogenic mechanisms following ischemic stroke. *Neurol Sci,* 38**,** 1167-1186.

KIM, K. M., ABDELMOHSEN, K., MUSTAPIC, M., KAPOGIANNIS, D. & GOROSPE, M. 2017. RNA in extracellular vesicles. *Wiley Interdiscip Rev RNA,* 8.

KOSSINOVA, O. A., GOPANENKO, A. V., TAMKOVICH, S. N., KRASHENININA, O. A., TUPIKIN, A. E., KISELEVA, E., YANSHINA, D. D., MALYGIN, A. A., VEN'YAMINOVA, A. G., KABILOV, M. R. & KARPOVA, G. G. 2017. Cytosolic YB-1 and NSUN2 are the only proteins recognizing specific motifs present in mRNAs enriched in exosomes. *Biochim Biophys Acta Proteins Proteom,* 1865**,** 664-673.

KOWAL, J., ARRAS, G., COLOMBO, M., JOUVE, M., MORATH, J. P., PRIMDAL-BENGTSON, B., DINGLI, F., LOEW, D., TKACH, M. & THERY, C. 2016a. Proteomic comparison defines novel markers to characterize heterogeneous populations of extracellular vesicle subtypes. *Proc Natl Acad Sci U S A,* 113**,** E968-77.

KOWAL, J., ARRAS, G., COLOMBO, M., JOUVE, M., MORATH, J. P., PRIMDAL-BENGTSON, B., DINGLI, F., LOEW, D., TKACH, M. & THÉRY, C. 2016b. Proteomic comparison defines novel markers to characterize heterogeneous

populations of extracellular vesicle subtypes. *Proc Natl Acad Sci U S A,* 113**,** E968-77.

KOWALSKI, R. G., LEDREUX, A., VIOLETTE, J. E., NEUMANN, R. T., ORNELAS, D., YU, X., GRIFFITHS, S. G., LEWIS, S., NASH, P., MONTE, A. A., COUGHLAN, C. M., DEIGHAN, C., GROTTA, J. C., JONES, W. J. & GRANER, M. W. 2023. Rapid Activation of Neuroinflammation in Stroke: Plasma and Extracellular Vesicles Obtained on a Mobile Stroke Unit. *Stroke,* 54**,** e52-e57.

KÜGLER, P. 2021. Extracellular RNA: from biomarkers to therapy in neurological diseases. Studienarbeit. *Universität Hamburg*.

KURIAKOSE, D. & XIAO, Z. 2020. Pathophysiology and Treatment of Stroke: Present Status and Future Perspectives. *Int J Mol Sci,* 21.

LADWIG, A., WALTER, H. L., HUCKLENBROICH, J., WILLUWEIT, A., LANGEN, K. J., FINK, G. R., RUEGER, M. A. & SCHROETER, M. 2017. Osteopontin Augments M2 Microglia Response and Separates M1- and M2-Polarized Microglial Activation in Permanent Focal Cerebral Ischemia. *Mediators Inflamm,* 2017**,** 7189421.

LÄSSER, C., SHELKE, G. V., YERI, A., KIM, D. K., CRESCITELLI, R., RAIMONDO, S., SJÖSTRAND, M., GHO, Y. S., VAN KEUREN JENSEN, K. & LÖTVALL, J. 2017. Two distinct extracellular RNA signatures released by a single cell type identified by microarray and next-generation sequencing. *RNA Biol,* 14**,** 58-72.

LÁZARO-IBÁÑEZ, E., LÄSSER, C., SHELKE, G. V., CRESCITELLI, R., JANG, S. C., CVJETKOVIC, A., GARCÍA-RODRÍGUEZ, A. & LÖTVALL, J. 2019. DNA analysis of low- and high-density fractions defines heterogeneous subpopulations of small extracellular vesicles based on their DNA cargo and topology. *J Extracell Vesicles,* 8**,** 1656993.

LEIN, E. S., HAWRYLYCZ, M. J., AO, N., AYRES, M., BENSINGER, A., BERNARD, A., BOE, A. F., BOGUSKI, M. S., BROCKWAY, K. S., BYRNES, E. J., CHEN, L., CHEN, L., CHEN, T. M., CHIN, M. C., CHONG, J., CROOK, B. E., CZAPLINSKA, A., DANG, C. N., DATTA, S., DEE, N. R., DESAKI, A. L., DESTA, T., DIEP, E., DOLBEARE, T. A., DONELAN, M. J., DONG, H. W., DOUGHERTY, J. G., DUNCAN, B. J., EBBERT, A. J., EICHELE, G., ESTIN, L. K., FABER, C., FACER, B. A., FIELDS, R., FISCHER, S. R., FLISS, T. P., FRENSLEY, C., GATES, S. N., GLATTFELDER, K. J., HALVERSON, K. R., HART, M. R., HOHMANN, J. G., HOWELL, M. P., JEUNG, D. P., JOHNSON, R. A., KARR, P. T., KAWAL, R., KIDNEY, J. M., KNAPIK, R. H., KUAN, C. L., LAKE, J. H., LARAMEE, A. R., LARSEN, K. D., LAU, C., LEMON, T. A., LIANG, A. J., LIU, Y., LUONG, L. T., MICHAELS, J., MORGAN, J. J., MORGAN, R. J., MORTRUD, M. T., MOSQUEDA, N. F., NG, L. L., NG, R., ORTA, G. J., OVERLY, C. C., PAK, T. H., PARRY, S. E., PATHAK, S. D., PEARSON, O. C., PUCHALSKI, R. B., RILEY, Z. L., ROCKETT, H. R., ROWLAND, S. A., ROYALL, J. J., RUIZ, M. J., SARNO, N. R., SCHAFFNIT, K., SHAPOVALOVA, N. V., SIVISAY, T., SLAUGHTERBECK, C. R., SMITH, S. C., SMITH, K. A., SMITH, B. I., SODT, A. J., STEWART, N. N., STUMPF, K. R., SUNKIN, S. M., SUTRAM, M., TAM, A., TEEMER, C. D., THALLER, C., THOMPSON, C. L., VARNAM, L. R., VISEL, A., WHITLOCK, R. M., WOHNOUTKA, P. E., WOLKEY, C. K., WONG, V. Y., et al. 2007. Genome-wide atlas of gene expression in the adult mouse brain. *Nature,* 445**,** 168-76.

LI, K., WONG, D. K., HONG, K. Y. & RAFFAI, R. L. 2018. Cushioned-Density Gradient Ultracentrifugation (C-DGUC): A Refined and High Performance Method for the Isolation, Characterization, and Use of Exosomes. *Methods Mol Biol,* 1740**,** 69-83.

LI, S. R., MAN, Q. W., GAO, X., LIN, H., WANG, J., SU, F. C., WANG, H. Q., BU, L. L., LIU, B. & CHEN, G. 2021a. Tissue-derived extracellular vesicles in cancers and non-cancer diseases: Present and future. *J Extracell Vesicles,* 10**,** e12175.

LI, Y., LIU, B., ZHAO, T., QUAN, X., HAN, Y., CHENG, Y., CHEN, Y., SHEN, X., ZHENG, Y. & ZHAO, Y. 2023. Comparative study of extracellular vesicles derived from mesenchymal stem cells and brain endothelial cells attenuating blood-brain barrier permeability via regulating Caveolin-1-dependent ZO-1 and Claudin-5 endocytosis in acute ischemic stroke. *J Nanobiotechnology,* 21**,** 70.

LI, Y., ZHAO, J., YU, S., WANG, Z., HE, X., SU, Y., GUO, T., SHENG, H., CHEN, J., ZHENG, Q., LI, Y., GUO, W., CAI, X., SHI, G., WU, J., WANG, L., WANG, P., HE, X. & HUANG, S. 2019. Extracellular Vesicles Long RNA Sequencing Reveals Abundant mRNA, circRNA, and lncRNA in Human Blood as Potential Biomarkers for Cancer Diagnosis. *Clin Chem,* 65**,** 798-808.

LI, Z., SONG, Y., HE, T., WEN, R., LI, Y., CHEN, T., HUANG, S., WANG, Y., TANG, Y., SHEN, F., TIAN, H. L., YANG, G. Y. & ZHANG, Z. 2021b. M2 microglial small extracellular vesicles reduce glial scar formation via the miR-124/STAT3 pathway after ischemic stroke in mice. *Theranostics,* 11**,** 1232-1248.

LIDDELOW, S. A., GUTTENPLAN, K. A., CLARKE, L. E., BENNETT, F. C., BOHLEN, C. J., SCHIRMER, L., BENNETT, M. L., MUNCH, A. E., CHUNG, W. S., PETERSON, T. C., WILTON, D. K., FROUIN, A., NAPIER, B. A., PANICKER, N., KUMAR, M., BUCKWALTER, M. S., ROWITCH, D. H., DAWSON, V. L., DAWSON, T. M., STEVENS, B. & BARRES, B. A. 2017. Neurotoxic reactive astrocytes are induced by activated microglia. *Nature,* 541**,** 481-487.

LIESZ, A., SURI-PAYER, E., VELTKAMP, C., DOERR, H., SOMMER, C., RIVEST, S., GIESE, T. & VELTKAMP, R. 2009. Regulatory T cells are key cerebroprotective immunomodulators in acute experimental stroke. *Nat Med,* 15**,** 192-9.

LINARES, R., TAN, S., GOUNOU, C., ARRAUD, N. & BRISSON, A. R. 2015. High-speed centrifugation induces aggregation of extracellular vesicles. *J Extracell Vesicles,* 4**,** 29509.

LINDOSO, R. S., COLLINO, F. & CAMUSSI, G. 2015. Extracellular vesicles derived from renal cancer stem cells induce a pro-tumorigenic phenotype in mesenchymal stromal cells. *Oncotarget,* 6**,** 7959-69.

LIPTON, P. 1999. Ischemic cell death in brain neurons. *Physiol Rev,* 79**,** 1431-568.

LISCHNIG, A., BERGQVIST, M., OCHIYA, T. & LÄSSER, C. 2022. Quantitative Proteomics Identifies Proteins Enriched in Large and Small Extracellular Vesicles. *Mol Cell Proteomics,* 21**,** 100273.

LIU, H., TIAN, Y., XUE, C., NIU, Q., CHEN, C. & YAN, X. 2022. Analysis of extracellular vesicle DNA at the single-vesicle level by nano-flow cytometry. *J Extracell Vesicles,* 11**,** e12206.

LIU, Z. & CHOPP, M. 2016. Astrocytes, therapeutic targets for neuroprotection and neurorestoration in ischemic stroke. *Prog Neurobiol,* 144**,** 103-20.

LIZARRAGA-VALDERRAMA, L. R. & SHERIDAN, G. K. 2021. Extracellular vesicles and intercellular communication in the central nervous system. *FEBS Lett,* 595**,** 1391-1410.

LO, E. H., DALKARA, T. & MOSKOWITZ, M. A. 2003. Mechanisms, challenges and opportunities in stroke. *Nature Reviews Neuroscience,* 4**,** 399-414.

LO, T. W., FIGUEROA-ROMERO, C., HUR, J., PACUT, C., STOLL, E., SPRING, C., LEWIS, R., NAIR, A., GOUTMAN, S. A., SAKOWSKI, S. A., NAGRATH, S. & FELDMAN, E. L. 2021. Extracellular Vesicles in Serum and Central Nervous

System Tissues Contain microRNA Signatures in Sporadic Amyotrophic Lateral Sclerosis. *Front Mol Neurosci,* 14**,** 739016.

LÖTVALL, J., HILL, A. F., HOCHBERG, F., BUZÁS, E. I., DI VIZIO, D., GARDINER, C., GHO, Y. S., KUROCHKIN, I. V., MATHIVANAN, S., QUESENBERRY, P., SAHOO, S., TAHARA, H., WAUBEN, M. H., WITWER, K. W. & THÉRY, C. 2014. Minimal experimental requirements for definition of extracellular vesicles and their functions: a position statement from the International Society for Extracellular Vesicles. *J Extracell Vesicles,* 3**,** 26913.

LU, J. H., TEH, B. K., WANG, L., WANG, Y. N., TAN, Y. S., LAI, M. C. & REID, K. B. 2008. The classical and regulatory functions of C1q in immunity and autoimmunity. *Cell Mol Immunol,* 5**,** 9-21.

LUND, S. A., GIACHELLI, C. M. & SCATENA, M. 2009. The role of osteopontin in inflammatory processes. *J Cell Commun Signal,* 3**,** 311-22.

MA, Y., WANG, J., WANG, Y. & YANG, G. Y. 2017. The biphasic function of microglia in ischemic stroke. *Prog Neurobiol,* 157**,** 247-272.

MAAS, S. L. N., BREAKEFIELD, X. O. & WEAVER, A. M. 2017. Extracellular Vesicles: Unique Intercellular Delivery Vehicles. *Trends Cell Biol,* 27**,** 172-188.

MALKIN, E. Z. & BRATMAN, S. V. 2020. Bioactive DNA from extracellular vesicles and particles. *Cell Death Dis,* 11**,** 584.

MATEESCU, B., KOWAL, E. J., VAN BALKOM, B. W., BARTEL, S., BHATTACHARYYA, S. N., BUZÁS, E. I., BUCK, A. H., DE CANDIA, P., CHOW, F. W., DAS, S., DRIEDONKS, T. A., FERNÁNDEZ-MESSINA, L., HADERK, F., HILL, A. F., JONES, J. C., VAN KEUREN-JENSEN, K. R., LAI, C. P., LÄSSER, C., LIEGRO, I. D., LUNAVAT, T. R., LORENOWICZ, M. J., MAAS, S. L., MÄGER, I., MITTELBRUNN, M., MOMMA, S., MUKHERJEE, K., NAWAZ, M., PEGTEL, D. M., PFAFFL, M. W., SCHIFFELERS, R. M., TAHARA, H., THÉRY, C., TOSAR, J. P., WAUBEN, M. H., WITWER, K. W. & NOLTE-'T HOEN, E. N. 2017. Obstacles and opportunities in the functional analysis of extracellular vesicle RNA - an ISEV position paper. *J Extracell Vesicles,* 6**,** 1286095.

MATTICK, J. S. & MAKUNIN, I. V. 2006. Non-coding RNA. *Hum Mol Genet,* 15 Spec No 1**,** R17-29.

MCNICHOLAS, K. & MICHAEL, M. Z. 2017. Immuno-characterization of Exosomes Using Nanoparticle Tracking Analysis. *Methods Mol Biol,* 1545**,** 35-42.

MENDELSON, S. J. & PRABHAKARAN, S. 2021. Diagnosis and Management of Transient Ischemic Attack and Acute Ischemic Stroke: A Review. *Jama,* 325**,** 1088-1098.

MICHINAGA, S. & KOYAMA, Y. 2019. Dual Roles of Astrocyte-Derived Factors in Regulation of Blood-Brain Barrier Function after Brain Damage. *International Journal of Molecular Sciences,* 20**,** 571.

MIFSUD, G., ZAMMIT, C., MUSCAT, R., DI GIOVANNI, G. & VALENTINO, M. 2014. Oligodendrocyte pathophysiology and treatment strategies in cerebral ischemia. *CNS Neurosci Ther,* 20**,** 603-12.

MOSKOWITZ, M. A., LO, E. H. & IADECOLA, C. 2010. The science of stroke: mechanisms in search of treatments. *Neuron,* 67**,** 181-98.

MURAOKA, S., LIN, W., CHEN, M., HERSH, S. W., EMILI, A., XIA, W. & IKEZU, T. 2020. Assessment of separation methods for extracellular vesicles from human and mouse brain tissues and human cerebrospinal fluids. *Methods,* 177**,** 35-49.

MURILLO, O. D., THISTLETHWAITE, W., ROZOWSKY, J., SUBRAMANIAN, S. L., LUCERO, R., SHAH, N., JACKSON, A. R., SRINIVASAN, S., CHUNG, A.,

LAURENT, C. D., KITCHEN, R. R., GALEEV, T., WARRELL, J., DIAO, J. A., WELSH, J. A., HANSPERS, K., RIUTTA, A., BURGSTALLER-MUEHLBACHER, S., SHAH, R. V., YERI, A., JENKINS, L. M., AHSEN, M. E., CORDON-CARDO, C., DOGRA, N., GIFFORD, S. M., SMITH, J. T., STOLOVITZKY, G., TEWARI, A. K., WUNSCH, B. H., YADAV, K. K., DANIELSON, K. M., FILANT, J., MOELLER, C., NEJAD, P., PAUL, A., SIMONSON, B., WONG, D. K., ZHANG, X., BALAJ, L., GANDHI, R., SOOD, A. K., ALEXANDER, R. P., WANG, L., WU, C., WONG, D. T. W., GALAS, D. J., VAN KEUREN-JENSEN, K., PATEL, T., JONES, J. C., DAS, S., CHEUNG, K. H., PICO, A. R., SU, A. I., RAFFAI, R. L., LAURENT, L. C., ROTH, M. E., GERSTEIN, M. B. & MILOSAVLJEVIC, A. 2019. exRNA Atlas Analysis Reveals Distinct Extracellular RNA Cargo Types and Their Carriers Present across Human Biofluids. *Cell,* 177**,** 463-477.e15.

NAKAMURA, K. & SHICHITA, T. 2019. Cellular and molecular mechanisms of sterile inflammation in ischaemic stroke. *J Biochem,* 165**,** 459-464.

O'BRIEN, K., BREYNE, K., UGHETTO, S., LAURENT, L. C. & BREAKEFIELD, X. O. 2020. RNA delivery by extracellular vesicles in mammalian cells and its applications. *Nat Rev Mol Cell Biol,* 21**,** 585-606.

ONÓDI, Z., PELYHE, C., TERÉZIA NAGY, C., BRENNER, G. B., ALMÁSI, L., KITTEL, Á., MANČEK-KEBER, M., FERDINANDY, P., BUZÁS, E. I. & GIRICZ, Z. 2018. Isolation of High-Purity Extracellular Vesicles by the Combination of Iodixanol Density Gradient Ultracentrifugation and Bind-Elute Chromatography From Blood Plasma. *Front Physiol,* 9**,** 1479.

OTERO-ORTEGA, L., LASO-GARCÍA, F., GÓMEZ-DE FRUTOS, M. D., RODRÍGUEZ-FRUTOS, B., PASCUAL-GUERRA, J., FUENTES, B., DÍEZ-TEJEDOR, E. & GUTIÉRREZ-FERNÁNDEZ, M. 2017. White Matter Repair After Extracellular Vesicles Administration in an Experimental Animal Model of Subcortical Stroke. *Sci Rep,* 7**,** 44433.

OZAKI, T., NAKAMURA, H. & KISHIMA, H. 2019. Therapeutic strategy against ischemic stroke with the concept of neurovascular unit. *Neurochem Int,* 126**,** 246-251.

PAN, B. T. & JOHNSTONE, R. M. 1983. Fate of the transferrin receptor during maturation of sheep reticulocytes in vitro: selective externalization of the receptor. *Cell,* 33**,** 967-78.

PANTONI, L., GARCIA, J. H. & GUTIERREZ, J. A. 1996. Cerebral white matter is highly vulnerable to ischemia. *Stroke,* 27**,** 1641-6; discussion 1647.

PAOLICELLI, R. C., SIERRA, A., STEVENS, B., TREMBLAY, M. E., AGUZZI, A., AJAMI, B., AMIT, I., AUDINAT, E., BECHMANN, I., BENNETT, M., BENNETT, F., BESSIS, A., BIBER, K., BILBO, S., BLURTON-JONES, M., BODDEKE, E., BRITES, D., BRÔNE, B., BROWN, G. C., BUTOVSKY, O., CARSON, M. J., CASTELLANO, B., COLONNA, M., COWLEY, S. A., CUNNINGHAM, C., DAVALOS, D., DE JAGER, P. L., DE STROOPER, B., DENES, A., EGGEN, B. J. L., EYO, U., GALEA, E., GAREL, S., GINHOUX, F., GLASS, C. K., GOKCE, O., GOMEZ-NICOLA, D., GONZÁLEZ, B., GORDON, S., GRAEBER, M. B., GREENHALGH, A. D., GRESSENS, P., GRETER, M., GUTMANN, D. H., HAASS, C., HENEKA, M. T., HEPPNER, F. L., HONG, S., HUME, D. A., JUNG, S., KETTENMANN, H., KIPNIS, J., KOYAMA, R., LEMKE, G., LYNCH, M., MAJEWSKA, A., MALCANGIO, M., MALM, T., MANCUSO, R., MASUDA, T., MATTEOLI, M., MCCOLL, B. W., MIRON, V. E., MOLOFSKY, A. V., MONJE, M., MRACSKO, E., NADJAR, A., NEHER, J. J., NENISKYTE, U., NEUMANN, H., NODA, M., PENG, B., PERI, F., PERRY, V.

H., POPOVICH, P. G., PRIDANS, C., PRILLER, J., PRINZ, M., RAGOZZINO, D., RANSOHOFF, R. M., SALTER, M. W., SCHAEFER, A., SCHAFER, D. P., SCHWARTZ, M., SIMONS, M., SMITH, C. J., STREIT, W. J., TAY, T. L., TSAI, L. H., VERKHRATSKY, A., VON BERNHARDI, R., WAKE, H., WITTAMER, V., WOLF, S. A., WU, L. J. & WYSS-CORAY, T. 2022. Microglia states and nomenclature: A field at its crossroads. *Neuron,* 110**,** 3458-3483.

PAPE, H.-C., KURTZ, A. & SILBERNAGL, S. (eds.) 2018. *Physiologie,* Stuttgart ; New York: Georg Thieme Verlag.

PEDRAGOSA, J., SALAS-PERDOMO, A., GALLIZIOLI, M., CUGOTA, R., MIRÓ-MUR, F., BRIANSÓ, F., JUSTICIA, C., PÉREZ-ASENSIO, F., MARQUEZ-KISINOUSKY, L., URRA, X., GIERYNG, A., KAMINSKA, B., CHAMORRO, A. & PLANAS, A. M. 2018. CNS-border associated macrophages respond to acute ischemic stroke attracting granulocytes and promoting vascular leakage. *Acta Neuropathol Commun,* 6**,** 76.

PEREZ-GONZALEZ, R., GAUTHIER, S. A., KUMAR, A. & LEVY, E. 2012. The exosome secretory pathway transports amyloid precursor protein carboxyl-terminal fragments from the cell into the brain extracellular space. *J Biol Chem,* 287**,** 43108-15.

PRADA, I., AMIN, L., FURLAN, R., LEGNAME, G., VERDERIO, C. & COJOC, D. 2016. A new approach to follow a single extracellular vesicle-cell interaction using optical tweezers. *Biotechniques,* 60**,** 35-41.

QIN, B., HU, X. M., SU, Z. H., ZENG, X. B., MA, H. Y. & XIONG, K. 2021. Tissue-derived extracellular vesicles: Research progress from isolation to application. *Pathol Res Pract,* 226**,** 153604.

QIN, C., ZHOU, L. Q., MA, X. T., HU, Z. W., YANG, S., CHEN, M., BOSCO, D. B., WU, L. J. & TIAN, D. S. 2019. Dual Functions of Microglia in Ischemic Stroke. *Neurosci Bull,* 35**,** 921-933.

RÄDLER, J., GUPTA, D., ZICKLER, A. & ANDALOUSSI, S. E. 2023. Exploiting the biogenesis of extracellular vesicles for bioengineering and therapeutic cargo loading. *Mol Ther,* 31**,** 1231-1250.

RIDDER, K., KELLER, S., DAMS, M., RUPP, A. K., SCHLAUDRAFF, J., DEL TURCO, D., STARMANN, J., MACAS, J., KARPOVA, D., DEVRAJ, K., DEPBOYLU, C., LANDFRIED, B., ARNOLD, B., PLATE, K. H., HÖGLINGER, G., SÜLTMANN, H., ALTEVOGT, P. & MOMMA, S. 2014. Extracellular vesicle-mediated transfer of genetic information between the hematopoietic system and the brain in response to inflammation. *PLoS Biol,* 12**,** e1001874.

RINALDO, L., RABINSTEIN, A. A., CLOFT, H., KNUDSEN, J. M., CASTILLA, L. R. & BRINJIKJI, W. 2019. Racial and Ethnic Disparities in the Utilization of Thrombectomy for Acute Stroke. *Stroke,* 50**,** 2428-2432.

RUSSELL, A. E., SNEIDER, A., WITWER, K. W., BERGESE, P., BHATTACHARYYA, S. N., COCKS, A., COCUCCI, E., ERDBRUGGER, U., FALCON-PEREZ, J. M., FREEMAN, D. W., GALLAGHER, T. M., HU, S., HUANG, Y., JAY, S. M., KANO, S. I., LAVIEU, G., LESZCZYNSKA, A., LLORENTE, A. M., LU, Q., MAHAIRAKI, V., MUTH, D. C., NOREN HOOTEN, N., OSTROWSKI, M., PRADA, I., SAHOO, S., SCHOYEN, T. H., SHENG, L., TESCH, D., VAN NIEL, G., VANDENBROUCKE, R. E., VERWEIJ, F. J., VILLAR, A. V., WAUBEN, M., WEHMAN, A. M., YIN, H., CARTER, D. R. F. & VADER, P. 2019. Biological membranes in EV biogenesis, stability, uptake, and cargo transfer: an ISEV position paper arising from the ISEV membranes and EVs workshop. *J Extracell Vesicles,* 8**,** 1684862.

SACCO, R. L., KASNER, S. E., BRODERICK, J. P., CAPLAN, L. R., CONNORS, J. J., CULEBRAS, A., ELKIND, M. S., GEORGE, M. G., HAMDAN, A. D., HIGASHIDA, R. T., HOH, B. L., JANIS, L. S., KASE, C. S., KLEINDORFER, D. O., LEE, J. M., MOSELEY, M. E., PETERSON, E. D., TURAN, T. N., VALDERRAMA, A. L. & VINTERS, H. V. 2013. An updated definition of stroke for the 21st century: a statement for healthcare professionals from the American Heart Association/American Stroke Association. *Stroke,* 44**,** 2064-89.

SAINI, V., GUADA, L. & YAVAGAL, D. R. 2021. Global Epidemiology of Stroke and Access to Acute Ischemic Stroke Interventions. *Neurology,* 97**,** S6-s16.

SAINT-POL, J., GOSSELET, F., DUBAN-DEWEER, S., POTTIEZ, G. & KARAMANOS, Y. 2020. Targeting and Crossing the Blood-Brain Barrier with Extracellular Vesicles. *Cells,* 9.

SCHAEFFER, S. & IADECOLA, C. 2021. Revisiting the neurovascular unit. *Nat Neurosci,* 24**,** 1198-1209.

SCHÄFER, M. K., SCHWAEBLE, W. J., POST, C., SALVATI, P., CALABRESI, M., SIM, R. B., PETRY, F., LOOS, M. & WEIHE, E. 2000. Complement C1q is dramatically up-regulated in brain microglia in response to transient global cerebral ischemia. *J Immunol,* 164**,** 5446-52.

SHAO, H., IM, H., CASTRO, C. M., BREAKEFIELD, X., WEISSLEDER, R. & LEE, H. 2018. New Technologies for Analysis of Extracellular Vesicles. *Chem Rev,* 118**,** 1917-1950.

SHEN, Z., XIANG, M., CHEN, C., DING, F., WANG, Y., SHANG, C., XIN, L., ZHANG, Y. & CUI, X. 2022. Glutamate excitotoxicity: Potential therapeutic target for ischemic stroke. *Biomed Pharmacother,* 151**,** 113125.

SHI, L., SUN, Z., SU, W., XU, F., XIE, D., ZHANG, Q., DAI, X., IYER, K., HITCHENS, T. K., FOLEY, L. M., LI, S., STOLZ, D. B., CHEN, K., DING, Y., THOMSON, A. W., LEAK, R. K., CHEN, J. & HU, X. 2021. Treg cell-derived osteopontin promotes microglia-mediated white matter repair after ischemic stroke. *Immunity,* 54**,** 1527-1542.e8.

SHI, Y., SHI, H., NOMI, A., LEI-LEI, Z., ZHANG, B. & QIAN, H. 2019. Mesenchymal stem cell-derived extracellular vesicles: a new impetus of promoting angiogenesis in tissue regeneration. *Cytotherapy,* 21**,** 497-508.

SILVA, A. M., ALMEIDA, M. I., TEIXEIRA, J. H., MAIA, A. F., CALIN, G. A., BARBOSA, M. A. & SANTOS, S. G. 2017. Dendritic Cell-derived Extracellular Vesicles mediate Mesenchymal Stem/Stromal Cell recruitment. *Sci Rep,* 7**,** 1667.

SIMAK, J., GELDERMAN, M. P., YU, H., WRIGHT, V. & BAIRD, A. E. 2006. Circulating endothelial microparticles in acute ischemic stroke: a link to severity, lesion volume and outcome. *J Thromb Haemost,* 4**,** 1296-302.

SPITZER, D., GUÉRIT, S., PUETZ, T., KHEL, M. I., ARMBRUST, M., DUNST, M., MACAS, J., ZINKE, J., DEVRAJ, G., JIA, X., CROLL, F., SOMMER, K., FILIPSKI, K., FREIMAN, T. M., LOOSO, M., GÜNTHER, S., DI TACCHIO, M., PLATE, K. H., REISS, Y., LIEBNER, S., HARTER, P. N. & DEVRAJ, K. 2022. Profiling the neurovascular unit unveils detrimental effects of osteopontin on the blood-brain barrier in acute ischemic stroke. *Acta Neuropathol,* 144**,** 305-337.

SRINIVASAN, S., YERI, A., CHEAH, P. S., CHUNG, A., DANIELSON, K., DE HOFF, P., FILANT, J., LAURENT, C. D., LAURENT, L. D., MAGEE, R., MOELLER, C., MURTHY, V. L., NEJAD, P., PAUL, A., RIGOUTSOS, I., RODOSTHENOUS, R., SHAH, R. V., SIMONSON, B., TO, C., WONG, D., YAN, I. K., ZHANG, X., BALAJ, L., BREAKEFIELD, X. O., DAABOUL, G., GANDHI, R., LAPIDUS, J., LONDIN, E., PATEL, T., RAFFAI, R. L., SOOD, A. K., ALEXANDER, R. P.,

DAS, S. & LAURENT, L. C. 2019. Small RNA Sequencing across Diverse Biofluids Identifies Optimal Methods for exRNA Isolation. *Cell,* 177**,** 446-462.e16.

STAM, J., BARTEL, S., BISCHOFF, R. & WOLTERS, J. C. 2021. Isolation of extracellular vesicles with combined enrichment methods. *J Chromatogr B Analyt Technol Biomed Life Sci,* 1169**,** 122604.

SUN, J., YUAN, Q., GUO, L., XIAO, G., ZHANG, T., LIANG, B., YAO, R., ZHU, Y., LI, Y. & HU, L. 2022. Brain Microvascular Endothelial Cell-Derived Exosomes Protect Neurons from Ischemia-Reperfusion Injury in Mice. *Pharmaceuticals (Basel),* 15.

SUZUKI, H., HASEGAWA, Y., KANAMARU, K. & ZHANG, J. H. 2010. Mechanisms of osteopontin-induced stabilization of blood-brain barrier disruption after subarachnoid hemorrhage in rats. *Stroke,* 41**,** 1783-90.

SZALAY, G., MARTINECZ, B., LÉNÁRT, N., KÖRNYEI, Z., ORSOLITS, B., JUDÁK, L., CSÁSZÁR, E., FEKETE, R., WEST, B. L., KATONA, G., RÓZSA, B. & DÉNES, Á. 2016. Microglia protect against brain injury and their selective elimination dysregulates neuronal network activity after stroke. *Nat Commun,* 7**,** 11499.

SZATANEK, R., BAJ-KRZYWORZEKA, M., ZIMOCH, J., LEKKA, M., SIEDLAR, M. & BARAN, J. 2017. The Methods of Choice for Extracellular Vesicles (EVs) Characterization. *Int J Mol Sci,* 18.

TAKAHASHI, A., OKADA, R., NAGAO, K., KAWAMATA, Y., HANYU, A., YOSHIMOTO, S., TAKASUGI, M., WATANABE, S., KANEMAKI, M. T., OBUSE, C. & HARA, E. 2017. Exosomes maintain cellular homeostasis by excreting harmful DNA from cells. *Nat Commun,* 8**,** 15287.

TAURO, B. J., GREENING, D. W., MATHIAS, R. A., JI, H., MATHIVANAN, S., SCOTT, A. M. & SIMPSON, R. J. 2012. Comparison of ultracentrifugation, density gradient separation, and immunoaffinity capture methods for isolating human colon cancer cell line LIM1863-derived exosomes. *Methods,* 56**,** 293-304.

THAKUR, B. K., ZHANG, H., BECKER, A., MATEI, I., HUANG, Y., COSTA-SILVA, B., ZHENG, Y., HOSHINO, A., BRAZIER, H., XIANG, J., WILLIAMS, C., RODRIGUEZ-BARRUECO, R., SILVA, J. M., ZHANG, W., HEARN, S., ELEMENTO, O., PAKNEJAD, N., MANOVA-TODOROVA, K., WELTE, K., BROMBERG, J., PEINADO, H. & LYDEN, D. 2014. Double-stranded DNA in exosomes: a novel biomarker in cancer detection. *Cell Res,* 24**,** 766-9.

THÉRY, C., OSTROWSKI, M. & SEGURA, E. 2009. Membrane vesicles as conveyors of immune responses. *Nat Rev Immunol,* 9**,** 581-93.

THÉRY, C., WITWER, K. W., AIKAWA, E., ALCARAZ, M. J., ANDERSON, J. D., ANDRIANTSITOHAINA, R., ANTONIOU, A., ARAB, T., ARCHER, F., ATKIN-SMITH, G. K., AYRE, D. C., BACH, J. M., BACHURSKI, D., BAHARVAND, H., BALAJ, L., BALDACCHINO, S., BAUER, N. N., BAXTER, A. A., BEBAWY, M., BECKHAM, C., BEDINA ZAVEC, A., BENMOUSSA, A., BERARDI, A. C., BERGESE, P., BIELSKA, E., BLENKIRON, C., BOBIS-WOZOWICZ, S., BOILARD, E., BOIREAU, W., BONGIOVANNI, A., BORRAS, F. E., BOSCH, S., BOULANGER, C. M., BREAKEFIELD, X., BREGLIO, A. M., BRENNAN, M. A., BRIGSTOCK, D. R., BRISSON, A., BROEKMAN, M. L., BROMBERG, J. F., BRYL-GORECKA, P., BUCH, S., BUCK, A. H., BURGER, D., BUSATTO, S., BUSCHMANN, D., BUSSOLATI, B., BUZAS, E. I., BYRD, J. B., CAMUSSI, G., CARTER, D. R., CARUSO, S., CHAMLEY, L. W., CHANG, Y. T., CHEN, C., CHEN, S., CHENG, L., CHIN, A. R., CLAYTON, A., CLERICI, S. P., COCKS, A., COCUCCI, E., COFFEY, R. J., CORDEIRO-DA-SILVA, A., COUCH, Y., COUMANS, F. A., COYLE, B., CRESCITELLI, R., CRIADO, M. F., D'SOUZA-

SCHOREY, C., DAS, S., DATTA CHAUDHURI, A., DE CANDIA, P., DE SANTANA, E. F., DE WEVER, O., DEL PORTILLO, H. A., DEMARET, T., DEVILLE, S., DEVITT, A., DHONDT, B., DI VIZIO, D., DIETERICH, L. C., DOLO, V., DOMINGUEZ RUBIO, A. P., DOMINICI, M., DOURADO, M. R., DRIEDONKS, T. A., DUARTE, F. V., DUNCAN, H. M., EICHENBERGER, R. M., EKSTROM, K., EL ANDALOUSSI, S., ELIE-CAILLE, C., ERDBRUGGER, U., FALCON-PEREZ, J. M., FATIMA, F., FISH, J. E., FLORES-BELLVER, M., FORSONITS, A., FRELET-BARRAND, A., et al. 2018. Minimal information for studies of extracellular vesicles 2018 (MISEV2018): a position statement of the International Society for Extracellular Vesicles and update of the MISEV2014 guidelines. *J Extracell Vesicles,* 7**,** 1535750.

TKACH, M. & THÉRY, C. 2016. Communication by Extracellular Vesicles: Where We Are and Where We Need to Go. *Cell,* 164**,** 1226-1232.

TOH, W. S., LAI, R. C., ZHANG, B. & LIM, S. K. 2018. MSC exosome works through a protein-based mechanism of action. *Biochem Soc Trans,* 46**,** 843-853.

TOHGI, H., UTSUGISAWA, K. & NAGANE, Y. 2000. Hypoxia-induced expression of C1q, a subcomponent of the complement system, in cultured rat PC12 cells. *Neurosci Lett,* 291**,** 151-4.

TRICARICO, C., CLANCY, J. & D'SOUZA-SCHOREY, C. 2017. Biology and biogenesis of shed microvesicles. *Small GTPases,* 8**,** 220-232.

TURCHINOVICH, A., DRAPKINA, O. & TONEVITSKY, A. 2019. Transcriptome of Extracellular Vesicles: State-of-the-Art. *Front Immunol,* 10**,** 202.

VALADI, H., EKSTROM, K., BOSSIOS, A., SJOSTRAND, M., LEE, J. J. & LOTVALL, J. O. 2007. Exosome-mediated transfer of mRNAs and microRNAs is a novel mechanism of genetic exchange between cells. *Nat Cell Biol,* 9**,** 654-9.

VAN NIEL, G., CHARRIN, S., SIMOES, S., ROMAO, M., ROCHIN, L., SAFTIG, P., MARKS, M. S., RUBINSTEIN, E. & RAPOSO, G. 2011. The tetraspanin CD63 regulates ESCRT-independent and -dependent endosomal sorting during melanogenesis. *Dev Cell,* 21**,** 708-21.

VAN NIEL, G., D'ANGELO, G. & RAPOSO, G. 2018. Shedding light on the cell biology of extracellular vesicles. *Nat Rev Mol Cell Biol,* 19**,** 213-228.

VEERMAN, R. E., TEEUWEN, L., CZARNEWSKI, P., GÜCLÜLER AKPINAR, G., SANDBERG, A., CAO, X., PERNEMALM, M., ORRE, L. M., GABRIELSSON, S. & ELDH, M. 2021. Molecular evaluation of five different isolation methods for extracellular vesicles reveals different clinical applicability and subcellular origin. *J Extracell Vesicles,* 10**,** e12128.

VELDMAN-JONES, M. H., BRANT, R., ROONEY, C., GEH, C., EMERY, H., HARBRON, C. G., WAPPETT, M., SHARPE, A., DYMOND, M., BARRETT, J. C., HARRINGTON, E. A. & MARSHALL, G. 2015. Evaluating Robustness and Sensitivity of the NanoString Technologies nCounter Platform to Enable Multiplexed Gene Expression Analysis of Clinical Samples. *Cancer Res,* 75**,** 2587-93.

VELLA, L. J., SCICLUNA, B. J., CHENG, L., BAWDEN, E. G., MASTERS, C. L., ANG, C. S., WILLAMSON, N., MCLEAN, C., BARNHAM, K. J. & HILL, A. F. 2017. A rigorous method to enrich for exosomes from brain tissue. *J Extracell Vesicles,* 6**,** 1348885.

VERGAUWEN, G., DHONDT, B., VAN DEUN, J., DE SMEDT, E., BERX, G., TIMMERMAN, E., GEVAERT, K., MIINALAINEN, I., COCQUYT, V., BRAEMS, G., VAN DEN BROECKE, R., DENYS, H., DE WEVER, O. &

HENDRIX, A. 2017. Confounding factors of ultrafiltration and protein analysis in extracellular vesicle research. *Sci Rep,* 7**,** 2704.

VICKERS, K. C., PALMISANO, B. T., SHOUCRI, B. M., SHAMBUREK, R. D. & REMALEY, A. T. 2011. MicroRNAs are transported in plasma and delivered to recipient cells by high-density lipoproteins. *Nat Cell Biol,* 13**,** 423-33.

WAGGOTT, D., CHU, K., YIN, S., WOUTERS, B. G., LIU, F. F. & BOUTROS, P. C. 2012. NanoStringNorm: an extensible R package for the pre-processing of NanoString mRNA and miRNA data. *Bioinformatics,* 28**,** 1546-8.

WANG, H., HORBINSKI, C., WU, H., LIU, Y., SHENG, S., LIU, J., WEISS, H., STROMBERG, A. J. & WANG, C. 2016. NanoStringDiff: a novel statistical method for differential expression analysis based on NanoString nCounter data. *Nucleic Acids Res,* 44**,** e151.

WANG, L., XIONG, X., ZHANG, L. & SHEN, J. 2021. Neurovascular Unit: A critical role in ischemic stroke. *CNS Neurosci Ther,* 27**,** 7-16.

WANG, R., ZHANG, X., ZHANG, J., FAN, Y., SHEN, Y., HU, W. & CHEN, Z. 2012. Oxygen-glucose deprivation induced glial scar-like change in astrocytes. *PLoS One,* 7**,** e37574.

WANG, X., LOUDEN, C., YUE, T. L., ELLISON, J. A., BARONE, F. C., SOLLEVELD, H. A. & FEUERSTEIN, G. Z. 1998. Delayed expression of osteopontin after focal stroke in the rat. *J Neurosci,* 18**,** 2075-83.

WEBB, R. L., KAISER, E. E., JURGIELEWICZ, B. J., SPELLICY, S., SCOVILLE, S. L., THOMPSON, T. A., SWETENBURG, R. L., HESS, D. C., WEST, F. D. & STICE, S. L. 2018a. Human Neural Stem Cell Extracellular Vesicles Improve Recovery in a Porcine Model of Ischemic Stroke. *Stroke,* 49**,** 1248-1256.

WEBB, R. L., KAISER, E. E., SCOVILLE, S. L., THOMPSON, T. A., FATIMA, S., PANDYA, C., SRIRAM, K., SWETENBURG, R. L., VAIBHAV, K., ARBAB, A. S., BABAN, B., DHANDAPANI, K. M., HESS, D. C., HODA, M. N. & STICE, S. L. 2018b. Human Neural Stem Cell Extracellular Vesicles Improve Tissue and Functional Recovery in the Murine Thromboembolic Stroke Model. *Transl Stroke Res,* 9**,** 530-539.

WEBER, G. F., ASHKAR, S., GLIMCHER, M. J. & CANTOR, H. 1996. Receptor-ligand interaction between CD44 and osteopontin (Eta-1). *Science,* 271**,** 509-12.

WEI, E. P., KONTOS, H. A. & BECKMAN, J. S. 1996. Mechanisms of cerebral vasodilation by superoxide, hydrogen peroxide, and peroxynitrite. *Am J Physiol,* 271**,** H1262-6.

WEI, Z., BATAGOV, A. O., SCHINELLI, S., WANG, J., WANG, Y., EL FATIMY, R., RABINOVSKY, R., BALAJ, L., CHEN, C. C., HOCHBERG, F., CARTER, B., BREAKEFIELD, X. O. & KRICHEVSKY, A. M. 2017. Coding and noncoding landscape of extracellular RNA released by human glioma stem cells. *Nat Commun,* 8**,** 1145.

WELSH, J. A., GOBERDHAN, D. C. I., O'DRISCOLL, L., BUZAS, E. I., BLENKIRON, C., BUSSOLATI, B., CAI, H., DI VIZIO, D., DRIEDONKS, T. A. P., ERDBRÜGGER, U., FALCON-PEREZ, J. M., FU, Q. L., HILL, A. F., LENASSI, M., LIM, S. K., MAHONEY, M. G., MOHANTY, S., MÖLLER, A., NIEUWLAND, R., OCHIYA, T., SAHOO, S., TORRECILHAS, A. C., ZHENG, L., ZIJLSTRA, A., ABUELREICH, S., BAGABAS, R., BERGESE, P., BRIDGES, E. M., BRUCALE, M., BURGER, D., CARNEY, R. P., COCUCCI, E., CRESCITELLI, R., HANSER, E., HARRIS, A. L., HAUGHEY, N. J., HENDRIX, A., IVANOV, A. R., JOVANOVIC-TALISMAN, T., KRUH-GARCIA, N. A., KU'ULEI-LYN FAUSTINO, V., KYBURZ, D., LÄSSER, C., LENNON, K. M.,

LÖTVALL, J., MADDOX, A. L., MARTENS-UZUNOVA, E. S., MIZENKO, R. R., NEWMAN, L. A., RIDOLFI, A., ROHDE, E., ROJALIN, T., ROWLAND, A., SAFTICS, A., SANDAU, U. S., SAUGSTAD, J. A., SHEKARI, F., SWIFT, S., TER-OVANESYAN, D., TOSAR, J. P., USECKAITE, Z., VALLE, F., VARGA, Z., VAN DER POL, E., VAN HERWIJNEN, M. J. C., WAUBEN, M. H. M., WEHMAN, A. M., WILLIAMS, S., ZENDRINI, A., ZIMMERMAN, A. J., THÉRY, C. & WITWER, K. W. 2024. Minimal information for studies of extracellular vesicles (MISEV2023): From basic to advanced approaches. *J Extracell Vesicles,* 13**,** e12404.

WEN, R. X., SHEN, H., HUANG, S. X., WANG, L. P., LI, Z. W., PENG, P., MAMTILAHUN, M., TANG, Y. H., SHEN, F. X., TIAN, H. L., YANG, G. Y. & ZHANG, Z. J. 2020. P2Y6 receptor inhibition aggravates ischemic brain injury by reducing microglial phagocytosis. *CNS Neurosci Ther,* 26**,** 416-429.

WICKS, E. E., RAN, K. R., KIM, J. E., XU, R., LEE, R. P. & JACKSON, C. M. 2022. The Translational Potential of Microglia and Monocyte-Derived Macrophages in Ischemic Stroke. *Front Immunol,* 13**,** 897022.

WITWER, K. W., GOBERDHAN, D. C., O'DRISCOLL, L., THÉRY, C., WELSH, J. A., BLENKIRON, C., BUZÁS, E. I., DI VIZIO, D., ERDBRÜGGER, U., FALCÓN-PÉREZ, J. M., FU, Q. L., HILL, A. F., LENASSI, M., LÖTVALL, J., NIEUWLAND, R., OCHIYA, T., ROME, S., SAHOO, S. & ZHENG, L. 2021. Updating MISEV: Evolving the minimal requirements for studies of extracellular vesicles. *J Extracell Vesicles,* 10**,** e12182.

WITWER, K. W. & THÉRY, C. 2019. Extracellular vesicles or exosomes? On primacy, precision, and popularity influencing a choice of nomenclature. *J Extracell Vesicles,* 8**,** 1648167.

XIN, D., LI, T., CHU, X., KE, H., LIU, D. & WANG, Z. 2021. MSCs-extracellular vesicles attenuated neuroinflammation, synapse damage and microglial phagocytosis after hypoxia-ischemia injury by preventing osteopontin expression. *Pharmacol Res,* 164**,** 105322.

XU, S., LU, J., SHAO, A., ZHANG, J. H. & ZHANG, J. 2020. Glial Cells: Role of the Immune Response in Ischemic Stroke. *Front Immunol,* 11**,** 294.

YANG, C., HAWKINS, K. E., DORÉ, S. & CANDELARIO-JALIL, E. 2019. Neuroinflammatory mechanisms of blood-brain barrier damage in ischemic stroke. *Am J Physiol Cell Physiol,* 316**,** C135-c153.

YANG, Y., BOZA-SERRANO, A., DUNNING, C. J. R., CLAUSEN, B. H., LAMBERTSEN, K. L. & DEIERBORG, T. 2018. Inflammation leads to distinct populations of extracellular vesicles from microglia. *J Neuroinflammation,* 15**,** 168.

YAO, Y., CHEN, Z. L., NORRIS, E. H. & STRICKLAND, S. 2014. Astrocytic laminin regulates pericyte differentiation and maintains blood brain barrier integrity. *Nat Commun,* 5**,** 3413.

YEUNG, C. C., DONDELINGER, F., SCHOOF, E. M., GEORG, B., LU, Y., ZHENG, Z., ZHANG, J., HANNIBAL, J., FAHRENKRUG, J. & KJAER, M. 2022. Circadian regulation of protein cargo in extracellular vesicles. *Sci Adv,* 8**,** eabc9061.

YILMAZ, G. & GRANGER, D. N. 2010. Leukocyte recruitment and ischemic brain injury. *Neuromolecular Med,* 12**,** 193-204.

YOSHIMURA, S., SAKAI, N., YAMAGAMI, H., UCHIDA, K., BEPPU, M., TOYODA, K., MATSUMARU, Y., MATSUMOTO, Y., KIMURA, K., TAKEUCHI, M., YAZAWA, Y., KIMURA, N., SHIGETA, K., IMAMURA, H., SUZUKI, I., ENOMOTO, Y., TOKUNAGA, S., MORITA, K., SAKAKIBARA, F., KINJO, N., SAITO, T., ISHIKURA, R., INOUE, M. & MORIMOTO, T. 2022. Endovascular

Therapy for Acute Stroke with a Large Ischemic Region. *N Engl J Med,* 386**,** 1303-1313.

ZHANG, D., REN, J., LUO, Y., HE, Q., ZHAO, R., CHANG, J., YANG, Y. & GUO, Z. N. 2021a. T Cell Response in Ischemic Stroke: From Mechanisms to Translational Insights. *Front Immunol,* 12**,** 707972.

ZHANG, L., WEI, W., AI, X., KILIC, E., HERMANN, D. M., VENKATARAMANI, V., BÄHR, M. & DOEPPNER, T. R. 2021b. Extracellular vesicles from hypoxia-preconditioned microglia promote angiogenesis and repress apoptosis in stroke mice via the TGF-β/Smad2/3 pathway. *Cell Death Dis,* 12**,** 1068.

ZHANG, Q., JEPPESEN, D. K., HIGGINBOTHAM, J. N., FRANKLIN, J. L. & COFFEY, R. J. 2023. Comprehensive isolation of extracellular vesicles and nanoparticles. *Nat Protoc,* 18**,** 1462-1487.

ZHANG, S., SHANG, D., SHI, H., TENG, W. & TIAN, L. 2021c. Function of Astrocytes in Neuroprotection and Repair after Ischemic Stroke. *Eur Neurol,* 84**,** 426-434.

ZHAO, Y., ZHANG, X., CHEN, X. & WEI, Y. 2022. Neuronal injuries in cerebral infarction and ischemic stroke: From mechanisms to treatment (Review). *Int J Mol Med,* 49.

ZHENG, K., LIN, L., JIANG, W., CHEN, L., ZHANG, X., ZHANG, Q., REN, Y. & HAO, J. 2022a. Single-cell RNA-seq reveals the transcriptional landscape in ischemic stroke. *J Cereb Blood Flow Metab,* 42**,** 56-73.

ZHENG, L., GUO, Y., ZHAI, X., ZHANG, Y., CHEN, W., ZHU, Z., XUAN, W. & LI, P. 2022b. Perivascular macrophages in the CNS: From health to neurovascular diseases. *CNS Neurosci Ther,* 28**,** 1908-1920.

ZHI, Z., SUN, Q. & TANG, W. 2022. Research advances and challenges in tissue-derived extracellular vesicles. *Front Mol Biosci,* 9**,** 1036746.

ZHOU, Y., YAO, Y., SHENG, L., ZHANG, J., ZHANG, J. H. & SHAO, A. 2020. Osteopontin as a candidate of therapeutic application for the acute brain injury. *J Cell Mol Med,* 24**,** 8918-8929.

ZICARI, S., ARAKELYAN, A., PALOMINO, R., FITZGERALD, W., VANPOUILLE, C., LEBEDEVA, A., SCHMITT, A., BOMSEL, M., BRITT, W. & MARGOLIS, L. 2018. Human cytomegalovirus-infected cells release extracellular vesicles that carry viral surface proteins. *Virology,* 524**,** 97-105.

ZIEREN, R. C., DONG, L., CLARK, D. J., KUCZLER, M. D., HORIE, K., MORENO, L. F., LIH, T. M., SCHNAUBELT, M., VERMEULEN, L., ZHANG, H., DE REIJKE, T. M., PIENTA, K. J. & AMEND, S. R. 2021. Defining candidate mRNA and protein EV biomarkers to discriminate ccRCC and pRCC from non-malignant renal cells in vitro. *Med Oncol,* 38**,** 105.

ZOMER, A., MAYNARD, C., VERWEIJ, F. J., KAMERMANS, A., SCHÄFER, R., BEERLING, E., SCHIFFELERS, R. M., DE WIT, E., BERENGUER, J., ELLENBROEK, S. I. J., WURDINGER, T., PEGTEL, D. M. & VAN RHEENEN, J. 2015. In Vivo imaging reveals extracellular vesicle-mediated phenocopying of metastatic behavior. *Cell,* 161**,** 1046-1057.

Internet references

Internet reference 1: WHO (2020) The top 10 causes of death. [online on the internet] URL: https://www.who.int/news-room/fact-sheets/detail/the-top-10-causes-of-death [retrieved on 13.02.2023, 17:38]

Internet reference 2: Serumwerk Bernburg AG (2020) OptiPrepTM Application Sheet S01. [online on the internet] URL: https://diagnostic.serumwerk.com/wp-content/uploads/2021/05/S01-Serumwerk.pdf [retrieved on 13.02.2023, 17:48]

Internet reference 3: Serumwerk Bernburg AG (2020) OptiPrepTM Application Sheet S09. URL: https://diagnostic.serumwerk.com/wp-content/uploads/2021/05/S09-Serumwerk.pdf [retrieved on 13.02.2023, 17:50]

Internet reference 4: NanoString Technologies, Inc. (2018) nCounter® Advanced Analysis 2.0, Plugin for nSolver Software, User Manual. URL: https://nanostring.com/wp-content/uploads/MAN-10030-03_nCounter®_Advanced_Analysis_2.0_User_Manual.pdf [retrieved on 13.02.2023, 17:53]

Internet reference 5: NanoString Technologies, Inc. (2018) nSolver™ 4.0, Analysis Software User Manual. URL: https://nanostring.com/wp-content/uploads/MAN-C0019-08_nSolver_4.0_Analysis_Software_User_Manual.pdf [retrieved on 13.02.2023, 17:55]

Internet reference 6: Beckman Coulter (2024) Calculator. URL: https://www.beckman.de/centrifuges/rotors/calculator [retrieved on 13.02.2023, 17:48]

Internet reference 7: NanoString Technologies, Inc. (2024) nCounter® Neuroinflammation Panel. URL: https://nanostring.com/products/ncounter-assays-panels/neuroscience/neuroinflammation/ [retrieved on 13.02.2023, 17:57]

11. Acknowledgement

This dissertation is the result of hard work, frustration and achievements. It would not have been possible without the help of several colleagues and friends.

I would like to express my deepest gratitude to my supervisor, PD Dr. rer. nat. Berta Puig, for her knowledge and guidance, which was especially important for me when I started my experiments. I thank her for the regular meetings, the constructive criticism and the feedback, which was invaluable during the writing of these pages.

Additionally, I am indebted to Prof. Dr. Tim Magnus, who encouraged me to start in the "Experimental Research of Stroke and Inflammation" working group. Furthermore, I am grateful for the support of the iPRIME doctoral committee, who financed my research.

Thanks should also be given to Santra Brenna, who taught me new experiments and helped me to improve my scientific work.

Lastly, I would not have hold out under the stress without my family, who always had an open ear when experiments failed, and Annika, who was always there for me.

12. Lebenslauf

Paul Christian Max Kügler
*30.04.1997 in Kiel

Schulsausbildung

2007 - 2015 Abitur, Gymnasium Buckhorn

Akademische Laufbahn

10/2015 – 11/2023 Studium der Humanmedizin (Staatsexamen)
10/2015 – 04/2016: Universität Greifswald
10/2016 – 11/2023: Universität Hamburg

seit 10/2019 Experimentelle Doktorarbeit
Titel: "Role of extracellular vesicles mRNA in neuroinflammation in a mouse model of stroke"
Stipendiat des iPRIME Promotionskollegs, Förderperiode 10/2019 – 09/2020
Betreuerin: PD Dr. Berta Puig

Veröffentlichung
BUB, A., BRENNA, S., ALAWI, M., KÜGLER, P., GUI, Y., KRETZ, O., ALTMEPPEN, H., MAGNUS, T. & PUIG, B. 2022. Multiplexed mRNA analysis of brain-derived extracellular vesicles upon experimental stroke in mice reveals increased mRNA content with potential relevance to inflammation and recovery processes. *Cell Mol Life Sci,* 79**,** 329.

Klinische Erfahrungen

07/2018 – 10/2021 Famulaturen in den Fachgebieten Allgemeinmedizin, Anästhesiologie, Neurologie, Nephrologie und Gastroenterologie

01/2019 – 04/2022 Studentische Hilfskraft in der Anästhesie am UKE (PACU)

11/2022 – 10/2023 Praktisches Jahr
1. Tertial: Gynäkologie und Geburtshilfe im Marienkrankenhaus in Hamburg
2. Tertial: Allgemein- und Unfallchirurgie im Klinikum Itzehoe
3. Tertial: Innere Medizin (Schwerpunkt Gastroenterologie, Kardiologie und Onkologie) am Universitätsklinikum Hamburg-Eppendorf (UKE)

Ärztliche Ausbildung

seit 03/2024 Arzt in Weiterbildung im Fachbereich Gynäkologie und Geburtshilfe

Hamburg, 25.11.2023

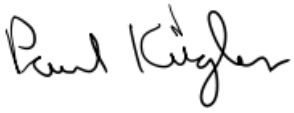

13. Eidesstattliche Versicherung

Ich versichere ausdrücklich, dass ich die Arbeit selbständig und ohne fremde Hilfe verfasst, andere als die von mir angegebenen Quellen und Hilfsmittel nicht benutzt und die aus den benutzten Werken wörtlich oder inhaltlich entnommenen Stellen einzeln nach Ausgabe (Auflage und Jahr des Erscheinens), Band und Seite des benutzten Werkes kenntlich gemacht habe.

Ferner versichere ich, dass ich die Dissertation bisher nicht einem Fachvertreter an einer anderen Hochschule zur Überprüfung vorgelegt oder mich anderweitig um Zulassung zur Promotion beworben habe.

Ich erkläre mich einverstanden, dass meine Dissertation vom Dekanat der Medizinischen Fakultät mit einer gängigen Software zur Erkennung von Plagiaten überprüft werden kann.

Unterschrift: .....